



Alexandre Olas de Sousa Martins

Bachelor Degree in Sciences of Physics Engineering

**Electrical Impedance Measurements of
DNA Molecules and Gold Nanoparticles
at low Temperatures**

Dissertation submitted in partial fulfillment
of the requirements for the degree of

Master of Science in
Physics Engineering

Co-advisers: Maria de Fátima Raposo,
Associate Professor,
NOVA University of Lisbon
Grégoire Bonfait, Associate
Professor, NOVA University of Lisbon

Examination Committee

Chair: Dr. Isabel Catarino, NOVA University of Lisbon
Members: Dr. Yuri Nunes, NOVA University of Lisbon
Dr. Grégoire Bonfait, NOVA University of Lisbon



FACULDADE DE
CIÊNCIAS E TECNOLOGIA
UNIVERSIDADE NOVA DE LISBOA

November, 2019

Electrical Impedance Measurements of DNA Molecules and Gold Nanoparticles at low Temperatures

Copyright © Alexandre Olas de Sousa Martins, Faculty of Sciences and Technology, NOVA University Lisbon.

The Faculty of Sciences and Technology and the NOVA University Lisbon have the right, perpetual and without geographical boundaries, to file and publish this dissertation through printed copies reproduced on paper or on digital form, or by any other means known or that may be invented, and to disseminate through scientific repositories and admit its copying and distribution for non-commercial, educational or research purposes, as long as credit is given to the author and editor.

ACKNOWLEDGEMENTS

I would like to express my thankfulness to all the people and institutions that contributed to the accomplishment of this work, especially to:

Professor Maria Fátima Raposo and Professor Grégoire Bonfait, my supervisors, for all the support and guidance, for being there for me on my first steps as a scientist, for all the opportunities they gave me throughout this year, and above all, for trusting me and helping me without giving all the answers. Professor Paulo Ribeiro, who was a constant help throughout this period.

The members of the laboratories LIBPhys and CEFITEC, such as Jorge Barreto who was always there to support me, as well as Thais Pivetta.

My friends, for always being there and for understanding my absence during this year, for all the friendly words that you always give to me. Specially to Francisco Mendes.

My family, for always believing in me, for the unconditional love, inspiration, strength and support. For all the patience and consolation that you always offer to me. Especially thanking to my parents and brother, I love you and you are always in my heart. I know that sometimes I was not easy to put up with. However, I never quit and I give all of me in everything that I do, just as you always taught me!

And last but not least, to my girlfriend, Rita Mendes, for being the foundation pillar to the building that is my life. Thank you for being there for me, even though it is not always easy.

I acknowledge the financial support from FEDER, through Programa Operacional Factores de Competitividade COMPETE and Fundação para a Ciência e a Tecnologia through research project grants UID/FIS/00068/2013 and PTDC/FIS-NAN/0909/2014.

ABSTRACT

Strand breaks occur naturally in the deoxyribonucleic acid (DNA) chain. Studies have shown that the amount of breaks increases with exposure to ultraviolet (UV) light. Additionally, it has been shown that low energy electrons, with energies below DNA's ionization energy, are capable of also inducing strand breaks on DNA. These breaks alter the length of the DNA molecule which in turn alters its electrical impedance. As such, the amount of strand breaks can be indirectly measured through an impedance spectroscopy (IS). This work presents the construction of a cryogenic unit capable to hold an interdigitated sensor, with a sample of DNA or DNA with gold nanoparticles (AuNPs), allowing IS measurements to occur. This cryogenic unit is able to withstand temperatures in the range of 77 to 300 K, while monitoring the temperature at which its sample is. Liquid nitrogen was used as the cold source, allowing the low temperatures mentioned above to be reached. Since the heating process lasts around 8 h, depending on the amount of liquid nitrogen used, it becomes hard to manually start a measurement at the appropriate time. To counter this, a user interface was developed that monitors the temperature, automatically starting a measurement when a temperature defined by the user is reached. Overall, a cryogenic system was built which can be applied in the future for the study of DNA and DNA+AuNPs thin films.

Keywords: Impedance Spectroscopy; Electrical Impedance; DNA; Gold Nanoparticles; Interdigitated Sensor; Low Temperatures

RESUMO

Quebras de cadeia ocorrem naturalmente na cadeia do ácido desoxirribunocleico (DNA). Estudos mostraram que a quantidade de quebras aumenta com a exposição a luz ultravioleta (UV). Adicionalmente, foi demonstrado que elétrons de baixa energia, com energias abaixo da energia de ionização do DNA, são capazes de induzir quebras de cadeia no DNA. Estas quebras alteram o comprimento da molécula de DNA, o que irá alterar a sua impedância elétrica. Como tal, a quantidade de quebras de cadeia pode ser indiretamente medida através de uma espectroscopia de impedância. Este trabalho apresenta a construção de uma unidade criogénica capaz de receber um sensor interdigitado, com uma amostra de DNA ou de DNA com nanopartículas de ouro (AuNPs), permitindo medidas de espectroscopia de impedância. Esta unidade criogénica é capaz de suportar temperaturas no intervalo de 77 a 300 K, enquanto monitoriza a temperatura à qual a amostra se encontra. Azoto líquido foi usado como fonte fria, permitindo que se chegasse às baixas temperaturas acima mencionadas. Uma vez que o processo de aquecimento demora à volta de 8 h - dependendo da quantidade de azoto utilizado - torna-se difícil de começar uma medição manual na altura adequada. Para resolver isto, foi desenvolvido um interface de utilizador que monitoriza a temperatura, começando automaticamente uma medição quando a temperatura definida pelo utilizador é alcançada. Em suma, um sistema criogénico foi construído, que poderá ser usado no estudo de filmes finos de DNA e DNA+AuNPs.

Palavras-chave: Espectroscopia de Impedância; Impedância Elétrica; ADN; Nanopartículas de Ouro; Sensor Interdigitado; Baixas Temperaturas

CONTENTS

1	Introduction	1
2	Theoretical Foundations	3
2.1	DNA	3
2.2	AuNPs	5
2.3	Electrical Impedance	5
2.4	Impedance Spectroscopy	7
2.4.1	Bode Plot	8
3	Materials and Methods	11
3.1	Interdigitated Sensors	12
3.1.1	DNA and DNA + AuNPs Thin Film Sensors	12
3.2	Impedance Spectrometer	13
3.3	Cryogenic System Design and Construction	13
3.3.1	Assembly A	15
3.3.2	Assembly B	16
3.4	Temperature Monitoring	16
3.4.1	Platinum Resistors: Pt100	16
3.4.2	Analog to Digital Converter MAX31865	18
3.4.3	Microcontroller Raspberry Pi	18
3.5	User Interface	20
3.5.1	Temperature Verification	21
3.5.2	1260A Interaction and Data Generation	23
3.5.3	Control Panel	24
3.6	Circuits and Connectors	26
4	Results and Discussion	29
4.1	Circuit and Assembly Validation	29
4.2	User Software Validation	31
4.3	Bare Sensors	33
4.4	Temperature Variation over Time	35
4.5	SMaRT vs LabVIEW™ and 1260A vs 1260A paired with 1296A	40

CONTENTS

4.6	Effects of Consecutive Measurements in the 5 to 25 mV Voltage Amplitude Range	43
4.7	Effect of UV Irradiation	48
5	Conclusion and Future Perspectives	53
	Bibliography	57
	Apêndices	61
A	Appendix 1: Technical Drawings	61
A.1	General Components	61
A.2	Assembly A	67
A.3	Assembly B	72
B	Appendix 2: Python Code	77
C	Appendix 3: Bode Plots of DNA and DNA+AuNPs, from 240 to 290 K	81
	Annexes	85
I	AuNPs Datasheet	85
II	MAX31865 Datasheet	87

LIST OF FIGURES

2.1	Illustration of a DNA molecule and its components [13].	3
2.2	Representation of the components that constitute impedance (adapted from [22]).	6
2.3	Representation the angle δ formed from the complex permittivity and its real component.	7
2.4	Representation of the ideal circuits composed of a) a capacitor, b) a resistor, c) a resistor in series with a capacitor and d) a resistor in parallel with a capacitor.	8
2.5	Impedance Bode plot of the ideal circuits composed of a) a capacitor, b) a resistor, c) a resistor in series with a capacitor and d) a resistor in parallel with a capacitor, shown in figure 2.4.	9
3.1	Global schematic of the project.	11
3.2	Illustration of the sensor (not to scale) with relevant measurements, in millimeters.	12
3.3	Representation of an ideal equivalent circuit to that of the sensor.	12
3.4	Prepared DNA (on the left) and DNA+AuNPs (on the right) sensors.	13
3.5	General schematic of the cryogenic system.	14
3.6	Electrodes responsible for making contact with the sensor.	14
3.7	Assembly A (bottom) and assembly B (top), with the screen in between. . . .	15
3.8	Assembly A viewed from a) the front and b) the side.	16
3.9	Assembly B viewed from a) the side and b) the back.	16
3.10	Photograph of a Cylindrical Pt100 (bottom) and a thin film Pt100 (top). . . .	17
3.11	Schematic of a four wire method Pt100 wiring.	17
3.12	A photograph of MAX31865.	18
3.13	Flowchart of the Python <i>While</i> algorithm.	19
3.14	User interface temperature table.	20
3.15	Flowchart of the state machine.	21
3.16	Flowchart of the temperature monitoring algorithm.	22
3.17	Example of the resulting spreadsheet.	24
3.18	Control panel, Monitoring tab.	25
3.19	Control panel, Definitions tab.	25
3.20	a) Schematic and b) photograph of the homemade circuit.	26
3.21	AMETEK SI [®] set of circuits a) from above and b) from the front.	26

3.22	Blue connector a) as a whole and b) its sensor slit.	27
4.1	Bode plot of the impedance modulus as a function of frequency.	30
4.2	Bode plot of the impedance phase as a function of frequency.	31
4.3	Bode plots of impedance modulus as a function of frequency, at several temperatures, of the homemade circuit.	32
4.4	Bode plots of impedance phase as a function of frequency, at several temperatures, of the homemade circuit. The points taken at frequencies lower than 13 Hz are not in the plot.	33
4.5	Bode plot of the impedance modulus as a function of frequency and temperature, of a bare sensor, measured with Assembly A.	34
4.6	Bode plot of the impedance modulus as a function of frequency and temperature, of a bare sensor, measured with Assembly B.	34
4.7	Bode plot of the impedance modulus as a function of frequency, at several temperatures, of a bare sensor, measured with Assembly A (red) and Assembly B (blue).	35
4.8	Temperature variation as a function of time, for the Pt100 placed inside the hole of the sensor support (red) and the Pt100 placed inside the hole of the electrode support (blue), of Assembly A.	36
4.9	Temperature variation as a function of time, for the Pt100 glued beneath the sensor support (red) and the Pt100 hanging in the air (blue), of Assembly B.	37
4.10	Temperature variation as a function of time, for Assembly A (red) and Assembly B (blue).	38
4.11	Plot of the difference of the temperature measured by each Pt100 as a function of time, for Assembly A (red) and Assembly B (blue).	39
4.12	Plot of the derivative of the average temperature with respect to time as a function of the average temperature, for Assembly A (red) and Assembly B (blue).	39
4.13	Bode plot of the impedance modulus as a function of frequency of a bare sensor measured with Assembly B, at around 300 K (red) and at 77 K (blue). For these measurements, 1260A paired with 1296A were used along with SMaRT software.	40
4.14	Bode plot of the impedance modulus as a function of frequency of a bare sensor measured with Assembly B, at around 300 K (red) and at 77 K (blue). For these measurements, 1260A was used along with SMaRT software.	41
4.15	Bode plot of the impedance modulus as a function of frequency of a bare sensor measured with Assembly B, at around 300 K (red) and at 77 K (blue). For these measurements, 1260A was used along with the developed LabVIEW™ program.	42

4.16	Bode plot of the impedance modulus as a function of frequency of a bare sensor measured with Assembly B, at around 300 K (red) and at 77 K (blue). For these measurements, 1260A was used along with the developed LabVIEW™ program.	42
4.17	Bode plot of the impedance modulus as a function of frequency and the number of measurements for a DNA sensor at the voltage amplitude of a) 5 mV, b) 10 mV, c) 15 mV, d) 20 mV, e) 25 mV and f) the first measurement of each of the previous voltage amplitudes.	44
4.18	Bode plot of the impedance phase as a function of frequency and the number of measurements for a DNA sensor at the voltage amplitude of a) 5 mV, b) 10 mV, c) 15 mV, d) 20 mV, e) 25 mV and f) the first measurement of each of the previous voltage amplitudes.	45
4.19	Bode plot of the impedance modulus as a function of frequency and the number of measurements for a DNA+AuNPs sensor at the voltage amplitude of a) 5 mV, b) 10 mV, c) 15 mV, d) 20 mV, e) 25 mV and f) the first measurement of each of the previous voltage amplitudes.	46
4.20	Bode plot of the impedance phase as a function of frequency and the number of measurements for a DNA+AuNPs sensor at the voltage amplitude of a) 5 mV, b) 10 mV, c) 15 mV, d) 20 mV, e) 25 mV and f) the first measurement of each of the previous voltage amplitudes.	47
4.21	Bode plot of the impedance modulus as a function of frequency and temperature, of the DNA sensor (from 240 to 290 K, with a step of 4 K).	49
4.22	Bode plot of the impedance modulus as a function of frequency and temperature, of the DNA+AuNPs sensor (from 240 to 290 K, with a step of 4 K).	49
4.23	Bode plot of the impedance modulus as a function of frequency and temperature, of the UV irradiated DNA sensor (from 240 to 290 K, with a step of 4 K).	50
4.24	Bode plot of the impedance modulus as a function of frequency and temperature, of the UV irradiated DNA+AuNPs sensor (from 240 to 290 K, with a step of 4 K).	50
4.25	Bode plot of the impedance modulus as a function of frequency at 290 K, of the DNA (red), DNA+AuNPs (blue), UV irradiated DNA (yellow) and UV irradiated DNA+AuNPs sensor (purple).	51
C.1	Bode plot of the impedance modulus as a function of frequency and temperature, of the DNA sensor.	81
C.2	Bode plot of the impedance modulus as a function of frequency and temperature, of the DNA+AuNPs sensor.	82
C.3	Bode plot of the impedance modulus as a function of frequency and temperature, of the UV irradiated DNA sensor.	82

C.4 Bode plot of the impedance modulus as a function of frequency and temperature, of the UV irradiated DNA+AuNPs sensor. 83

LIST OF TABLES

3.1	Configuration VIs, with their variables and respective default values.	23
-----	--	----

LISTINGS

B.1	A listing of Python code used to establish communication between the Raspberry Pi and the computer.	77
-----	---	----

ACRONYMS

AC	Alternating Current
ADC	Analog to Digital Converter
AuNPs	Gold Nanoparticles
DC	Direct Current
DNA	Deoxyribonucleic Acid
DS-DNA	Double Stranded DNA
DSB	Double Strand Break
GPIO	General Purpose Input Output
IR	Infrared
IS	Impedance Spectroscopy
NIR	Near Infrared
NPs	Nanoparticles
PID	Proportional–Integral–Derivative
RS-232	Recommended Standard 232
SPI	Serial Peripheral Interface
SPR	Surface Plasmonic Resonance
SS-DNA	Single Stranded DNA
SSB	Single Strand Break
TTL	Transistor-Transistor Logic
USB	Universal Serial Bus

ACRONYMS

UV Ultraviolet

*

VI Virtual Instrument

INTRODUCTION

Radiotherapy is one of the main techniques of malignant cell elimination due to the radiation's lethal effect on the tumor. However, this technique has two limitations: the increased radioresistance of the surviving cells and the tumor's location within the body. In order to increase the treatment's effectiveness, antitumor chemicals are used alongside radiation. A similar effect may be obtained with the presence of gold nanoparticles (AuNPs) when irradiated by a laser with its wavelength in the visible section of the electromagnetic spectrum. In Photothermal Therapy (PTT), AuNPs are used due to their extraordinary ability to absorb photons in the visible and Near-infrared (NIR) and convert that energy into heat, significantly raising the temperature of vicinity which leads to the death of the tumor cells [3].

On the other hand, the damage that low energy radiation causes to biomolecules is currently a subject of importance in molecular physics, due to it has been experimentally proven that irradiation with particles and photons with lower energies than the ionization potential may induce damage in the Deoxyribonucleic Acid (DNA) [5, 27].

The analysis of the electrical impedance temporal evolution in alternating current (AC) of ultraviolet (UV) light irradiated DNA thin films has revealed that the electric conduction in the DNA chain is caused by electron hopping between base pairs and phosphate groups [17]. The hopping distance is calculated by the conduction by correlated barrier hopping model and it takes the value of $3,3899 \pm 0.0002 \text{ \AA}$ which corresponds to the distance between DNA base pairs. This result is consistent with the conductivity loss with radiation time.

As such, the understanding of electric conduction processes in thin films of DNA and AuNPs mixtures can be useful in the study of smart breaks in the DNA chain, by virtue of the electron jump from the AuNPs to the DNA.

The purpose behind this project is to develop system which allows the impedance

measurement of DNA and DNA + AuNPs, in the frequency range of 1 to 10^6 Hz and in the temperature range of 77 to 300 K. In order to achieve this, it was necessary to design and build a cryogenic system that would allow the sample measurements in the temperature range mentioned previously, but also able to allow an easy and reliable sample change. The design of the cryogenic system developed in this project was based upon the design of a colleague's previous work [14], where a cryogenic cell was developed in order to study the electrical resistivity of metals and its change with temperature variation.

The temperatures mentioned above were achieved by pouring liquid nitrogen into the dewar and purposely letting it evaporate, making the temperature slowly increase from 77 K to room temperature. This process would take from 6 to 8 hours, forcing the whole acquisition process to be automatized. As such, in order to control when measurements are made, an interface software was developed. It receives the temperature measurements from the microcontroller and communicates with the impedance spectrometer, giving the order to begin the measurement, as well as receiving the data from it. This software will also serve as the user interface, showing how the plots of temperature as a function of time and the plot of impedance as a function of frequency, among other functionalities.

This work is composed of an additional four chapters. On the second chapter, the theoretical foundations needed for this project are given. On the third, the materials needed throughout the project are detailed, as well as some of the procedures. On the fourth chapter, the results obtained are shown and discussed. Finally, on the last chapter, a review of the project is made and future perspectives are given.

THEORETICAL FOUNDATIONS

2.1 DNA

The nucleotide is the base unit of the DNA molecule and it is composed of a pentose sugar bounded to both a phosphate group and a nitrogen-containing heterocyclic base, which may be adenine (A), thymine (T), guanine (G) or cytosine (C). Double stranded DNA (DS-DNA) is formed when two complementary single stranded DNA (SS-DNA) combine through hydrogen bonds, forming a double helix, as shown in figure 2.1. Thus, DS-DNA may be seen as one dimensional semiconductor [29].

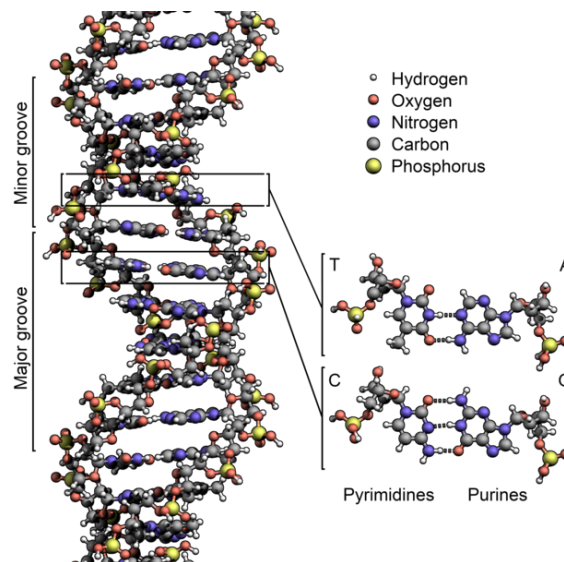


Figure 2.1: Illustration of a DNA molecule and its components [13].

DNA's conductivity and dielectric properties were studied [21] in the range of frequencies of 1 to 10^5 Hz and temperatures of 80 to 330 K, through an impedance spectroscopy

(IS). It was found that most charge carriers move in the vicinity of DNA phosphate groups.

The effect of the distortion of a DNA molecule on its impedance was studied [29]. It was found that an AC impedance spectroscopy (IS) is better suited for the study of DNA than its direct current (DC) counterpart. Additionally, in a normal state, DNA molecules are coiled and randomly distributed. Those molecules did not exhibit electric conduction, unlike those that would stretch and fill the electrodes; i.e. there is a proportional relation between DNA's conductivity and the number of DNA molecules stretched between the electrodes. Furthermore, it was found that after using an enzyme to degrade the DNA molecules, the charge-transfer resistances would increase. This demonstrated that the DNA molecules were responsible for the electrical conduction seen with an AC IS. Also, the author found no traces of ionic conduction. Finally, the author suggests that double stranded DNA behaves like a one-dimensional semiconductor, as opposed to the previous hypothesis of DNA being a metallically conductive molecule.

The correlation between low energy free secondary electrons and DNA strand breaks was studied [6]. This work revealed that low energy electrons could induce DNA strand breaks, even at energies below the ionization limit of DNA and that the amount of DNA damage done by the electrons depends on their initial kinetic energy. This led to the conclusion that the amount of damage inflicted to DNA molecules depends both on the amount of energy absorbed and the nature of the incident particle. Additionally, the observation that electrons with energies below the energy required for two ionizations cause double strand breaks led the authors to suggest that the fragmentation products of a single strand break may react locally with other DNA components, leading to a break on the opposing strand.

In 2012 [17], the electrical conductivity of ultraviolet (UV) irradiated DNA thin films was studied through IS. Results demonstrated that DNA conductivity exponentially decreases with exposure time increase of the DNA molecules to UV light. This happens because phosphate groups are affected by UV radiation, leading to an increase in the molecules damage. The authors suggest that the reason behind the decrease in conductivity is due to the fact that conductivity is governed by electron hopping between DNA base pairs and phosphate groups, with electrical conduction in the DNA molecule occurring along its length. Thus, electrical conductivity can be used to measure DNA damage.

The effects of UV radiation on the DNA molecule were studied, as well as the effects of secondary electrons generated by it [16]. It was found that low energy photoelectrons are emitted from the most peripheral nitrogen groups which subsequently migrate through DNA bases. Since energies below 3.5 eV are sufficient to induce breaks in DNA phosphate groups, this migration causes DNA base fragmentation, inducing DNA strand breaks which leads to irreversible cell damage.

Since electrical conduction in the DNA molecule occurs along its length, when either a single strand break (SSB) or a double strand break (DSB) occur on a DNA molecule, its length is reduced. This will then alter its electrical properties, decreasing the molecule's

conductivity - i.e., increasing its impedance. As such, an IS can indirectly measure the density of damage on a given sample [17, 29].

In order to understand which processes enable electrical conduction in a given material, measurements should be made at different temperatures - preferably below ambient temperature in order to avoid sample decomposition. In fact, conduction might be caused by electrons, ions, dipolar orientation or electron hops. In either of these situations, the mobility of the charge carriers has its own temperature dependency. Thus, since biologic molecules lose their properties at higher temperatures, the temperature dependency will have to be studied at lower temperatures.

2.2 AuNPs

In recent years, gold nanoparticles (AuNPs) have taken the spotlight with regards to scientific research due to their biocompatibility and unique physical and chemical properties [23], such as their size (10^{-9} m), easy synthesis and biomedical applications.

Another important physical property is based on the interaction between an electromagnetic wave with the conduction electrons on its surface, causing them to oscillate coherently in resonance with the frequency of visible light, which results in strong magnetic fields. This effect, known as Surface Plasmonic Resonance (SPR), greatly enhances radiative, such as absorption and scattering, and nonradiative properties, such as the conversion of absorbed light into thermal energy. These properties make the AuNPs an attractive solution for some biological or medical problems [15, 24].

Nanoparticles show great promise for biomedical applications, for instance in cancer diagnostics and therapeutics. Their unique features - specially their size - allow their preferential accumulation in tumor sites due to the Enhanced Permeability and Retention (EPR) effect that occurs in solid tumors [11]. This effect is due to the physiopathological characteristics of tumors, since they have a leaky vasculature with wider fenestrations and a poor lymphatic drainage, which not only leads to the extravasation of NPs from the surrounding vessels into its inner ones but also their accumulation in the tumor cells surroundings.

2.3 Electrical Impedance

The electrical resistance $R = \Delta V/I$ is the degree to which a certain material opposes the electric current and its SI unit is the Ohm (Ω). In an AC circuit, coils and capacitors also contribute to the voltage-to-current ratio. Along with the resistance, the total contribution of these three types of components to this ratio is measured by the electrical impedance and is represented by Z [22, 28].

By applying a voltage that harmonically oscillates in time $V = V_0 \cos(\omega t)$ to an RLC circuit, a current $I = I_0 \cos(\omega t - \theta)$ will be formed. The electrical impedance is the complex

equivalent of Ohm's law and is given by

$$Z = \frac{V_0}{I_0} e^{j\theta} = R + jX, \quad (2.1)$$

where θ is the phase angle, R is the resistance of the circuit and $X = X_L - X_C$ is the complex component of the impedance [9, 22]. The impedance modulus is given by

$$|Z| = \sqrt{R^2 + (X_L - X_C)^2} = \sqrt{R^2 + \left(\omega L - \frac{1}{\omega C}\right)^2}, \quad (2.2)$$

where $X_L = \omega L$ and $X_C = 1/(\omega C)$ are the inductive reactance and the capacitive reactance, respectively. One can draw the each of the components of equation 2.2 in the complex plane, as shown in figure 2.2.

The phase angle is represented by θ and is given by

$$\theta = \arctan\left(\frac{X_L - X_C}{R}\right) = \arctan\left(\frac{Z''}{Z'}\right) \quad (2.3)$$

and represents the phase between the AC potential difference and the current.

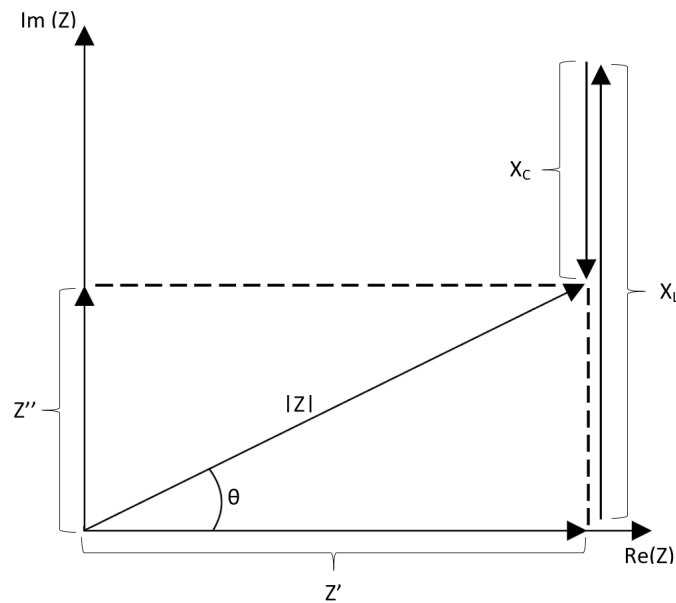


Figure 2.2: Representation of the components that constitute impedance (adapted from [22]).

When $|Z|$ and θ are known, it is possible to derive the real and imaginary impedance components through the trigonometric ratio shown in figure 2.2, by

$$Z' = |Z| \times \cos \theta \quad (2.4)$$

and

$$Z'' = |Z| \times \sin \theta. \quad (2.5)$$

Moreover, the capacitance depends on the dielectric permittivity ($\epsilon(\omega)$), which describes its degree of electrical polarization caused by an external electric field [10, 30]. The permittivity has real and imaginary parts due to the polarization not changing instantly with the change of the electric field, causing a phase difference to be produced. Its real part is associated with the lossless energy exchange between the electric field and the medium and is given by

$$\epsilon' = -\frac{Z''}{2\pi f \epsilon_0 (Z'{}^2 + Z''{}^2)} \frac{s}{A} = -\frac{Z''}{\omega \epsilon_0 Z^2} \frac{s}{A} \quad (2.6)$$

where ϵ_0 is the vacuum permittivity with a value of approximately 8.85×10^{-12} F m⁻¹ and s and A are the sample thickness and area, respectively [25]. On the other hand, its imaginary part represents the energy dissipation associated with the polarization process that is converted into heat and it is given by

$$\epsilon'' = \frac{Z'}{2\pi f \epsilon_0 (Z'{}^2 + Z''{}^2)} \frac{s}{A} = \frac{Z'}{\omega \epsilon_0 Z^2} \frac{s}{A}. \quad (2.7)$$

By plotting the imaginary component as a function of the real component of the dielectric permittivity, it is possible to define the loss angle δ as shown in figure 2.3 [7, 12, 30].

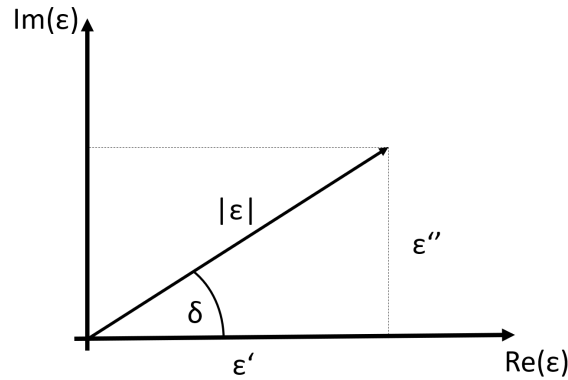


Figure 2.3: Representation the angle δ formed from the complex permittivity and its real component.

The loss tangent $\tan(\delta)$ and is a measure of dissipation that occurs in nonideal capacitors, due to the energy dissipation by the charged particles [12, 26]

$$\tan(\delta) = \frac{\epsilon''}{\epsilon'} \quad (2.8)$$

2.4 Impedance Spectroscopy

Impedance spectroscopy is a technique which - by varying the frequency of the AC signal - allows the study of a substance's electrical properties, of either solids or liquids;

conductors, insulator or dielectric; chemical solutions and samples of biologic origins [8, 17].

The standard electrical stimuli used in IS is based on the application of a single-frequency voltage on the sample and measuring the complex impedance output of the resulting current, be it both its amplitude and phase, or its real and imaginary components [22]. Therefore, this technique allows the electrical characterization of materials and comparison of its properties with an electrical circuit.

In an RLC circuit, resistors, capacitors and coils are discrete elements that make the circuit itself. However, a sample of a given material can be represented by a set of R and C components in parallel and/or in series, where Z' and Z'' correspond respectively to the resistance and capacitance of the whole, and sometimes complex, circuits mimicking the microscopic phenomena. By varying the frequency of the applied voltage, one can observe several interface conduction, polarization and ionic phenomena.

In the case of this project, through the software SMaRT, the impedance spectrometer (1260A) would apply a voltage and would measure the impedance amplitude and phase at defined frequencies between the given range. From these three variables, the remaining impedance components were derived.

2.4.1 Bode Plot

There are several possible ways to convey the information obtained from an AC IS, such as a Bode, Nyquist or Cole-Cole plots. In a Bode plot the impedance modulus or phase are plotted against the frequency [19, 20, 22].

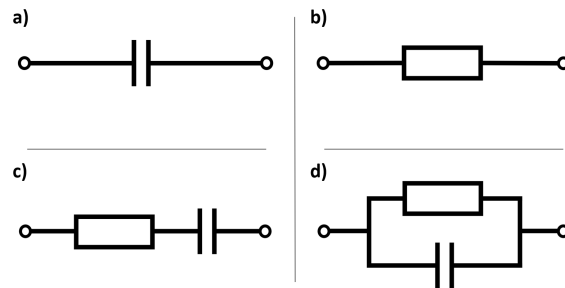


Figure 2.4: Representation of the ideal circuits composed of a) a capacitor, b) a resistor, c) a resistor in series with a capacitor and d) a resistor in parallel with a capacitor.

For instance, by measuring the four simple circuits represented in figure 2.4 with an IS and presenting the data as a bode plot of the impedance modulus as a function of frequency, the four corresponding plots shown in figure 2.5 would be obtained.

It is possible to apply equation 2.2 with $L = 0$, to the circuits shown in figure 2.4, which results in

$$|Z| = \sqrt{R^2 + \left(-\frac{1}{\omega C}\right)^2}. \quad (2.9)$$

The impedance modulus value of a capacitor would be inversely proportional to the frequency, as can be seen in equation 2.9 with $R = 0$. This occurs because the impedance associated to a capacitor is associated with its charge, which means that if the capacitor is charged it will oppose current flow and vice-versa. As such, as frequency increases, the capacitor is being discharged and recharged at a higher rate, lowering its impedance. This is corroborated by the slope seen in the plot, which is proportional to $1/(\omega C)$. Secondly, in the case of the circuit shown in b), the impedance modulus value would be independent of the frequency, with its value equal to the value R of the resistor. This occurs because the degree to which a resistor opposes current is intrinsic to the resistor itself, which means that it does not depend on the frequency, as can be seen in equation 2.2. In the case of the circuit shown in c), the plot would be an amalgamation of a) and b). For low frequencies, the impedance modulus value decays linearly (with both axes being in logarithmic scale). And for high frequencies, the capacitor does not oppose current, which makes the resistor the main source of impedance, resembling the plot of a low-pass filter. Finally, in the case of the circuit shown in d), the plot would be an inverted version of the c) circuit plot. For low frequencies, the capacitor does not allow current flow, the impedance modulus value is equal to the value R of the resistor. And for high frequencies, the current favors flowing to the capacitor, making the impedance decay linearly (with both axis being in logarithmic scale), resembling the plot of a low-pass filter [4, 19, 20, 22]. Each resulting Bode plot can be seen in figure 2.5.

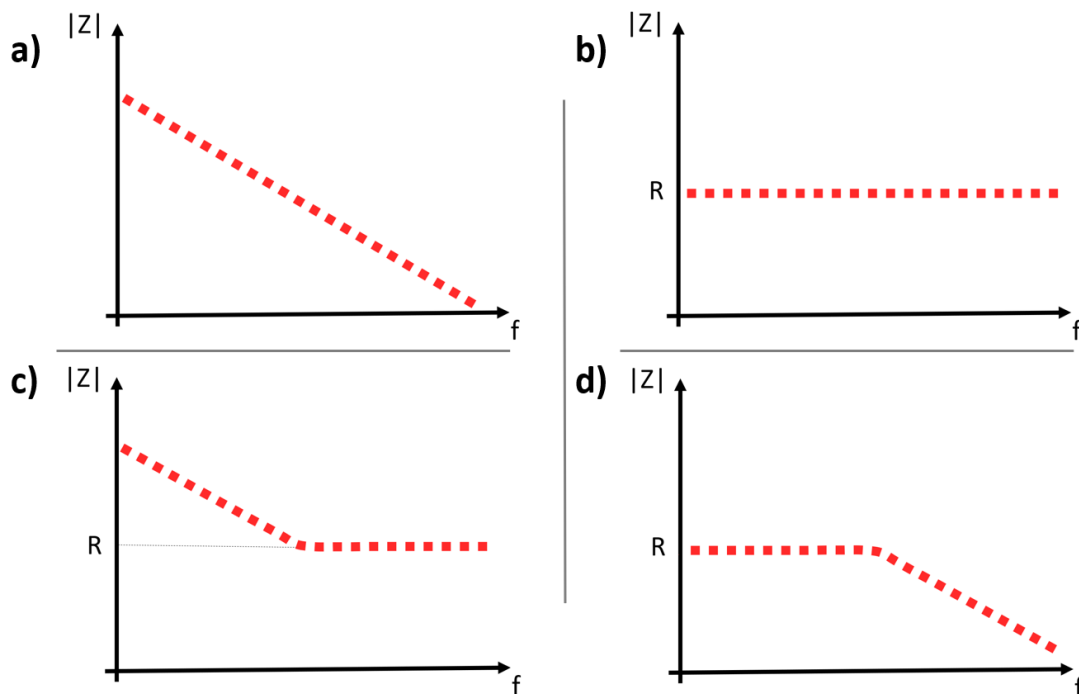


Figure 2.5: Impedance Bode plot of the ideal circuits composed of a) a capacitor, b) a resistor, c) a resistor in series with a capacitor and d) a resistor in parallel with a capacitor, shown in figure 2.4.

MATERIALS AND METHODS

The objective of this project was to build a system that would be able to withstand a temperature range of 77 to 300 K. Its upper end would be exposed at room temperature and receive all electrical connections, allowing its connection to the impedance spectrometer. While its bottom end is equipped to receive the sensors inside its cryogenic cell, making it be able to withstand temperatures of 77 K. There are two platinum resistors with the purpose of indicating the temperature of the medium which surrounds the sample. Each of these two resistors is connected to one analog-to-digital converter, which applies a voltage to the resistor's terminals, reading the originated electric current and then calculates the resistance of the platinum resistors. It then sends this value to a Raspberry Pi board. The Raspberry Pi is connected to both analog-to-digital converters and to the computer, functioning as a bridge between them. Specifically, its function is to wait for the inquiry made by the computer and then read the signal sent by the converter back to the computer. Finally, the impedance spectrometer is connected to the computer through a GPIB-USB interface and to the cryogenic system. This way, the computer is able to monitor the variation of temperature over time and whenever a measurement is to be taken, the signal is sent to the impedance spectrometer which will take a measurement, sending the results back to the computer. This whole process can be seen in figure 3.1.

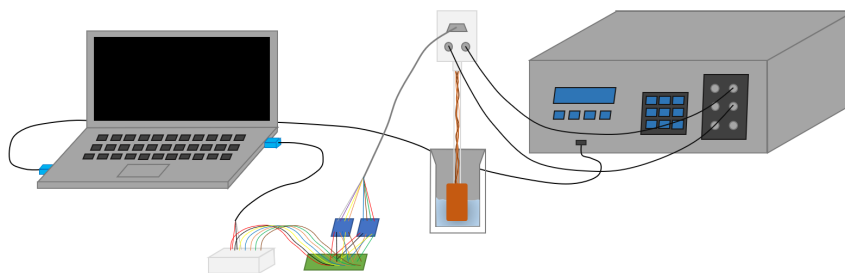


Figure 3.1: Global schematic of the project.

3.1 Interdigitated Sensors

With the purpose of measuring the electric properties of DNA and DNA+AuNPs thin films, gold interdigitated sensors were used, as shown in figure 3.2. These sensors consist of a ceramic upon which was deposited gold in order to form the interdigitated area, as well as the tracks that lead to it. The interdigitated electrodes act as multiple capacitors in parallel, with an equivalent representation made in figure 3.3. This configuration grants more sensibility, allowing impedance measurements of small samples.

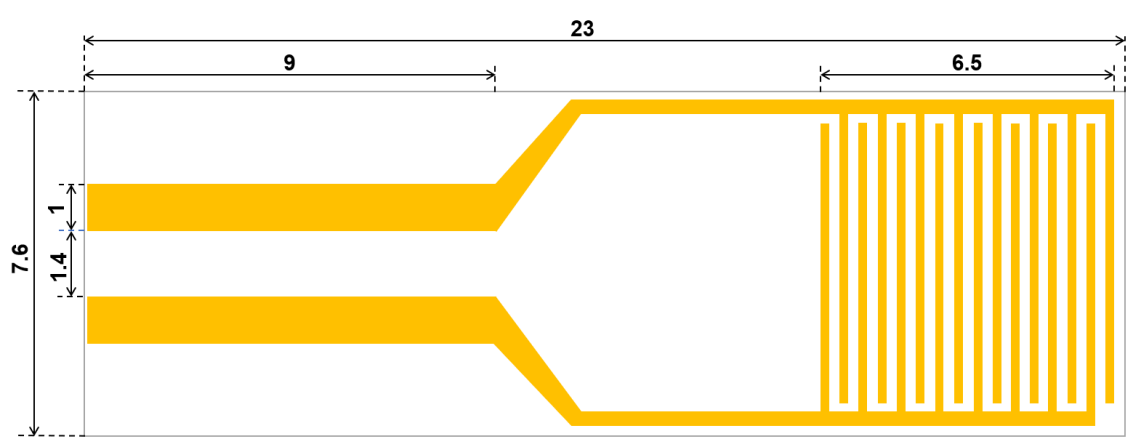


Figure 3.2: Illustration of the sensor (not to scale) with relevant measurements, in millimeters.

The sample to measure is deposited on top of the interdigitated area of the sensor, so that it covers both the gold electrodes and the area between them.



Figure 3.3: Representation of an ideal equivalent circuit to that of the sensor.

3.1.1 DNA and DNA + AuNPs Thin Film Sensors

DNA and DNA+AuNPs thin films were prepared using 10 mg of DNA extracted from a lyophilized calf thymus DNA (cas number 73049-39-5). In order to make the DNA sensor, 500 μL of ultrapure water was used to dissolve the DNA. On the other hand, to make the DNA+AuNPs sensor, 500 μL of a 40 nm AuNPs solution purchased from BBI SolutionsTM (product code EM. GC40), was used to dissolve the DNA. The datasheet of the AuNPs solution can be seen in annex I. Then, the DNA solutions were gently stirred and left to rest in the fridge. After 30 min, the DNA solutions were removed from the fridge and using a micropipette 50 μL were deposited in the interdigitated area of the sensor. Finally, the sensor were left in a dark and closed environment with silica for 2 h,

in order to remove the water from the sensors. The result of this process is shown in figure 3.4.

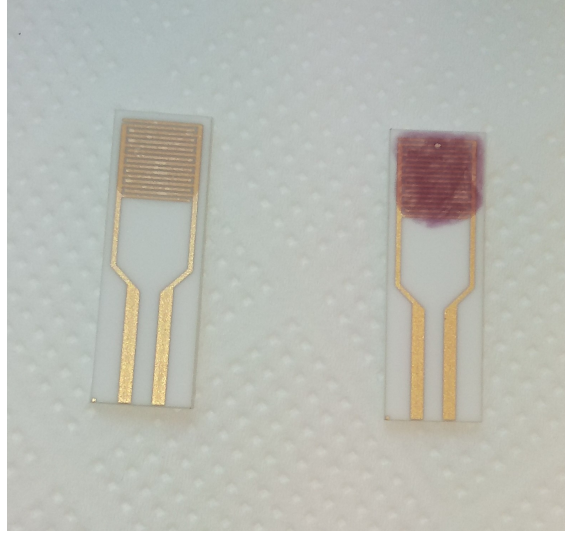


Figure 3.4: Prepared DNA (on the left) and DNA+AuNPs (on the right) sensors.

3.2 Impedance Spectrometer

The impedance spectrometer used in this project was the 1260A *Impedance Analyzer* [1] along with 1296A *Dielectric Interface System* [2], from AMETEK Scientific Instruments® (AMETEK SI®). 1260A was controlled by software SMaRT which acts as the user interface, allowing control over the measurement parameters mentioned in subsection 3.5.2.

Despite SMaRT having an option to add a temperature control device such as Lake Shore Cryotronics, Inc. model 350, this option was not taken due to its high cost. Instead, since AMETEK SI® provides the ability to interact with 1260A with LabVIEW™, a low budget option was taken. However, by choosing this option, the ability to communicate with 1296A was lost, consequently losing the ability to measure impedance magnitude values upwards of $10^8 \Omega$.

3.3 Cryogenic System Design and Construction

This project's design was built upon the general design of Ana Francisco's [14] project. The objective was to build a cryogenic cell able to withstand a temperature difference of around 220 K, using liquid nitrogen as a cold source. Additionally, it would have to be able to receive the sensors mentioned in section 3.1 while allowing measurements to take place. The parts that composed the cryogenic system were designed using SolidWorks® and the corresponding technical drawings are shown in appendix A.

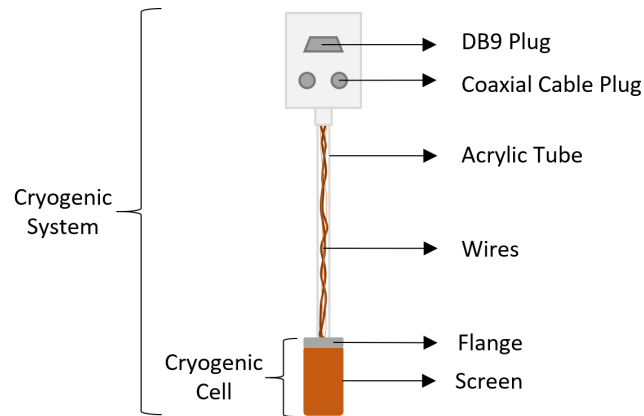


Figure 3.5: General schematic of the cryogenic system.

A general schematic of the cryogenic system is shown in figure 3.5. The cryogenic cell is located on the bottom end of the cryogenic system. This cell is comprised of a screen, a flange, a sensor support and an electrode support. The screen was made out of a copper tube with a brass lid soldered to it, which was attached to the flange, shielding the rest of the cryogenic cell. The donut-shaped flange is made out of aluminum and it serves as a support, where the acrylic tube is glued to and where the sensor support is screwed to. This sensor support is the component which receives the support in its groove, making it unable to move. The electrode support is the component which receives and holds the two electrodes in place, so that they can maintain their position relative to the sensor, so that consecutive measurements can occur. The electrodes which make contact with the gold tracks of the interdigitated sensors, are shown in figure 3.6 and are composed of two halves connected by a spring. Additionally, they are slightly pushed against the gold tracks of the interdigitated sensor, avoiding bad electrical contact, which could be a source of noise for electrical impedance measurements.

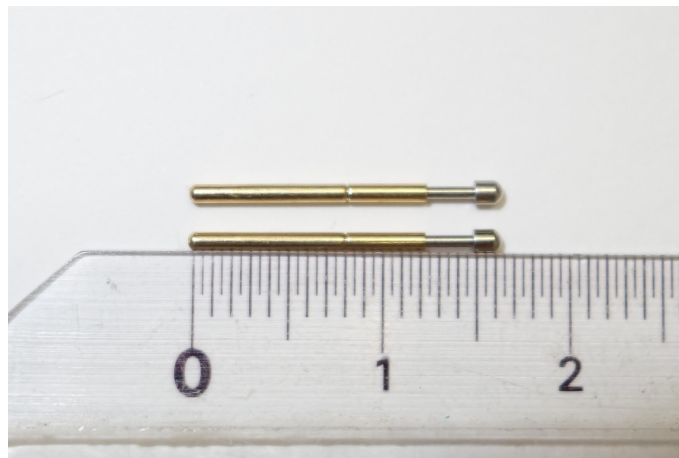


Figure 3.6: Electrodes responsible for making contact with the sensor.

As mentioned before, an acrylic tube of around 20 cm was glued to the center hole

of the flange, allowing the wires to be soldered to the electrodes and to two platinum resistors (Pt100). The other end of the tube is glued a parallelepiped casing which was printed using a 3D printer. This casing has two lids of opposing faces. One of the lids is prepared to receive a GPIB and two coaxial plugs, where the other end of the wires threaded through the tube are soldered. The purpose of the other lid is to grant access the back of the previously mentioned lid, in order to solder the wires to the plugs.

During the design phase, two layouts of the sensor support and the electrode support were developed, as shown in figure 3.7. As such, two cryogenic systems were built, with the only difference being the way the sensor is facing and the way the flange holds the assembly. In order to distinguish them, a name was given to each: Assembly A and Assembly B.



Figure 3.7: Assembly A (bottom) and assembly B (top), with the screen in between.

3.3.1 Assembly A

Assembly A was built out of aluminum and it holds the sensor so that it is facing upwards when the unit is standing, as shown in figure 3.8. Its design has a structure that forces the electrodes in place, so that strain in the solder between the wires and the electrodes can be avoided. Since aluminum is an electrical conductor, it was of the utmost importance that contact between the electrodes and the aluminum structure was avoided. Considering this fact, a plastic cylinder was designed and 3D printed. This cylinder has two holes that hold both electrodes in place and is placed in the electrode support. This support is then fastened between two L-shaped stems, which in turn are being held by two screws against the flange.

The sensor support holds the sensor in a groove of appropriate dimensions, forcing it to be aligned with the electrodes. This support has a hole on each side, so that two screws hold the support in place between the two L-shaped stems while also maintaining contact with the electrode support. This setup was designed to allow an easy sample swap.

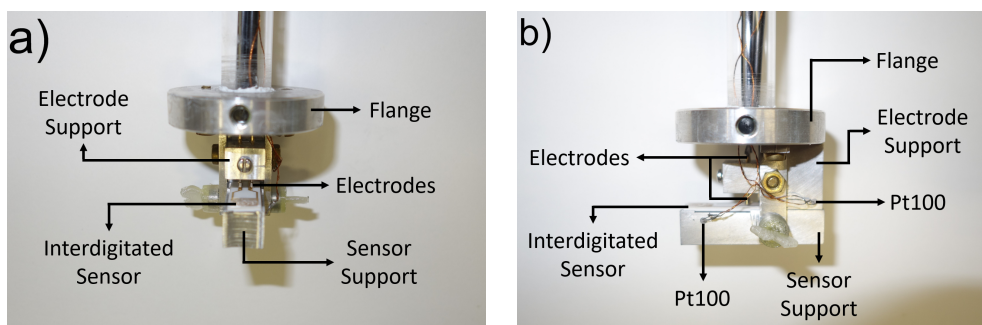


Figure 3.8: Assembly A viewed from a) the front and b) the side.

3.3.2 Assembly B

Contrary to Assembly A, every piece that composes Assembly B was made out of plastic and 3D printed. This was due to the fact that this assembly's pieces had some design traits that were harder to machine, while the 3D printer did not have the same problem.

As shown in figure 3.9, its design has the sensor support connected directly to the flange and a groove which holds the sensor in place. Before the groove, there is a platform, on top of which the structure which holds the electrodes is placed. On its front, the structure has two holes where the electrodes are inserted and around these holes there's an indent to facilitate soldering of the electrodes to the central conductor of a coaxial wires. This structure is held in place against the support with a spring, pressing the structure against the support. Assembly B was designed so that sensors could be swapped by manually lifting the electrode structure, as opposed to Assembly A, where the sensor support has to be removed.

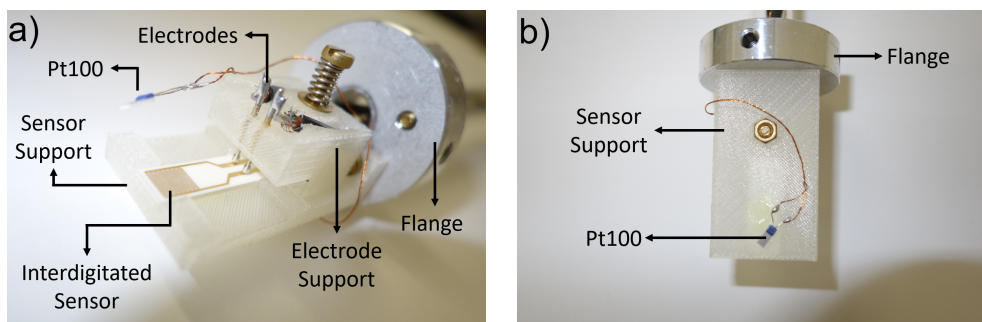


Figure 3.9: Assembly B viewed from a) the side and b) the back.

3.4 Temperature Monitoring

3.4.1 Platinum Resistors: Pt100

The objective of this project was to measure the electrical impedance at specific temperatures, within the 77 to 300 K range. To this end, two Pt100 resistors were used to

measure the temperature at which the sample is. The resistance of platinum resistors is proportional to their temperature and in the case of Pt100, its value is of $100\ \Omega$ at $0\ ^\circ\text{C}$. This project's temperature ranges from liquid nitrogen's to room temperature (around $25\ ^\circ\text{C}$) which translates in a resistance range of around 20 to $110\ \Omega$.

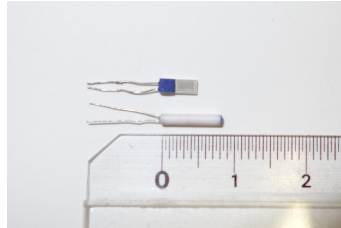


Figure 3.10: Photograph of a Cylindrical Pt100 (bottom) and a thin film Pt100 (top).

Since it was needed to know the temperature near the sample, two Pt100 were used for each cryogenic system. Two cylindrical Pt100 were used for Assembly A and two thin film Pt100 were used for Assembly B. Regarding Assembly A, a hole was made both in the sensor support and in the electrode support, in order to fit in each a cylindrical Pt100. This option was taken so that it was possible to see if there was a thermal equilibrium between both aluminum pieces. As to Assembly B, one thin film Pt100 was glued to the bottom of the structure, right under the sample, while the other was left hanging roughly half a centimeter above the sample. This was chosen so that it was possible to measure if a thermal gradient existed around the sample.

In order to avoid adding the wire's resistance to the Pt100 resistance value, four wires were used with two connecting to each resistor terminal. By wiring it how it is shown in figure 3.11 (a four wire method), it is possible to measure the voltage drop across the Pt100 alone. Knowing the voltage drop and the current it is then possible to calculate the resistance and consequently the temperature.

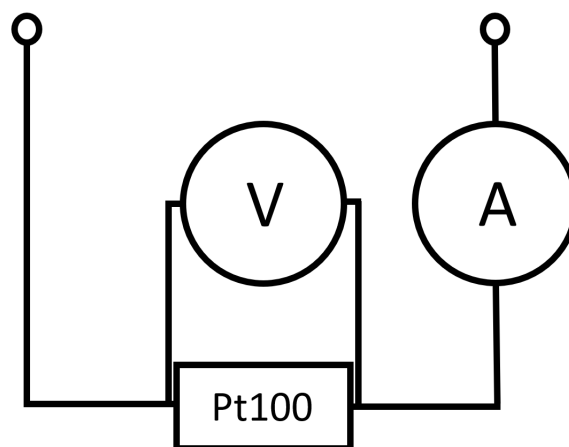


Figure 3.11: Schematic of a four wire method Pt100 wiring.

3.4.2 Analog to Digital Converter MAX31865

The device chosen to measure the Pt100 was MAX31865, shown in figure 3.12. It was chosen due to its ability to measure by applying a constant voltage and obtaining a varying current. Through Ohm's law, by measuring this current it obtains the resistance, indirectly obtaining the temperature value. The resistance and temperature values are obtained digitally, which allows temperature monitoring to be made in a digital format while the circuit is analog.

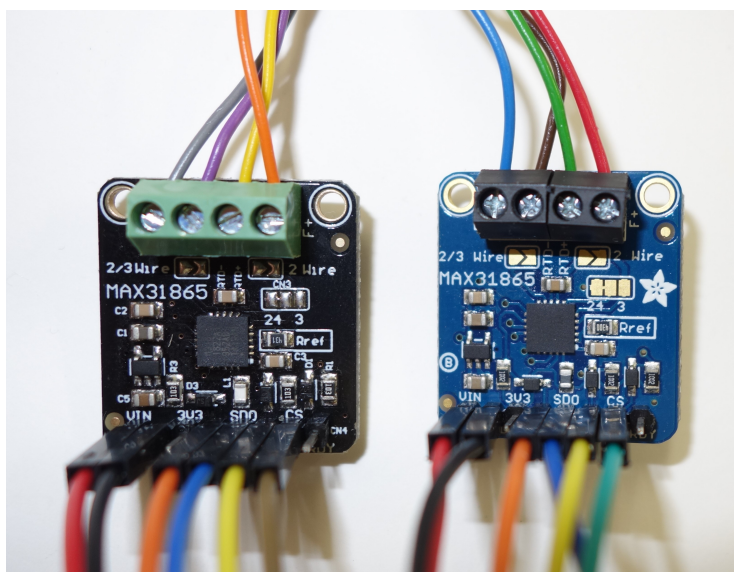


Figure 3.12: A photograph of MAX31865.

MAX31865's other perks include its compatibility with Serial Peripheral Interface (SPI) communication protocol, compatibility with four wire resistors, low price, a total accuracy of 0.5 °C and 15 bit Analog to Digital Converter (ADC) resolution - nearly 0.03 °C resolution. The first page of MAX31865's datasheet is shown in annex II.

In this project two MAX31865 were used, with each one connecting to a Pt100.

3.4.3 Microcontroller Raspberry Pi

Microcontrollers are widely used in engineering projects where automation is required, be it monitoring or control. In this project it was needed to monitor the sample temperature and, to that end, Raspberry Pi 3 B+ was chosen. Despite of Raspberry Pi being a single board computer instead of a microcontroller, it can act as one. It was chosen due to its SPI compatibility, access to Python programming language and its ability to receive a touch screen monitor - which was important for future implementation.

Raspberry Pi is equipped with forty General Purpose Input Output (GPIO) pins, which can be used with a several alternative functions [18]. One set of specific pins was used to communicate using the SPI communication protocol with both MAX31865.

Python was chosen due to its wide range of options for communication, such as Recommended Standard 232 (RS-232) serial communication - which was the one chosen for implementation. To this end, a Universal Serial Bus (USB) to Transistor-Transistor Logic (TTL) Serial Cable was used. On one end, this cable has four TTL pin plugs which were connected to the Raspberry Pi GPIO pins and on the other end it has a USB plug which was connected to the computer, enabling RS-232 serial communication.

The Python code that was written in order to read and send the resistance and corresponding temperature of each of the two Pt100. The loop used for such operation is shown in the flowchart of figure 3.13 and the full code is shown in appendix B. This loop, awaits user input from the computer. Upon receiving something, it reads the values of temperature and resistance and then sends the former, the latter or both back to the computer.

Another advantage provided by the chosen set is the fact that Python already has a MAX31865 library, making it simple to obtain the temperature and resistance values, as can be seen from the lines 36 to 39 from the listing B.1.

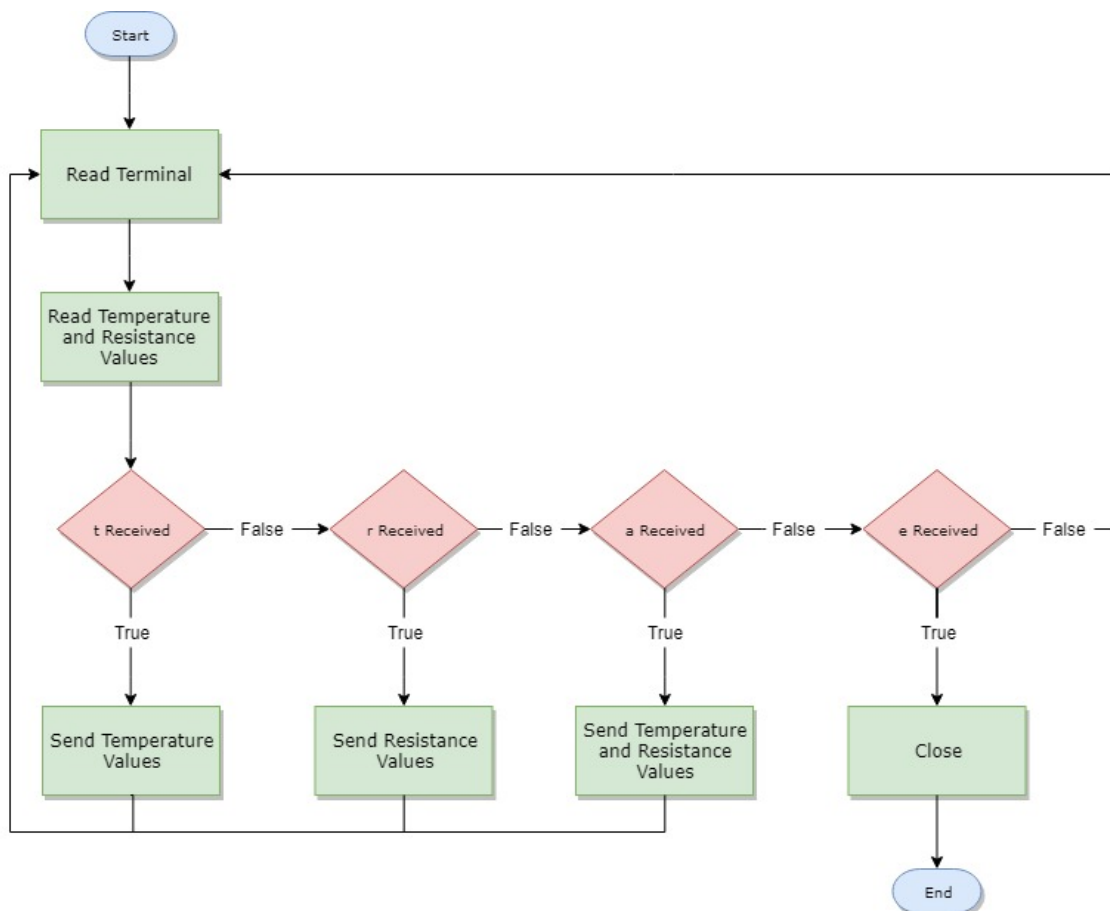


Figure 3.13: Flowchart of the Python *While* algorithm.

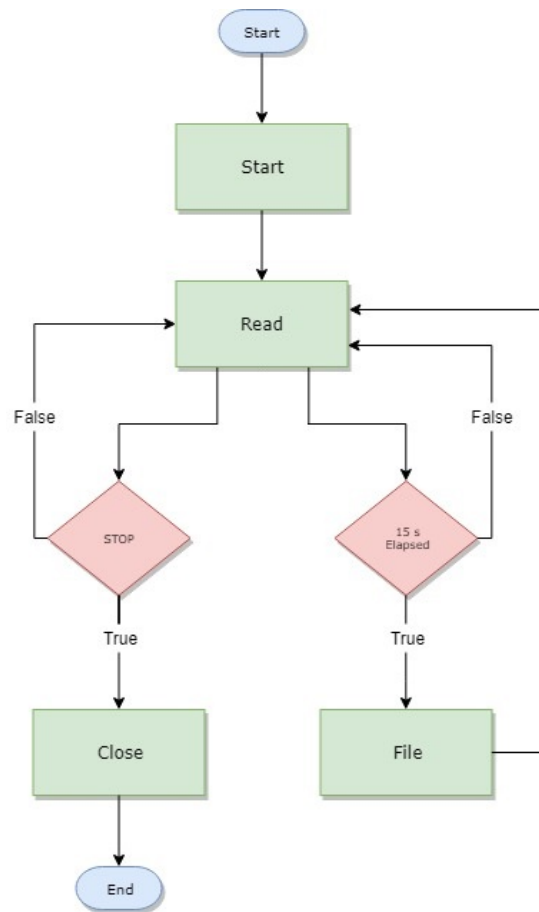


Figure 3.15: Flowchart of the state machine.

3.5.1 Temperature Verification

It is crucial that measures are initiated when the temperature of the sample is at each of the values defined by the user. Hence, it is of the utmost importance that the algorithm decides when to start measuring at the right temperature.

In the state Read of the state machine, the Raspberry Pi is contacted, which in turn sends the temperature values. The program has a mechanism to minimize the effect of fluctuation in the temperature measurement. This mechanism is that the last ten values obtained from average of the two temperature values received are stored in a ten-slot array. The average of this array is then compared with the value stored in the first index of the array generated by the values in the temperature table of figure 3.14, for the purpose of minimizing the effects of temperature oscillation. With every new measurement this comparison is repeated. If the result of this comparison is true, the signal for a measurement is sent to the impedance spectrometer, as will be explained in subsection 3.5.2. As shown in the flowchart in figure 3.16, this process is repeated for the following index until it runs through all the indexes of the table array.

There are two switches present in the control panel shown in figure 3.18 that affect when measurements begin. The first is the *Ready to Measure* switch which needs to be

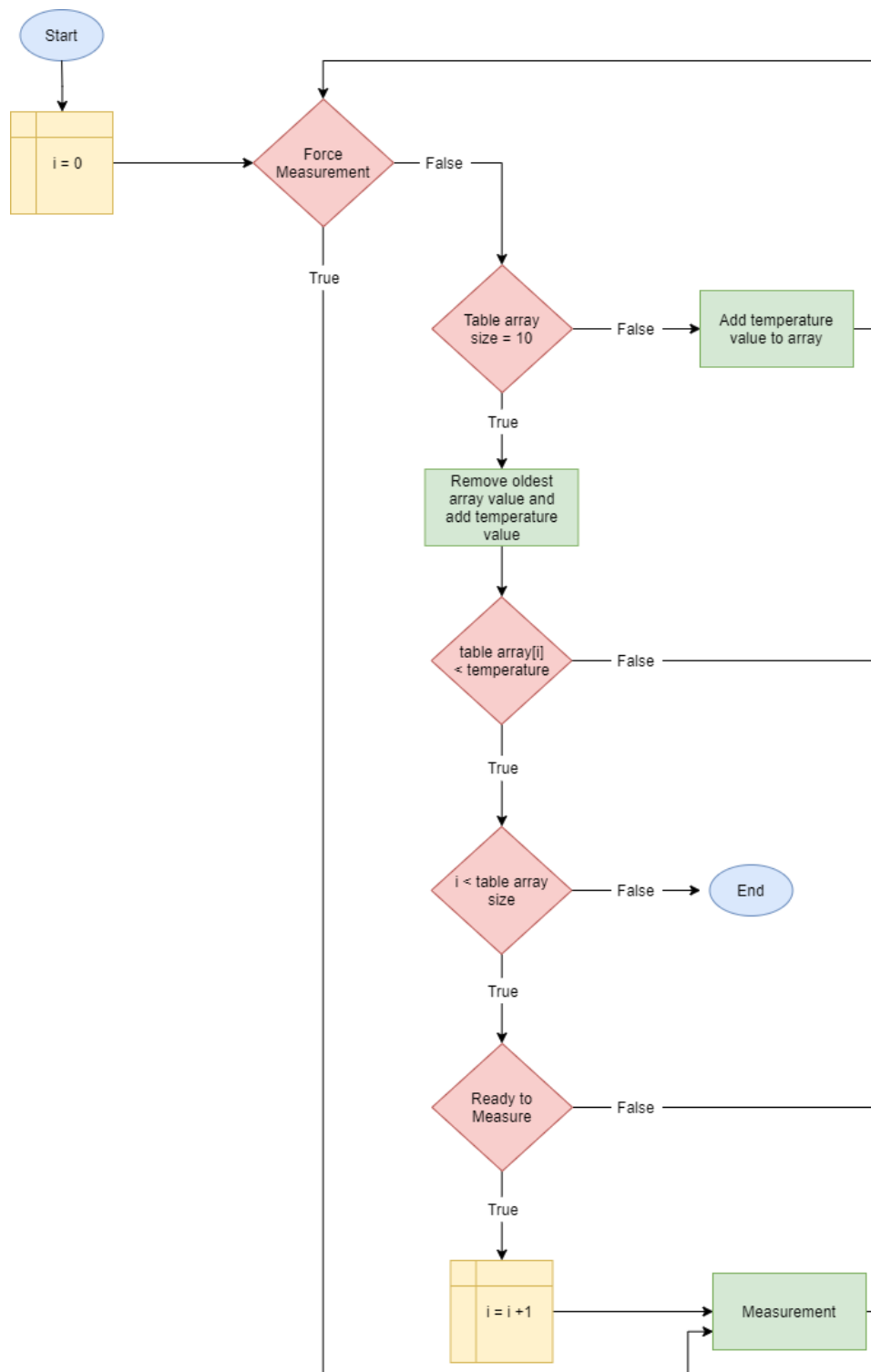


Figure 3.16: Flowchart of the temperature monitoring algorithm.

turned on so that the signal to the impedance spectrometer can be sent. And the second is the *Force Measurement* switch which can force a measure to occur, without affecting the position of the table array.

3.5.2 1260A Interaction and Data Generation

After the measurement signal is given, LabVIEW™ communicates with 1260A with the provided virtual instruments (VIs). Each VI has an effect, from measurement configuration to multiple measure ways.

The VIs were selected according to the objective at hand, as shown in table 3.1. The first couple of VIs configure the generator voltage amplitude and bias (25 mV and 0 V by default, respectively) and set the GPIB to All. The second couple of VIs configure the sweep, which was the chosen way to measure the impedance over the desired frequency range as opposed to the option of running multiple single frequency measurements. These VIs configure the sweep direction (if it starts from the lowest frequency value and ends on the highest or vice-versa, with the former by default), the sweep type (logarithmic by default), the number of points per sweep (31 points by default) and the minimum and maximum frequency values for the sweep (1 Hz and 1 MHz by default, respectively). The last configuration VI configures the display, which will configure the equivalent circuit that is seen by the 1260 model (since there are no biologic elements that are inductive, the default is parallel RC circuit) and what variables are output (with the impedance magnitude and phase as well as the frequency at which both were measured as defaults).

Table 3.1: Configuration VIs, with their variables and respective default values.

VI	Variable	Default Value
Configure Generator	Voltage Amplitude	25 mV
	Voltage Bias	0 V
Configure Sweep	Sweep Direction	Up
	Sweep Type	log
	Points per Sweep	31
	Minimum Frequency	1 Hz
	Maximum Frequency	10^6 Hz
Configure Display	Circuit	Parallel RC
	Result Type	$ Z , \theta$

After the configuration mentioned in the previous paragraph, the VI for *Read Multiple* is run, outputting the frequency and the impedance magnitude and phase as one-dimensional arrays. These arrays are ordered so that the first to last positions correspond to the first to last measurements. The rest of the data is derived from these arrays through equations 2.4 to 2.8.

Afterwards, the algorithm takes all these arrays and builds a two-dimensional array,

along with a temperature array made out of the average of the temperature obtained of each Pt100 and an array composed of a single number, starting with 1 and having an increment of one for each sweep made. Finally, this is written into a spreadsheet that can be accessed with an appropriate software. With each sweep, another two-dimensional array is appended to the bottom of the previous one. By the end of the experiment, a spreadsheet with all data is obtained with each column corresponding to each of the arrays and each line corresponding to each measurement, as shown in figure 3.17. For each sweep, the frequency increases with each line with the rest of the elements of the line corresponding to the values obtained at said frequency. After the last frequency comes the first frequency of the following sweep.

	A	B	C	D	E	F	G	H	I	J	K
1	f/Hz	w/(rad/s)	Z /Ohm	Z'/Ohm	Z''/Ohm	Phase	epsilon'	epsilon''	Loss Tg	T/K	n
2	1	6.283	1.2E+08	7.7E+07	-8.9E+07	49.252	-116.004	99.948	0.862	200.195	1
3	1.585	9.958	5E+07	3.2E+07	-3.8E+07	50.559	-175.785	144.602	0.823	200.195	1
4	2.512	15.783	6.3E+07	-5.8E+07	-2.4E+07	156.99	-44.661	-105.163	-2.355	200.195	1
5	3.981	25.014	4.7E+08	-4.1E+08	2.4E+08	209.79	4.738	-8.277	1.747	200.195	1
6	6.31	39.644	1.1E+08	9.3E+07	-6.6E+07	35.234	-14.403	20.392	1.416	200.195	1
7	10	62.832	1.8E+08	6.5E+07	-1.6E+08	68.323	-9.457	3.759	0.397	200.195	1
8	15.849	99.582	2.4E+08	1.3E+08	-2E+08	57.422	-3.934	2.514	0.639	200.195	1
9	25.119	157.827	1.8E+08	-1.6E+08	-6.6E+07	158.09	-1.503	-3.737	-2.486	200.195	1
10	39.811	250.139	1.2E+08	-1E+08	-6.8E+07	147.02	-1.979	-3.05	-1.541	200.195	1
11	63.096	396.444	1.7E+08	-1.6E+08	5.8E+07	200.48	0.6	-1.605	2.677	200.195	1
12	100	628.321	1.1E+08	-7.4E+07	7.8E+07	226.42	1.212	-1.153	0.952	200.195	1
13	158.49	995.823	8.3E+07	-2.9E+07	7.8E+07	249.79	1.277	-0.47	0.368	200.195	1
14	251.19	1578.27	8.8E+07	-367574	8.8E+07	269.76	0.815	-0.003	0.004	200.195	1
15	398.11	2501.4	5.6E+07	8106351	5.5E+07	278.36	0.801	0.118	-0.147	200.195	1
16	630.962	3964.45	4.3E+07	1.8E+07	3.8E+07	295.25	0.606	0.286	-0.472	200.195	1
17	1000.01	6283.23	3.2E+07	7481594	3.1E+07	283.39	0.541	0.129	-0.238	200.195	1
18	1584.91	9958.25	1.6E+07	-945943	1.6E+07	266.67	0.695	-0.04	0.058	200.195	1
19	2511.91	15782.8	1.1E+07	847463	1.1E+07	274.44	0.652	0.051	-0.078	200.195	1
20	3981.11	25014	6905300	-372227	6895260	266.91	0.653	-0.035	0.054	200.195	1
21	6309.63	39644.6	4608900	121451	4607300	271.51	0.618	0.016	-0.026	200.195	1

Figure 3.17: Example of the resulting spreadsheet.

3.5.3 Control Panel

The control panel is the means through which the user interacts with the experiment. As can be seen in figure 3.18, the control panel has two graphs. The one on the left of the figure is the temperature plot, where the temperature is shown as a function of time, from the time the program starts. While the other is the impedance plot, where for the last measurement made, the magnitude of impedance is shown as a function of frequency. The former was introduced so that the user can see how the temperature varies throughout the experiment and the latter so that the user can see how the measurements progress and so that anomalies can be detected.

On the top left corner of figure 3.18 it is possible to see that the elements mentioned previously are on a tab named *Monitoring*. *Definitions* is the name of the second tab, expanded in figure 3.19, which contains the ports corresponding to the Raspberry Pi and 1260A connections, as well as the values that are used as inputs for the configurations mentioned in the subsection 3.5.2.

3.6 Circuits and Connectors

In order to test the software, test circuits were used. A homemade circuit composed of a $100\text{ k}\Omega$ resistor in series with a 10 nF capacitor, in parallel with a 100 pF capacitor was made on a printed circuit board, as shown in figure 3.20. This circuit is composed of two copper tracks, one for each electrode, allowing its impedance measurement.

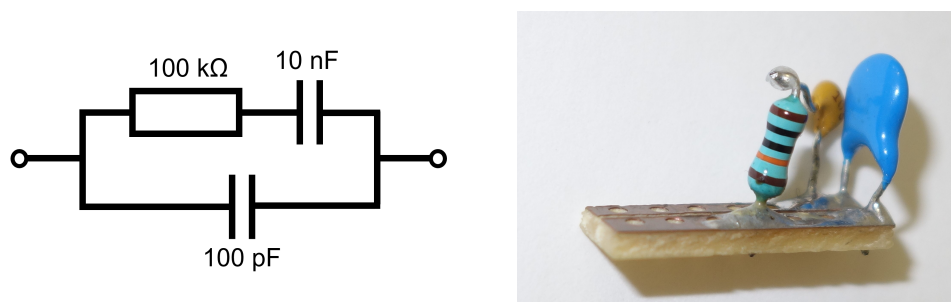


Figure 3.20: a) Schematic and b) photograph of the homemade circuit.

Additionally, the circuit from AMETEK SI[®] was also used, as shown in figure 3.21, of which its *Test Circuit* is equivalent to that of figure 3.20 a).

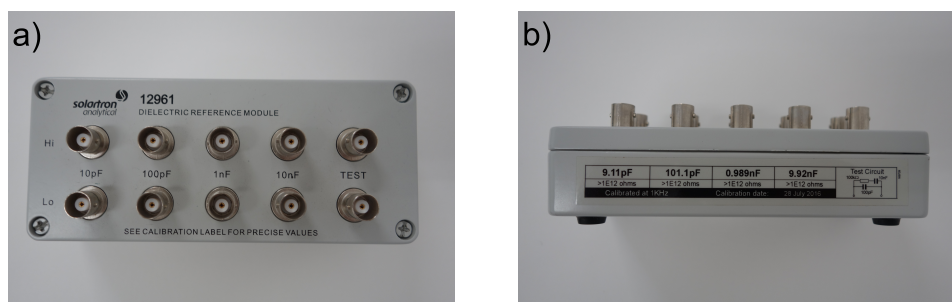


Figure 3.21: AMETEK SI[®] set of circuits a) from above and b) from the front.

The blue connector shown in figure 3.22 has one of its ends prepared to receive and hold sensors with its two electrodes, splitting into two coaxial cables with male coaxial plugs at their ends. The distance between the two electrodes is equal to that of the sensor tracks, as shown in figure 3.22 b), making it appropriate to receive and hold the sensor in place, while making contact with its electrodes, enabling measurements.

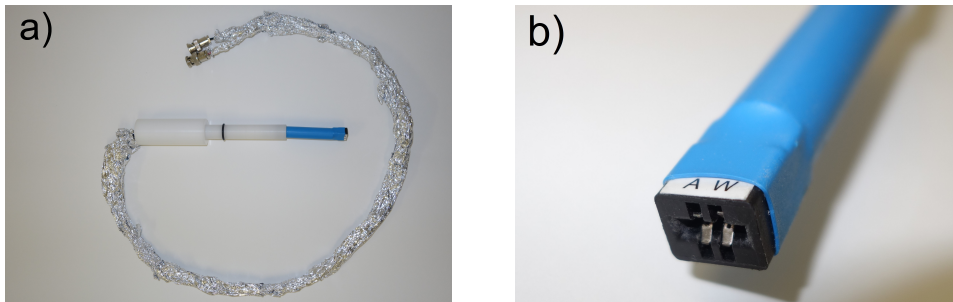


Figure 3.22: Blue connector a) as a whole and b) its sensor slit.

RESULTS AND DISCUSSION

It is important to note that before this project began, the established impedance spectrometer was comprised of 1260A and 1296A, with the interface software SMaRT along with the blue connector mentioned in sections 3.6.

The aim of each step detailed in each of this chapter's sections is to compare it to what was established in order to validate what was being tested - with exception to the experiment detailed in sections 4.6 and 4.7. Throughout this chapter, the detailed experiments were performed at room temperature, around 300 K, and the defined parameters were 25 mV voltage amplitude and 0 V bias voltage, with thirty-one frequency points between 1 and 10^6 Hz, unless the contrary is specified.

Whenever a cryogenic system is used in a measurement detailed in this chapter, the screen was attached to the flange, shielding the sample. Then the cryogenic cell was placed inside the dewar (a commercial thermal cup) and liquid nitrogen was poured into it, until the desired temperature was reached.

4.1 Circuit and Assembly Validation

In order to test Assembly B, the circuit would have to be put directly on the assembly sensor support, under the two electrodes, like an interdigitated sensor. Since this was not possible with the circuit provided by AMETEK SI[®], the homemade circuit described in section 3.6 was built. Thus the first experiment performed had the aim of determining if the homemade circuit described in section 3.6 could be used as a reference circuit for the following experiments. Another aim of this experiment was to verify if the measurements done with the assembly would be similar to those done with the connector shown in figure 3.22.

Three experimental setups were tested with the Impedance Analyzer 1260A along

with 1296A, using SMaRT software. The results obtained from each measurement are the average of three frequency sweeps. Firstly, the circuit provided by AMETEK SI[®] was directly connected to 1260A and measured. Afterwards, the homemade circuit was measured using the blue connector, which was connected to 1260A and measured. Finally, the homemade circuit was measured using Assembly B, which was also connected to 1260A and measured. The resulting plots are shown in figures 4.1 and 4.2.

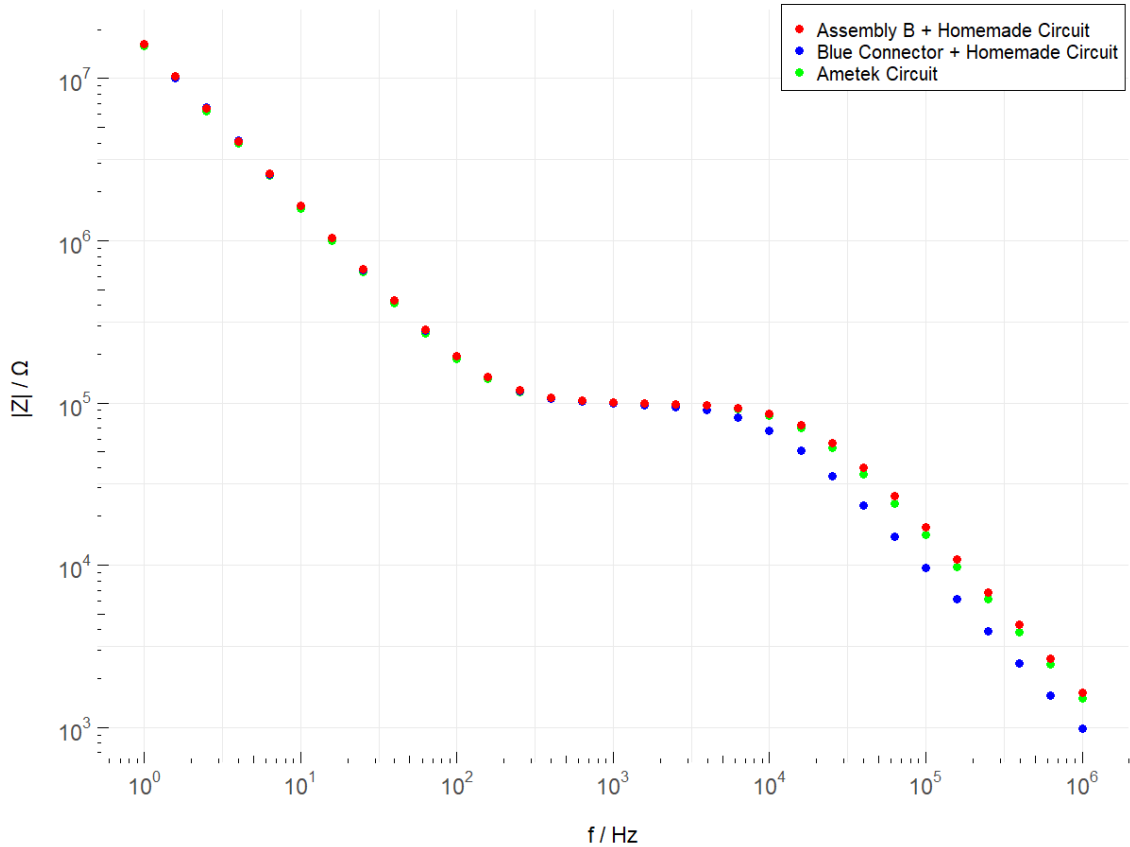


Figure 4.1: Bode plot of the impedance modulus as a function of frequency.

By analyzing the plots shown in figure 4.1, it is possible to see that for frequencies lower than 10^3 Hz the plots are indistinguishable. However, for frequencies above 10^4 Hz, the impedance magnitude values from the blue connector with the built circuit diverge from the remaining two, while only a slight difference can be seen between the other two.

The same type of discrepancies occur with the phase angle, as can be seen in the plot shown in figure 4.2, for frequencies between 1.5×10^2 and 10^5 Hz, in spite of having differing phase values all around, the phase values obtained from the blue connector with the homemade circuit are significantly lower than the remaining two. However, at frequencies greater than 1.2×10^5 Hz the opposite happens, with the ones from the Assembly B with the built circuit increase proportionally to the frequency, unlike the remaining two.

As explained in subsection 2.4.1, the impedance measured at higher frequencies is

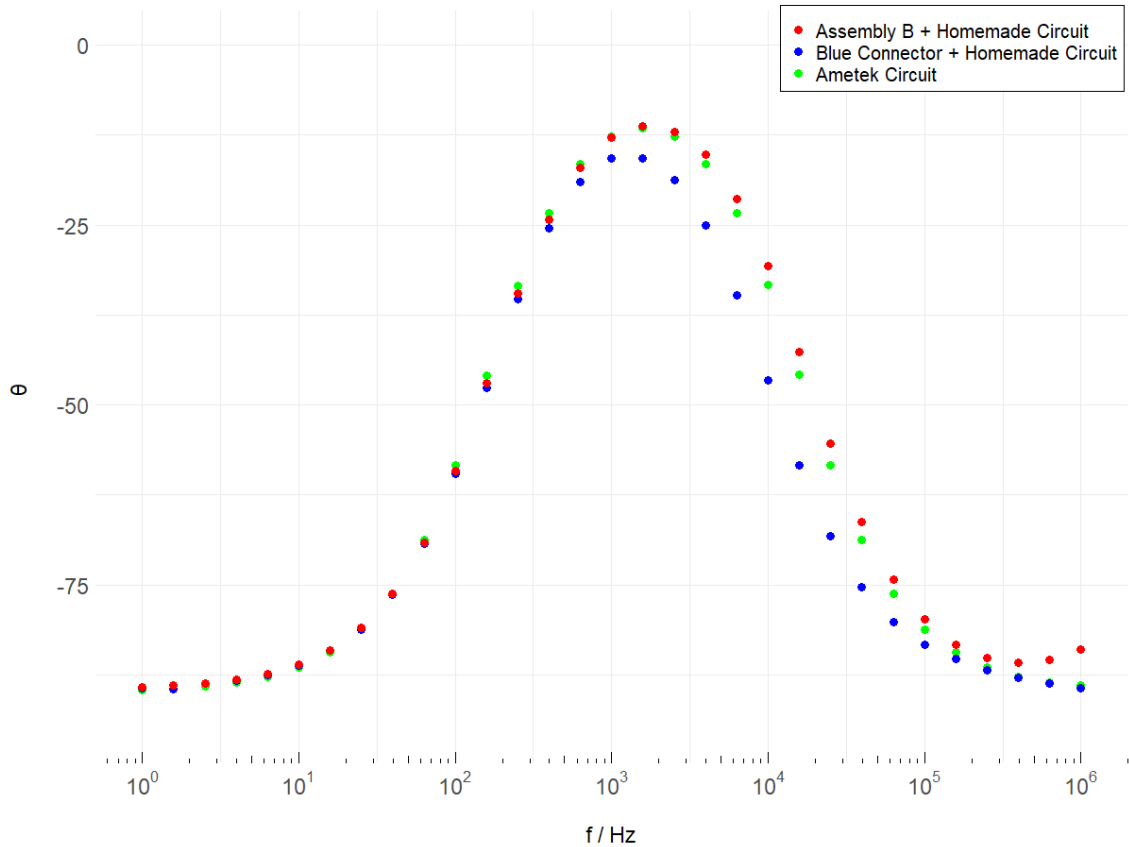


Figure 4.2: Bode plot of the impedance phase as a function of frequency.

due to the parallel capacitor. Additionally, equation 2.9 shows that higher capacitance translates into a lower electric impedance. Thus, these results might indicate that there is a parasitic capacitance associated with the blue connector, which is corroborated by the consistently lower in the impedance magnitude values at high frequencies.

Thus Assembly B could replace the blue connector as the intermediate between 1260A and the sensor, since the results obtained with Assembly B were almost identical to the ones obtained with the circuit provided by AMETEK SI[®], while the ones obtained with the blue connector were not. This and the fact that consecutively inserting and removing sensors from the blue connector would deteriorate the gold tracks, reducing the contact area between sensor and electrodes and altering the results, led to the abandonment of the blue connector. Additionally, these results show that the circuit described in section 3.6 could be used as a reference circuit for the following experiments.

4.2 User Software Validation

In order to test the developed LabVIEW[™] program, the temperature dependence of the electrical impedance homemade circuit was measured, along the temperature range of 85 to 280 K - specifically from 85 to 150 K with a step of 5 K and from there to 280 K with a step of 10 K, totaling twenty-seven different temperatures.

The homemade circuit was placed on the sensor support of Assembly B and the cooling process was performed as described in the beginning of chapter 4, until the temperature of 85 K was reached.

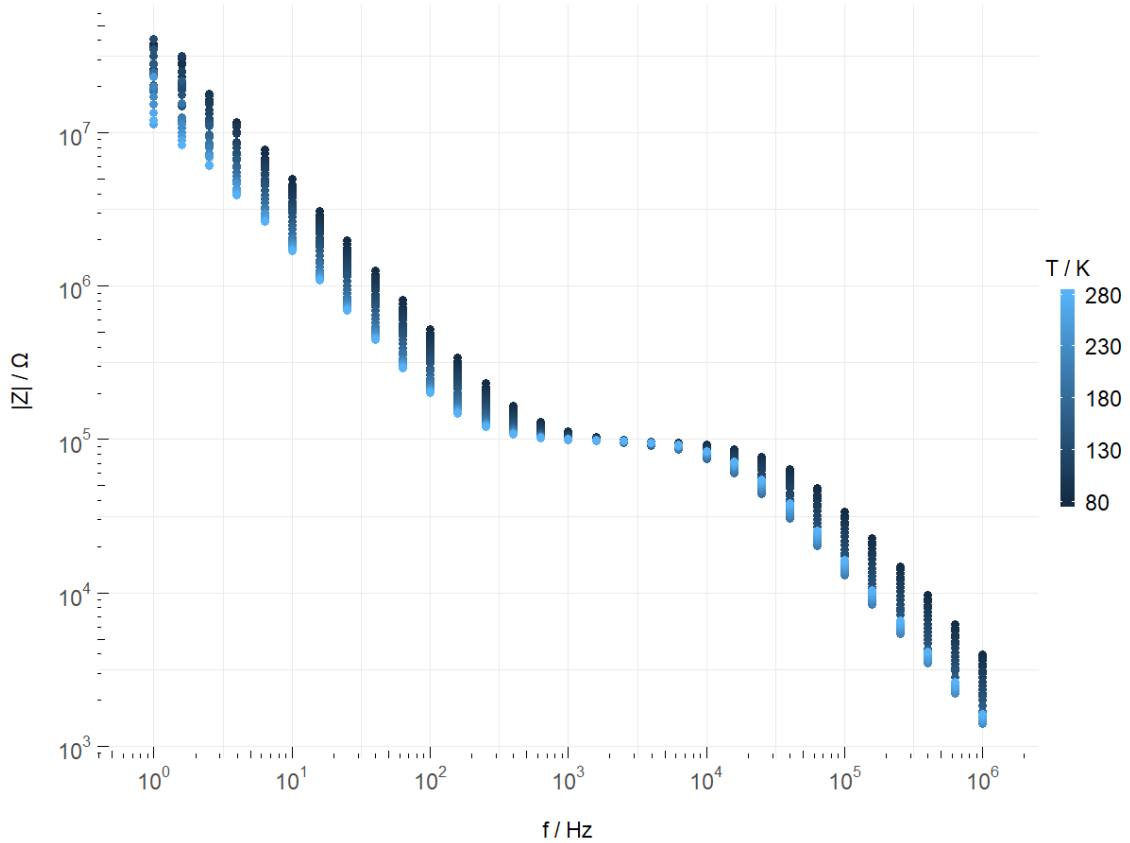


Figure 4.3: Bode plots of impedance modulus as a function of frequency, at several temperatures, of the homemade circuit.

By analyzing figures 4.3 and 4.4, one can see that the general shape of the plots is the same as shown in figures 4.1 and 4.2, respectively. It should be noted that for figure 4.4, the points taken at frequencies lower than 13 Hz were cut from the plot, because they do not correspond to the sample's correct impedance values. This occurs due to the fact that 1260A's impedance limit is somewhere near $10^7 \Omega$ and samples with values above this limit will cause 1260A to read erratically. Since the samples in this project only surpass this limit at lower frequencies, the cuts are made around 10 Hz. This was done in order to reduce clutter and facilitate the extraction of information.

The temperature variation from lower to higher temperatures, can be seen due to the color variation from dark to light blue, respectively. As can be seen in the Bode plot of figure 4.3, the increase in temperature seems to cause a decrease in the impedance of the circuit where the plot has a slope different from zero. These results seem to indicate that the capacitance of the capacitors used to build this circuit increases with the temperature - as can be seen by the decrease in the impedance. On the other hand, the impedance of the resistor does not vary with the temperature, as can be seen in the middle region

of the plot, where the impedance is equal to that of the circuit's resistor of $10^5 \Omega$. The same effect can be seen on the Bode plot of figure 4.4, due to the shift in the peak as temperature increases.

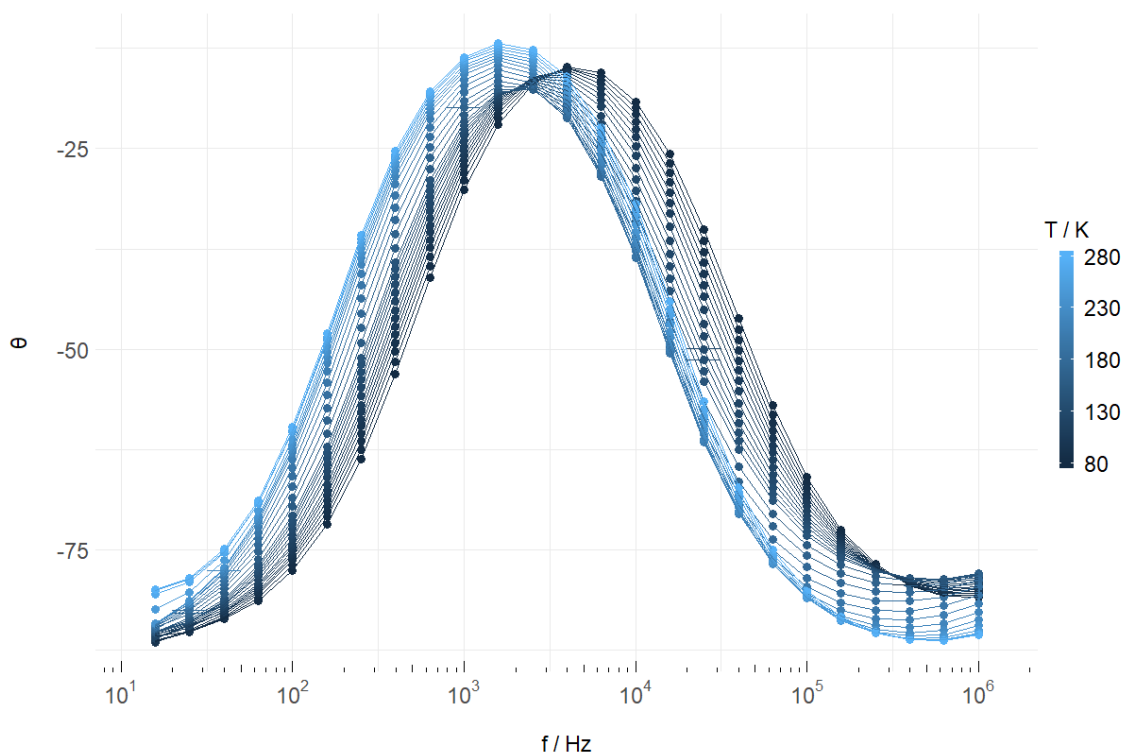


Figure 4.4: Bode plots of impedance phase as a function of frequency, at several temperatures, of the homemade circuit. The points taken at frequencies lower than 13 Hz are not in the plot.

4.3 Bare Sensors

With the intent of distinguishing whether the measurements reflect the presence of either DNA or DNA+AuNPs the sensor and not just the sensor itself, the response of a bare sensor to an IS had to be known. In light of this, Assembly A and Assembly B were used to measure an interdigitated sensor without a sample (i.e. a bare sensor), using the developed LabVIEWTM program with 1260A. The temperature range of this experiment was from 77 to 290 K.

A bare sensor was placed on the sensor support of Assembly A and the cooling process was performed as described in the beginning of chapter 4, until the temperature of 77 K was reached. After all measurements were taken, the same process was repeated for Assembly B.

The Bode plots shown in figures 4.5 and 4.6 were obtained by measuring a bare sensor with Assembly A and Assembly B, respectively. By analyzing both plots, it is possible to see that the data shows a linear pattern independent of the temperature, similar to that of

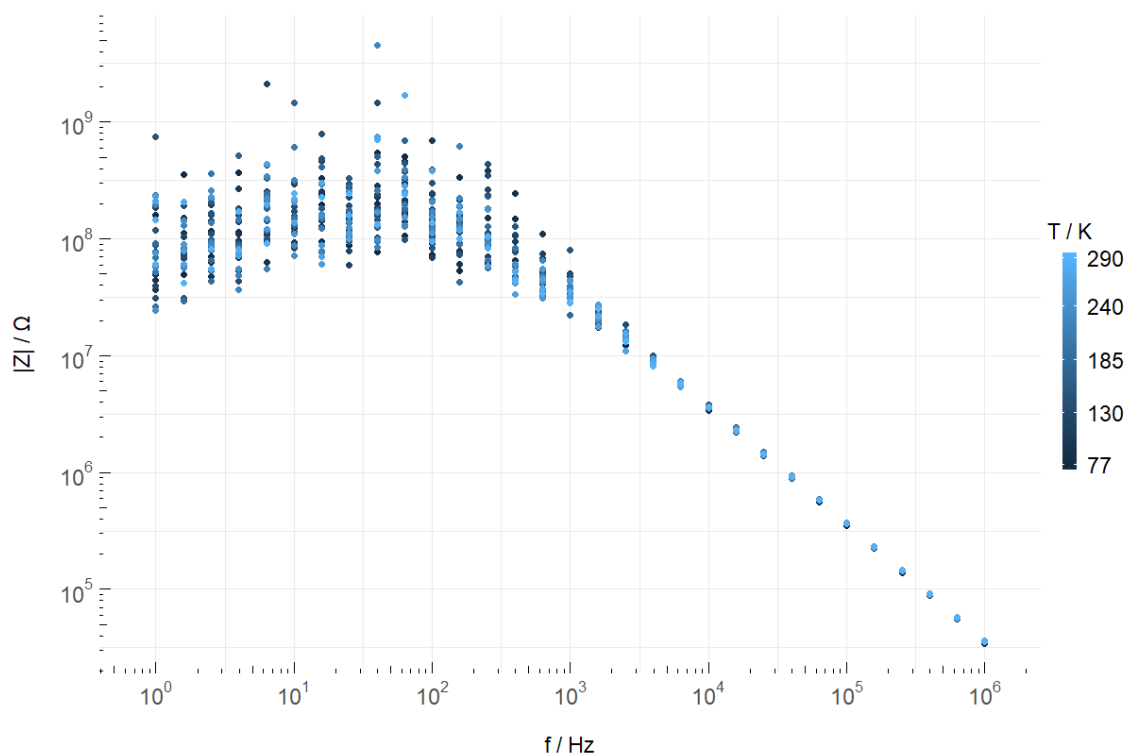


Figure 4.5: Bode plot of the impedance modulus as a function of frequency and temperature, of a bare sensor, measured with Assembly A.

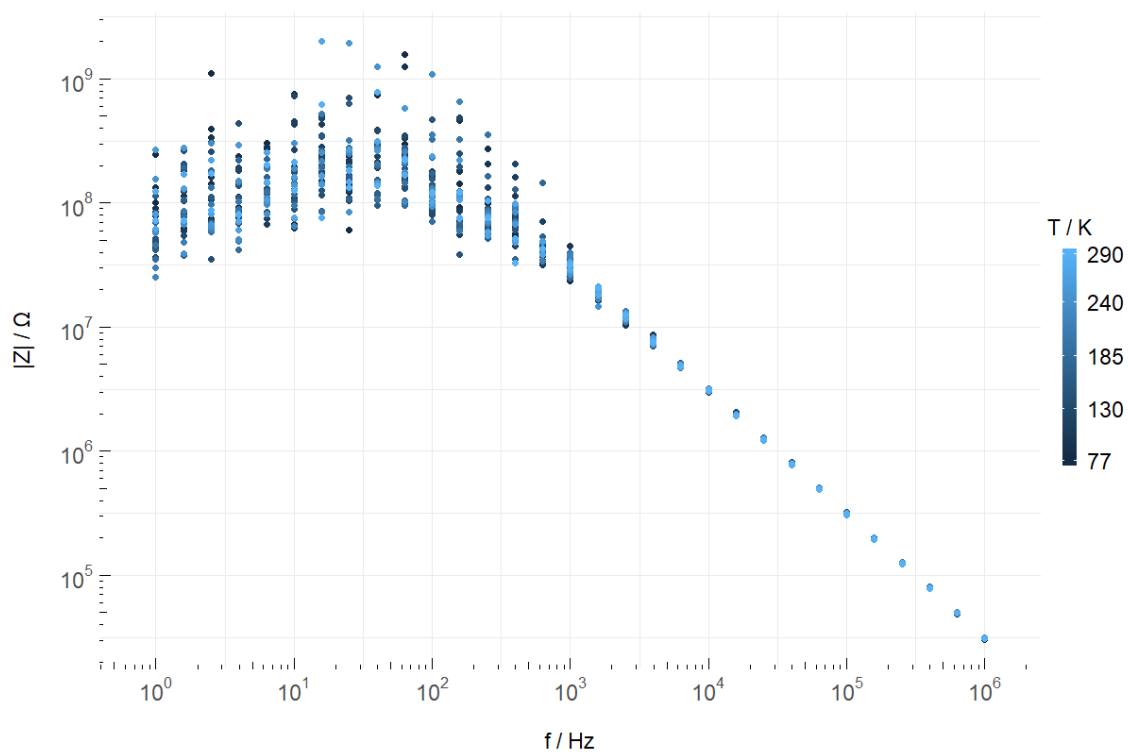


Figure 4.6: Bode plot of the impedance modulus as a function of frequency and temperature, of a bare sensor, measured with Assembly B.

a capacitor as shown in figure 2.5 a), up to around $10^7 \Omega$. From this point on, it loses this pattern while seeming to gain some random distribution. This effect will be discussed in section 4.5.

The Bode plot shown in figure 4.7 is both plots of figures 4.5 and 4.6 in one with no regard for temperatures, so that it is possible to compare differences between both assemblies. With regards to the linear pattern shown up until $10^7 \Omega$, the constant difference between the two assemblies might indicate that there is a parasitic capacitance associated with Assembly B, which is corroborated by the consistently lower in the impedance magnitude values. This parasitic capacitance has a value of 0.9 pF.

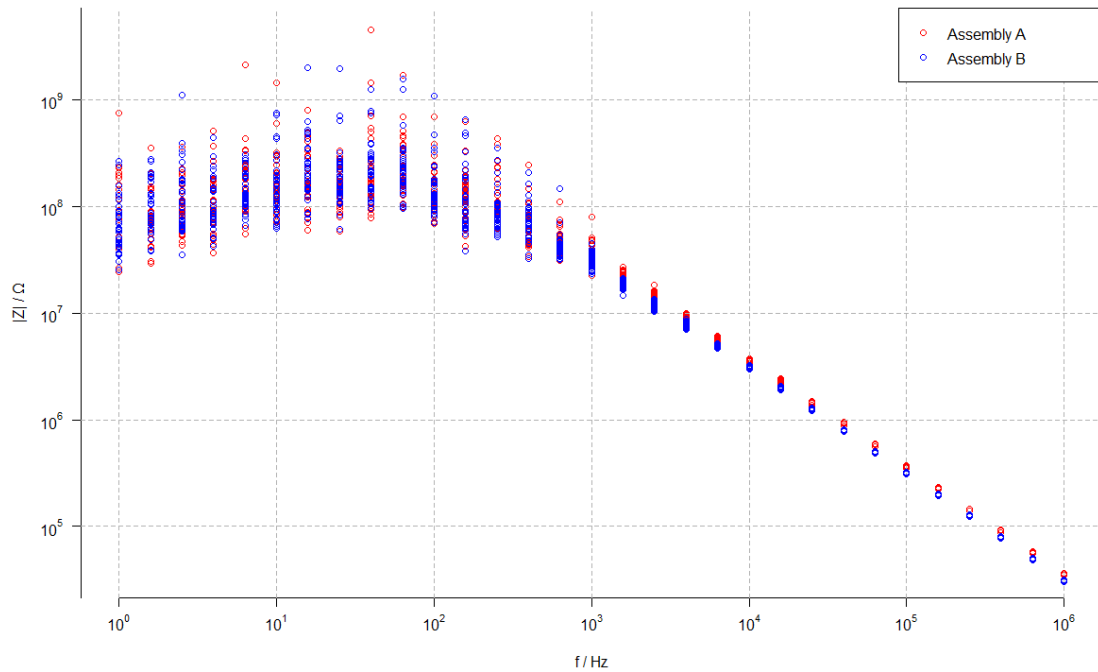


Figure 4.7: Bode plot of the impedance modulus as a function of frequency, at several temperatures, of a bare sensor, measured with Assembly A (red) and Assembly B (blue).

4.4 Temperature Variation over Time

In this experiment the temperature variation over time was measured for Assembly A and Assembly B.

The cooling process was performed as described in the beginning of chapter 4, until the temperature of 77 K was reached, for both cryogenic systems. Since it was not possible to measure the amount of liquid nitrogen poured each time, the cooling process can be slightly different from Assembly A to Assembly B. After the reaching 77 K, a cloth was wrapped around the acrylic tube, on the top of the dewar to isolate it from water. With the surrounding air serving as a heat source, the assemblies were left to heat for 12 h.

The temperature variation over time of Assembly A can be seen in figure 4.8. Each of the two plots, red and blue, correspond to a Pt100, with the red corresponding to the one placed in the hole directly underneath the area where the sample is placed and the blue corresponding to the one placed inside the hole in the electrode support. The temperature drop seen in $t < 1$ h is due to the cooling of the system, followed by a flat period where the temperature is equal to 77 K, while there is still liquid nitrogen in contact with the screen. Slightly before the 2 h mark, the temperature rose again, remaining steady for nearly another hour. At $t \approx 3$ h, the last drop of liquid nitrogen evaporated and the temperature starts to increase continuously at a higher rate. As the temperature of the system increases, the temperature difference with the outside air decreases, which slows the exchange of thermal energy resulting up to the point where the whole system reaches room temperature.

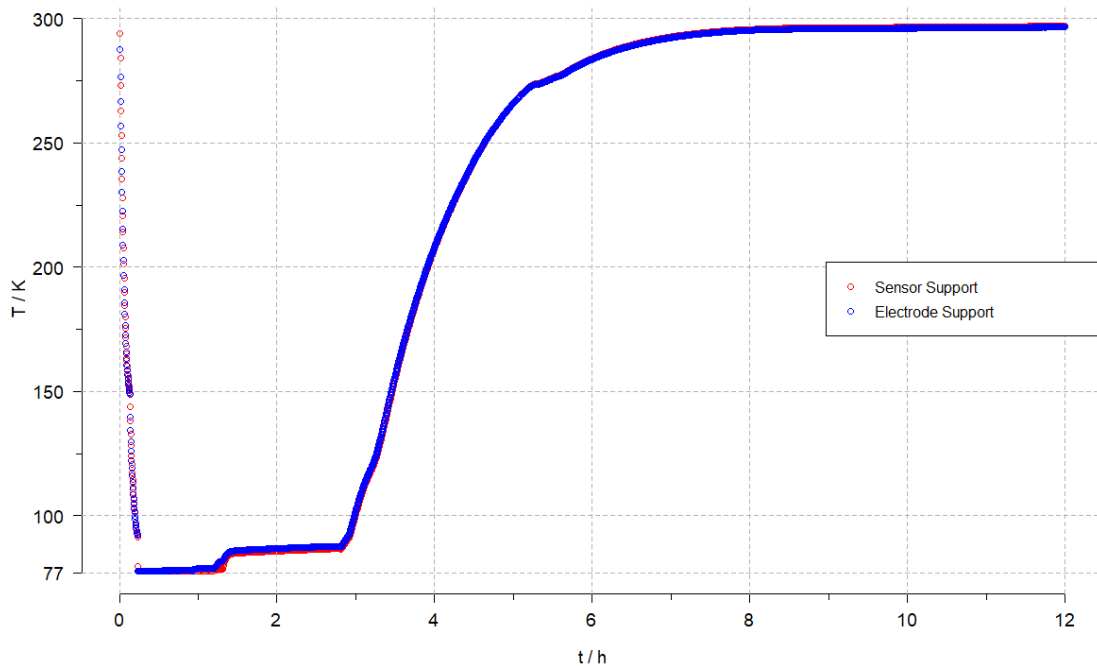


Figure 4.8: Temperature variation as a function of time, for the Pt100 placed inside the hole of the sensor support (red) and the Pt100 placed inside the hole of the electrode support (blue), of Assembly A.

The temperature variation over time of Assembly B can be seen in figure 4.9. As before, each of the two plots, red and blue, correspond to a Pt100, with the red corresponding to the one which was glued under the sensor support and the blue to the one left hanging, measuring the air temperature. The rest of the process is equivalent to that of Assembly A described previously.

In order to see how similar the warming process between assemblies is, the results for each assembly were plotted as shown in figure 4.10. The values for this plot were

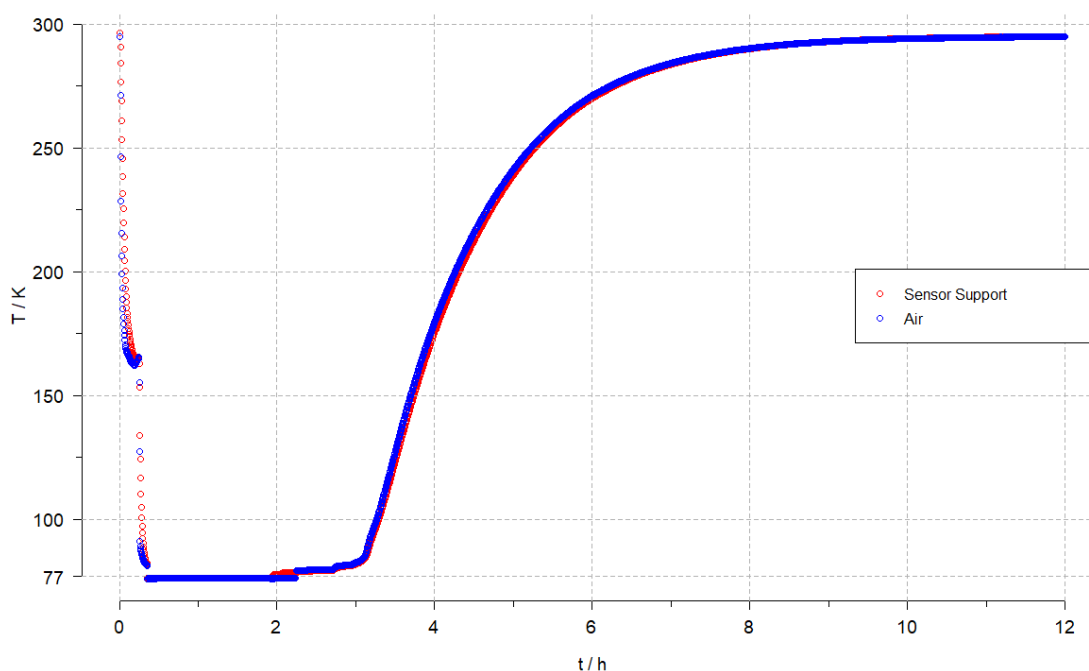


Figure 4.9: Temperature variation as a function of time, for the Pt100 glued beneath the sensor support (red) and the Pt100 hanging in the air (blue), of Assembly B.

obtained through a mean of the two temperature values for each assembly. Visiting for a fair comparison, the plotted values were selected to be equal or above 90 K and the total duration of 8 h. The difference in temperature of the horizontal regions of the plots might be due to the difference in the distance of the bottom of the screen to the bottom of the dewar, which also explains the difference in duration. Specifically, when the distance is greater, the screen loses contact with the liquid nitrogen sooner, which causes the nitrogen to last longer. For instance, the distance for Assembly A to the bottom of the dewar might have been greater than that of Assembly B, as can be seen for the duration of time before getting to the "shoulder" region.

It is also possible to note that for Assembly A, higher temperatures are achieved faster than Assembly B. This was expected since the parts that compose Assembly A are mostly made out of aluminum which is a better thermal conductor than plastic. However, the difference is smaller than expected, having little impact on the amount of time taken. This might be due to the fact that, when submerged in liquid nitrogen, the copper screen also acts like a cold source to the sample by cooling the amount of air inside the screen.

The difference between the temperature values recorded by each Pt100 as a function of the average temperature of the two Pt100 is shown in figure 4.11, with regards to the warming process only. For Assembly A, the values were obtained by subtracting the temperature recorded by the Pt100 placed inside the sensor support's hole from that of the one inside of the electrode support's hole. For Assembly B, the values were obtained

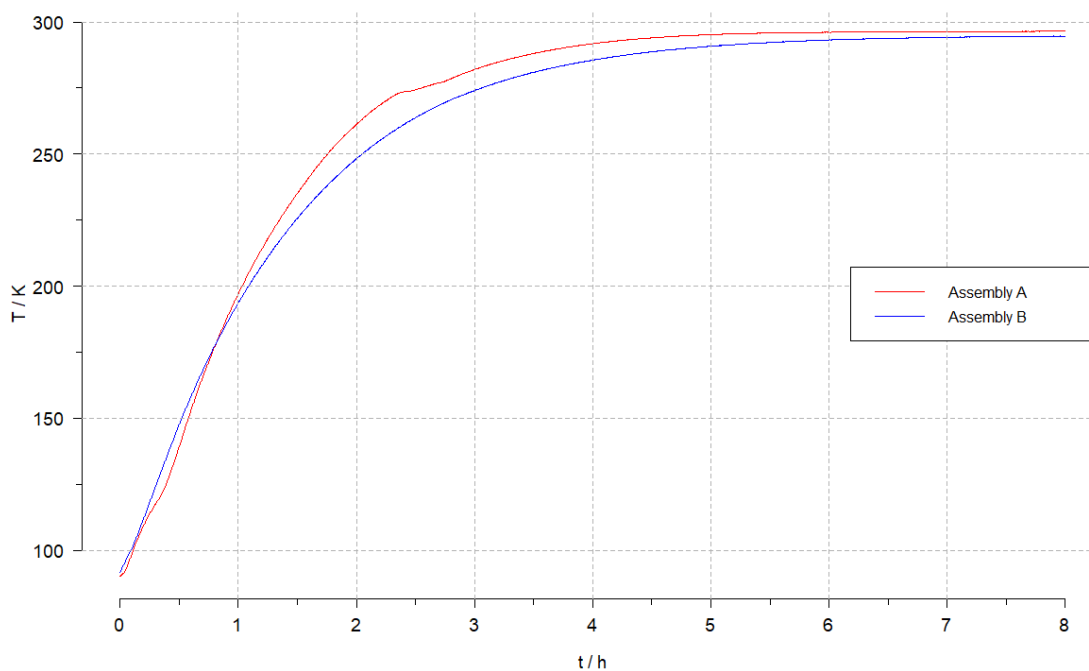


Figure 4.10: Temperature variation as a function of time, for Assembly A (red) and Assembly B (blue).

by subtracting the temperature recorded by the Pt100 which was left hanging from the one which was glued to the sensor support. By analyzing the plot, it is possible to see that the results obtained with respect to Assembly A are generally closer to zero than those of Assembly B. This was expected due to the fact that both Pt100 are placed inside aluminum, which is a good thermal conductor. The results obtained for Assembly B were also expected due to the fact that, when warming up, the gas around the sample is colder than the structure. This happens because, despite not being a good thermal conductor, the plastic that composes the sensor support is a better than the air.

The derivative of the average temperature with respect to time as a function of the average temperature for each assembly is shown in figure 4.12, with regards to the heating process only. As will be shown in section 4.7, the samples were only detected after the 250 K threshold. This means that the most relevant region of the plot figure 4.12 is from 250 to 290 K. In this range, the temperature rises less than a Kelvin per minute. Since the measurements take around 30 s, there is an increase of less than half a Kelvin during measurement. This is important considering that ideally the temperature would not rise while a measurement is taking place.

4.4. TEMPERATURE VARIATION OVER TIME

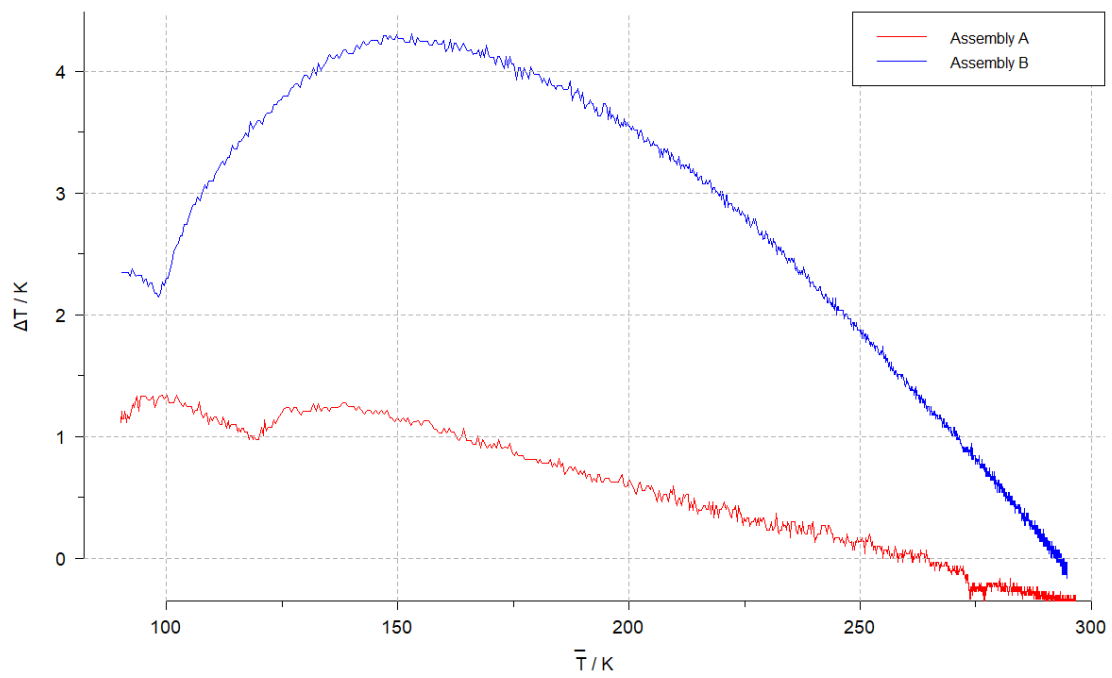


Figure 4.11: Plot of the difference of the temperature measured by each Pt100 as a function of time, for Assembly A (red) and Assembly B (blue).

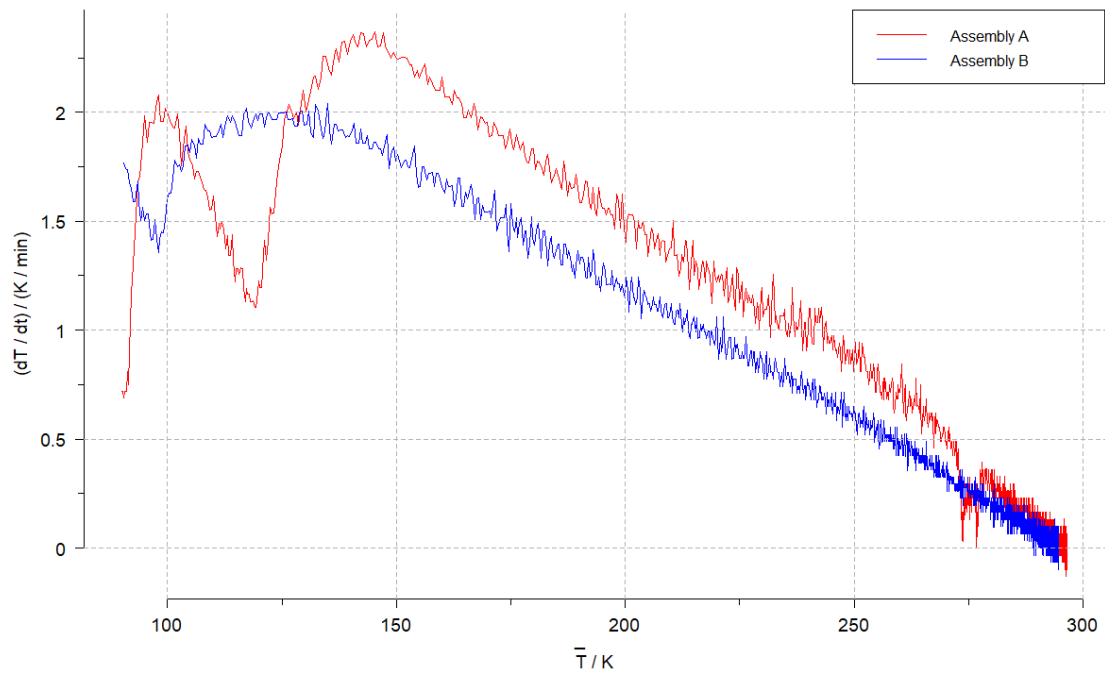


Figure 4.12: Plot of the derivative of the average temperature with respect to time as a function of the average temperature, for Assembly A (red) and Assembly B (blue).

4.5 SMaRT vs LabVIEW™ and 1260A vs 1260A paired with 1296A

With the purpose of determining if 1260A alone with the developed LabVIEW™ is equivalent to 1260A paired with 1269A and with SMaRT software as a means of measurement, Assembly A and Assembly B were used to measure a bare sensor, using either the SMaRT software or the developed LabVIEW™ program, with either 1260A or 1260A along with 1296A. This experiment was made at 77 K and at room temperature.

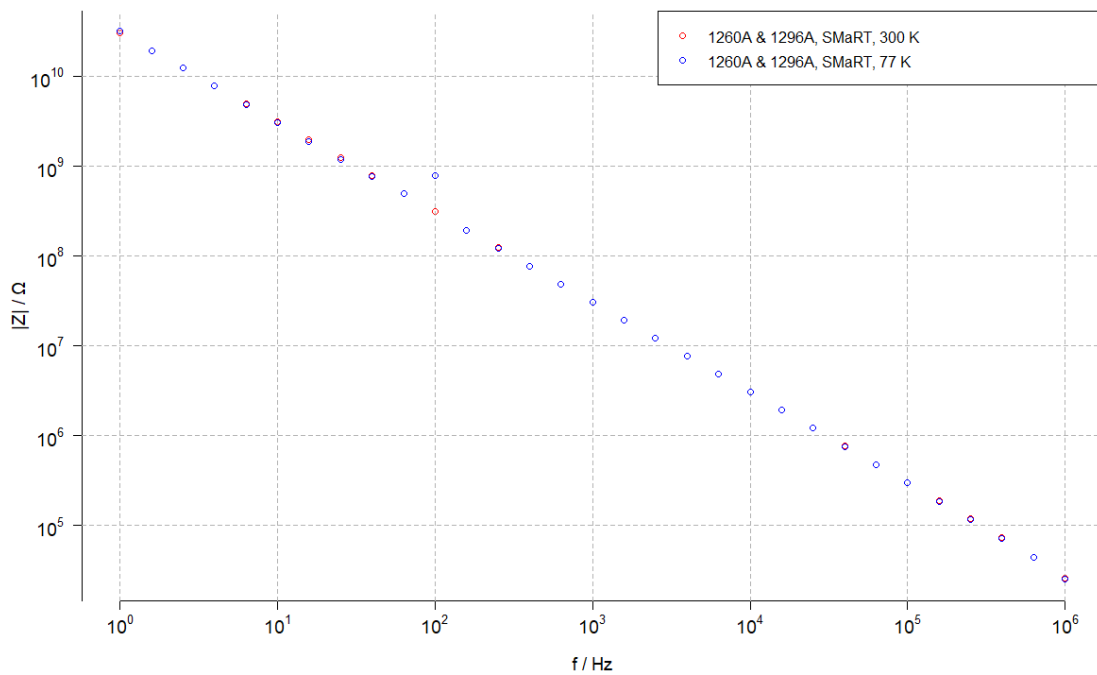


Figure 4.13: Bode plot of the impedance modulus as a function of frequency of a bare sensor measured with Assembly B, at around 300 K (red) and at 77 K (blue). For these measurements, 1260A paired with 1296A were used along with SMaRT software.

A bare sensor was placed on the sensor support of Assembly A, which was connected to 1296A, which in turn was connected to 1260A and a measurement was taken. Afterwards, Assembly A and 1260A were disconnected from 1269A and connected to one another, in a different manner as before and another measurement was taken using the SMaRT software. Then, another measurement was taken through the developed LabVIEW™ program, the measurements were made with the same parameters and connections between Assembly A and 1260A as before. Liquid nitrogen was then poured into the dewar until the temperature of 77 K was reached and the measurements with these three setups were repeated. Finally, the same process was repeated with Assembly B. Despite this experiment having been conducted with each test replicated with each assembly, since the purpose of this section is not to compare assemblies - since this has

already been discussed in section 4.3 - only data obtained with Assembly B will be shown.

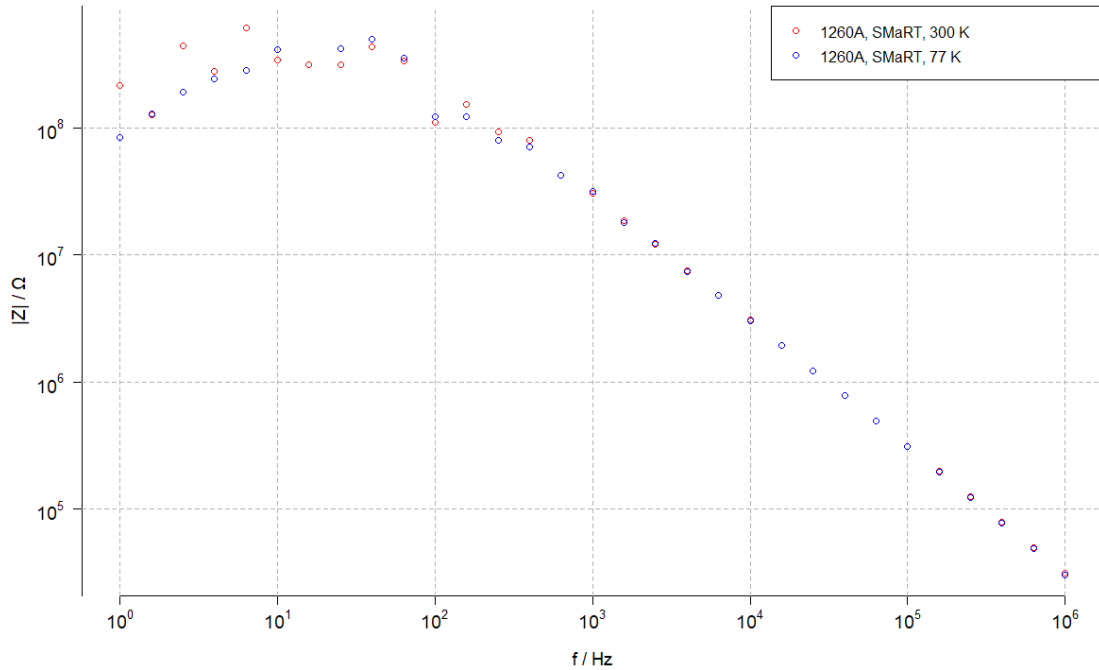


Figure 4.14: Bode plot of the impedance modulus as a function of frequency of a bare sensor measured with Assembly B, at around 300 K (red) and at 77 K (blue). For these measurements, 1260A was used along with SMaRT software.

Regarding measurements done with 1260A paired with 1296A, using SMaRT software as a means to control the parameters associated with the measurement, the results are shown in figure 4.13. It is possible to see that the general shape of the plots is linear - in logarithmic axis - corresponding to the response of a capacitor, as shown in figure 2.5. There seems to be little difference between the values measured at different temperatures, in concordance to what was seen in section 4.3. The biggest difference between the two sets of data occurs at 10^2 Hz, which might be caused due to some intrinsic property of 1260A when sweeping frequencies.

By removing 1296A out of the setup while keeping the rest unchanged, the linear shape is lost at higher impedance values, as shown in figure 4.14. This occurs due to the fact that 1260A's impedance limit is somewhere near 10^7 Ω and samples with values above this limit will cause 1260A to read erratically, which could be expected since 1296A's function is to aid in the measurement of dielectric materials such as polymers and ceramics [2]. However, for values under 10^7 Ω , the linear shape is maintained. This indicates that, for values under 10^7 Ω , using 1260A paired with 1296A or alone is equivalent. Disregarding values above 10^7 Ω , there seems to be little difference between the values measured at different temperatures, in concordance to the setup mentioned previously.

By swapping SMaRT software for the developed LabVIEW™ program, as the means

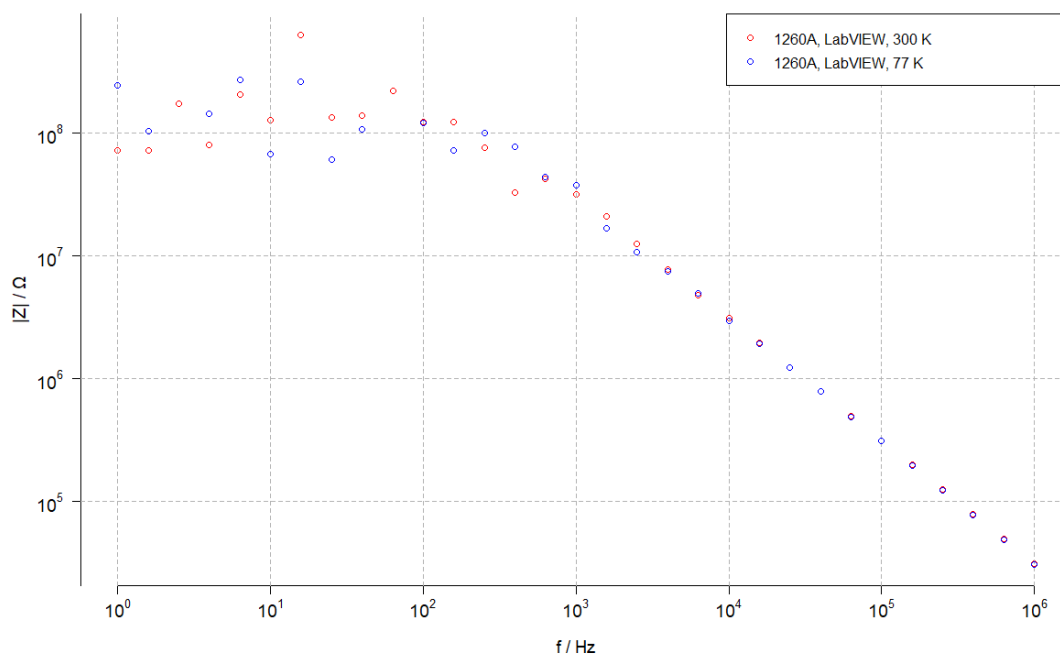


Figure 4.15: Bode plot of the impedance modulus as a function of frequency of a bare sensor measured with Assembly B, at around 300 K (red) and at 77 K (blue). For these measurements, 1260A was used along with the developed LabVIEWTM program.

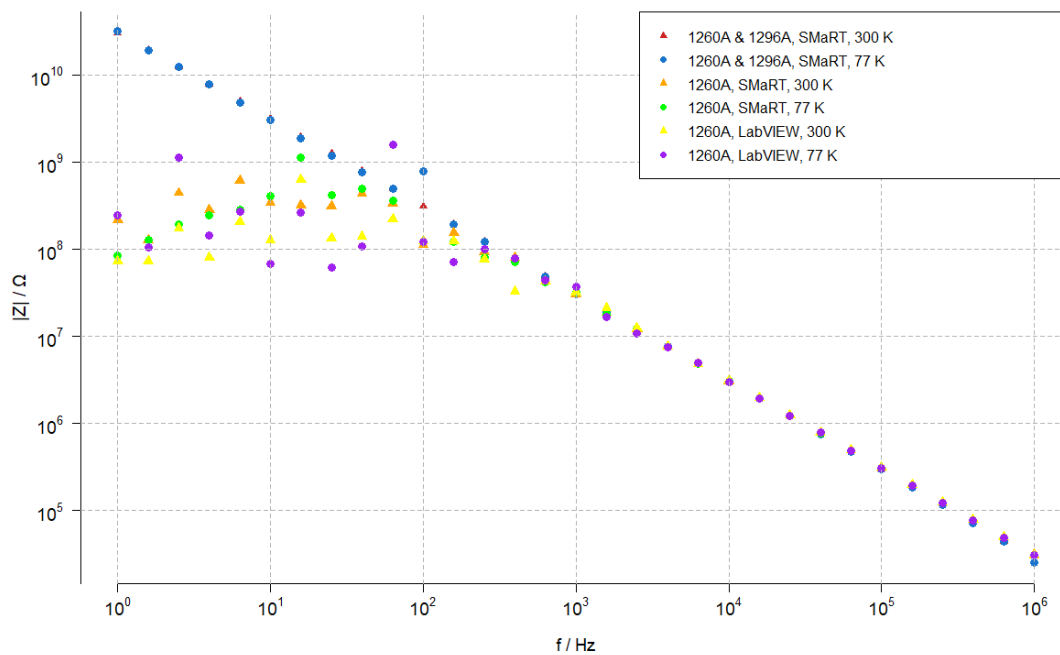


Figure 4.16: Bode plot of the impedance modulus as a function of frequency of a bare sensor measured with Assembly B, at around 300 K (red) and at 77 K (blue). For these measurements, 1260A was used along with the developed LabVIEWTM program.

of controlling the parameters associated with the measurement, no notable differences arise, as shown in figure 4.15. This indicates that as long as the Impedance Analyzer 1260A receives the required information it matters not what delivers it, as was expected. Therefore, the usage of the developed LabVIEW™ program is preferable to that of the SMaRT software, due to its ability to control when measurements are taken and also because it allows changes, being adaptable to future demands.

Figure 4.16 shows the data from the previous three plots in the same Bode plot. Here it is easier to see that for values under $10^7 \Omega$, there is little difference between all setups at both temperatures, indicating that they are equivalent ways of measuring the impedance of a sample. However, if the impedance values of said sample are higher than $10^7 \Omega$, the only way to measure those values would be with 1260A paired with 1296A.

4.6 Effects of Consecutive Measurements in the 5 to 25 mV Voltage Amplitude Range

The effects of consecutive measurements and the effect of the electrical field amplitude had to be tested before studying the response of DNA and DNA+AuNPs over a temperature span, where multiple measurements would take place. With this in mind, five different voltage amplitudes were chosen, with a number of ten measurements per voltage amplitude. These values were defined so that the voltage amplitude would gradually increase up to 25 mV - the value of the previous experiments - so that it would be possible to identify at which point the current would start damaging the sample, or if at all.

In this experiment two sensors were measured at room temperature, one with DNA and the other with DNA+AuNPs - prepared as detailed in subsection 3.1.1. The sensors were placed on the sensor support of Assembly B and the measurements were made with the developed LabVIEW™ program and 1260A. First, the DNA sensor was placed on the sensor support of Assembly B. Then the voltage amplitude was set at 5 mV and ten consecutive measurements were made. This process was repeated for 10, 15, 20 and 25 mV. Finally, the DNA sensor was swapped for the DNA+AuNPs sensor and another ten measurements were made for each of the previously specified voltage amplitudes.

The number n corresponding to the measurement from the first to the tenth, can be seen through the color variation from dark to light blue, respectively. By analyzing the plots shown in figure 4.17, it is possible to see that for the DNA sample there the impedance is independent of electrical field applied and does not change with consecutive measurements, as can also be seen in figure 4.18.

Regarding the DNA+AuNPs sample, it is possible to see in figures 4.19 and 4.20 that a variation with consecutive measurements occurs at 5 mV, maintaining this value for the following measurements. This might indicate that either some sort of anomaly took place before or during the measurement (e.g. humidity on the sample), or the sample was

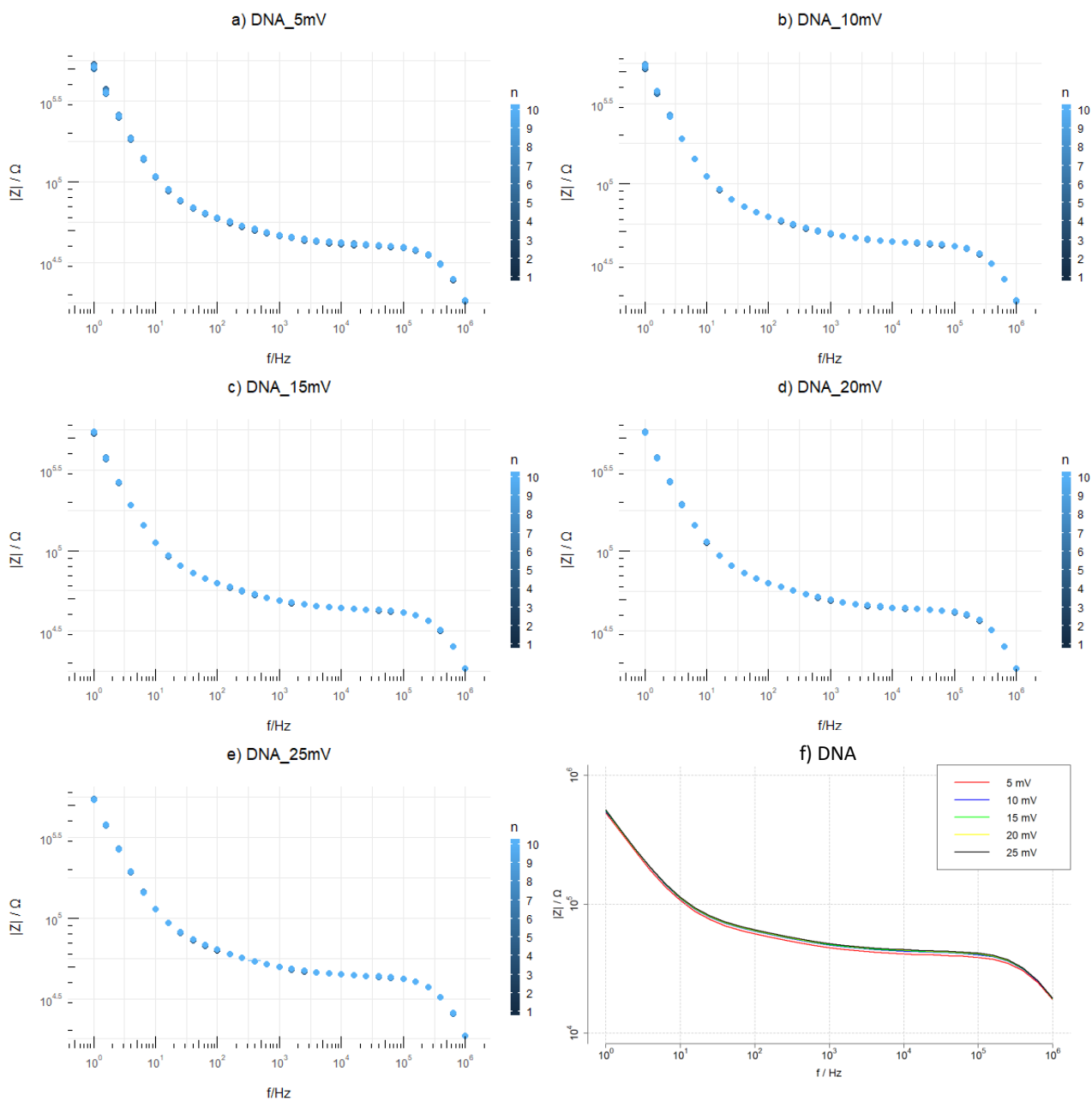


Figure 4.17: Bode plot of the impedance modulus as a function of frequency and the number of measurements for a DNA sensor at the voltage amplitude of a) 5 mV, b) 10 mV, c) 15 mV, d) 20 mV, e) 25 mV and f) the first measurement of each of the previous voltage amplitudes.

4.6. EFFECTS OF CONSECUTIVE MEASUREMENTS IN THE 5 TO 25 MV VOLTAGE AMPLITUDE RANGE

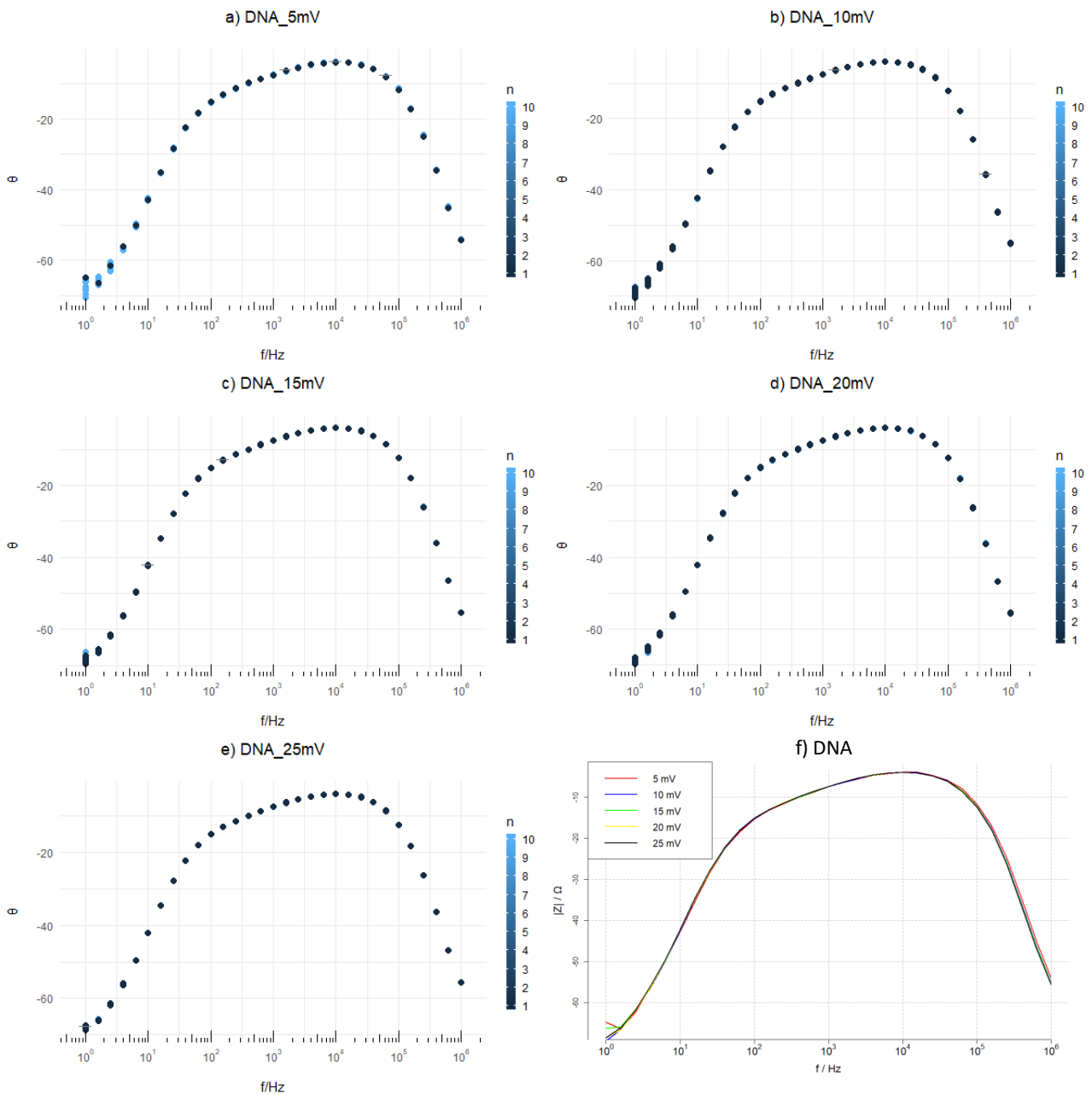


Figure 4.18: Bode plot of the impedance phase as a function of frequency and the number of measurements for a DNA sensor at the voltage amplitude of a) 5 mV, b) 10 mV, c) 15 mV, d) 20 mV, e) 25 mV and f) the first measurement of each of the previous voltage amplitudes.

damaged by the flow of current associated with the measurement.

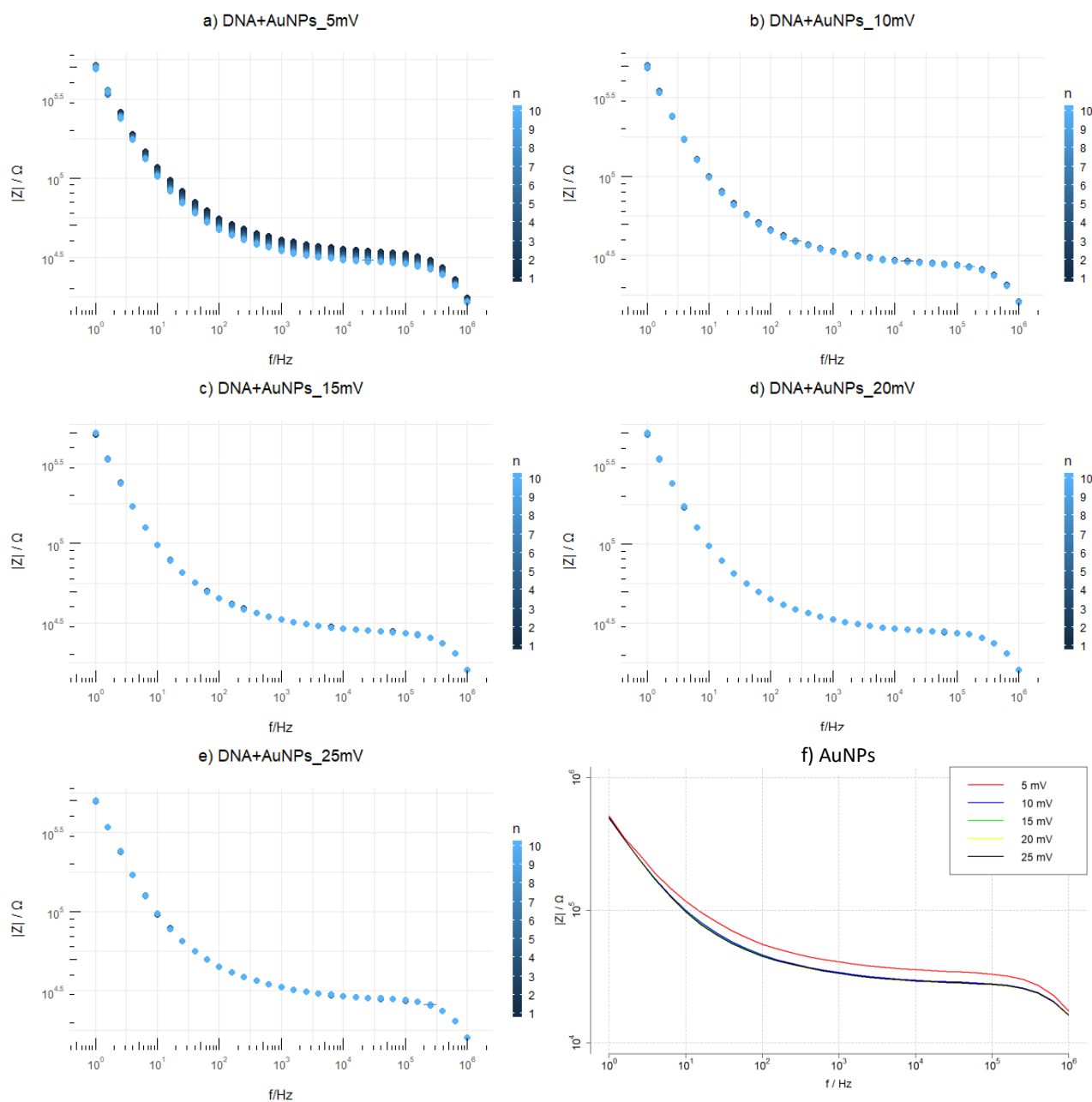


Figure 4.19: Bode plot of the impedance modulus as a function of frequency and the number of measurements for a DNA+AuNPs sensor at the voltage amplitude of a) 5 mV, b) 10 mV, c) 15 mV, d) 20 mV, e) 25 mV and f) the first measurement of each of the previous voltage amplitudes.

Overall, it would appear that up to 25 mV, the measuring current does not affect the DNA sample, while irreversibly affecting the DNA+AuNPs. However, this needs to be confirmed with more samples in order to more accurately state that this is what is happening.

4.6. EFFECTS OF CONSECUTIVE MEASUREMENTS IN THE 5 TO 25 MV VOLTAGE AMPLITUDE RANGE

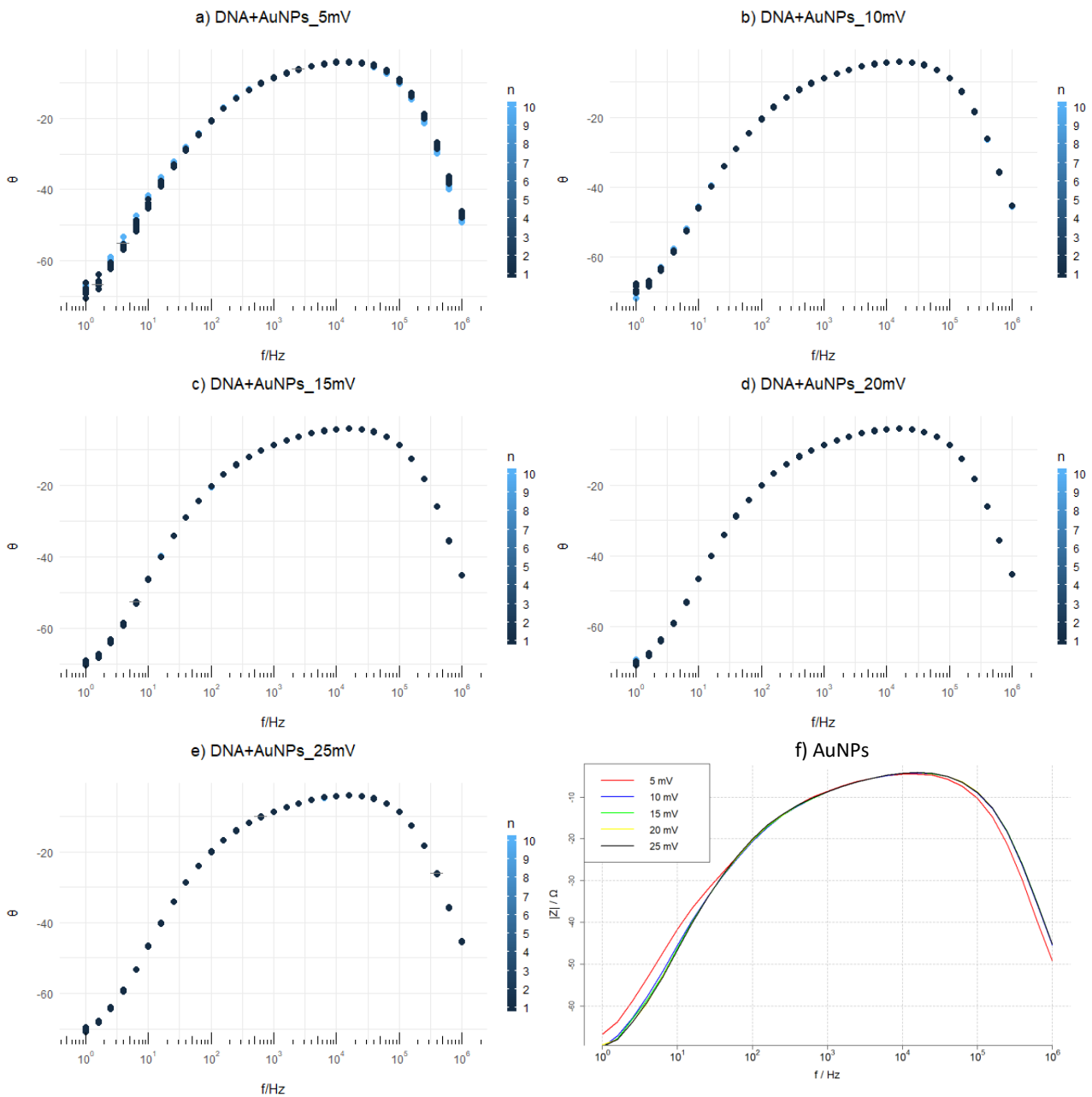


Figure 4.20: Bode plot of the impedance phase as a function of frequency and the number of measurements for a DNA+AuNPs sensor at the voltage amplitude of a) 5 mV, b) 10 mV, c) 15 mV, d) 20 mV, e) 25 mV and f) the first measurement of each of the previous voltage amplitudes.

4.7 Effect of UV Irradiation

To find what is the effect of UV radiation on DNA and DNA+AuNPs samples, one sensor with DNA and another with DNA+AuNPs, prepared as detailed in subsection 3.1.1, were measured. These sensors were placed on the sensor support of Assembly B and the measurements were made with the developed LabVIEW™ program and 1260A, within the temperature range of 200 to 290 K with a step of 2 K. The DNA sensor was placed on the sensor support of Assembly B and the cooling process was performed as described in the beginning of chapter 4, until the temperature of 200 K was reached. This process was repeated for the DNA+AuNPs sensor.

Both samples were then left exposed to UV light with a wavelength of 256 nm, for a total of 16 h at a temperature of 297 K and relative humidity of 50 %, with an irradiance of 10.05 W/m² which results in a dose of $\approx 5.8 \times 10^5$ J/m². Measurements of the UV irradiated DNA and DNA+AuNPs sensors were then made, through the same process as the one mentioned in the previous paragraph.

A previous experiment showed that from 77 to around 250 K the measurement results were the same. In this temperature range, the response would be equivalent to the one shown on figure 4.6. As such, this experiment's lowest measurement temperature was 200 K. However, the results show the lowest temperature as 240 K in order to reduce noise at high impedance values.

The Bode plots of figures 4.21, 4.22, 4.23 and 4.24 show how the impedance modulus varies with the frequency at several temperatures. Only half of the measurements are plotted in these plots; plots with all measurements are shown in appendix C. In the last section the effect of multiple consecutive measurements was studied and it was concluded that it might not have an effect on the studied samples. Thus, the variation of impedance at each measured frequency would be due to the variation of temperature. However, due to the lack of a measurement before cooling it is impossible to state if the values are converging to the values that would be obtained before cooling - i.e. it is not known if a cycle of cooling and warming irreversibly alters the electrical impedance of the sample.

Figure 4.25 shows the measurement at 290 K of each sensor, before and after irradiation. AuNPs are conductive and, as such, the impedance value of the DNA sensor before irradiation (figure 4.25, red plot) are not supposed to be lower than that of DNA+AuNPs, both before and after UV irradiation. The fact that this is not the case might be an anomaly and more testing should be done with varying DNA concentrations.

It is also possible to note that irradiation increases the impedance of each sample, as expected. In the case of the DNA sample, irradiation resulted in an increase of one order of magnitude to the sample's impedance. This confirms that UV radiation is irreversibly damages the DNA molecule, altering its electrical properties [16, 29]. As to the DNA+AuNPs sample (figure 4.25, blue and green plots), although there is an increase in its impedance, it is much smaller than that of the DNA sample. This might be due to the fact that AuNPs keep conducting the electrical current associated to the spectroscopy,

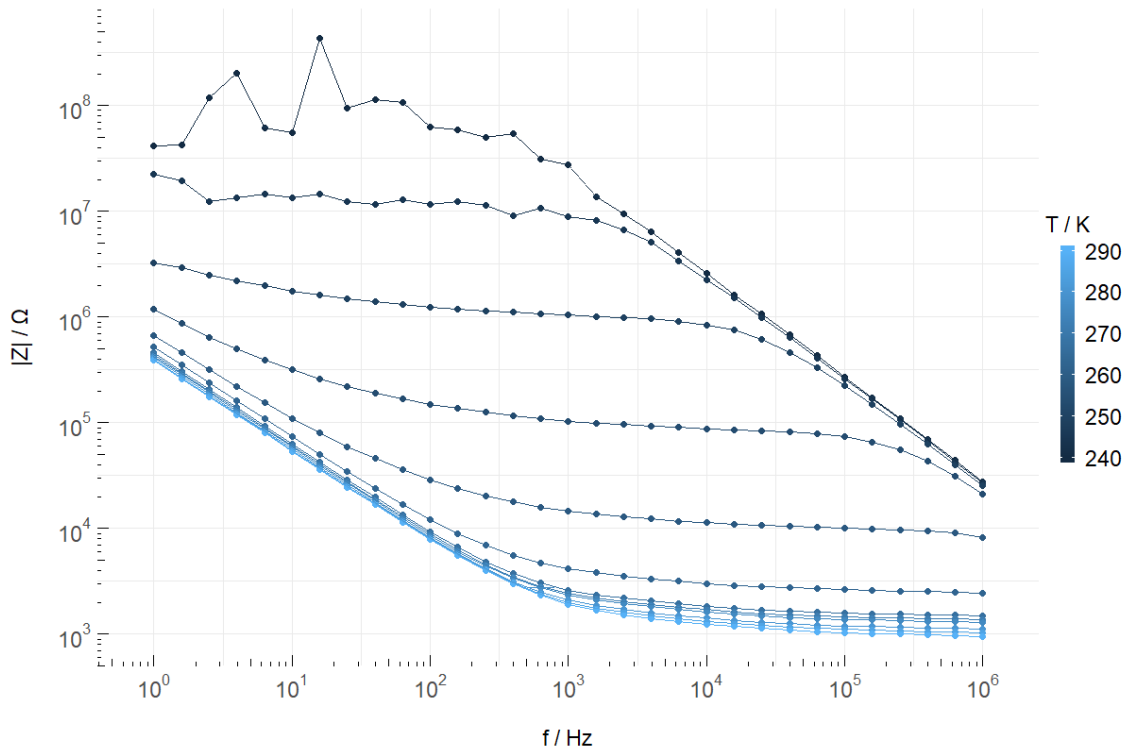


Figure 4.21: Bode plot of the impedance modulus as a function of frequency and temperature, of the DNA sensor (from 240 to 290 K, with a step of 4 K).

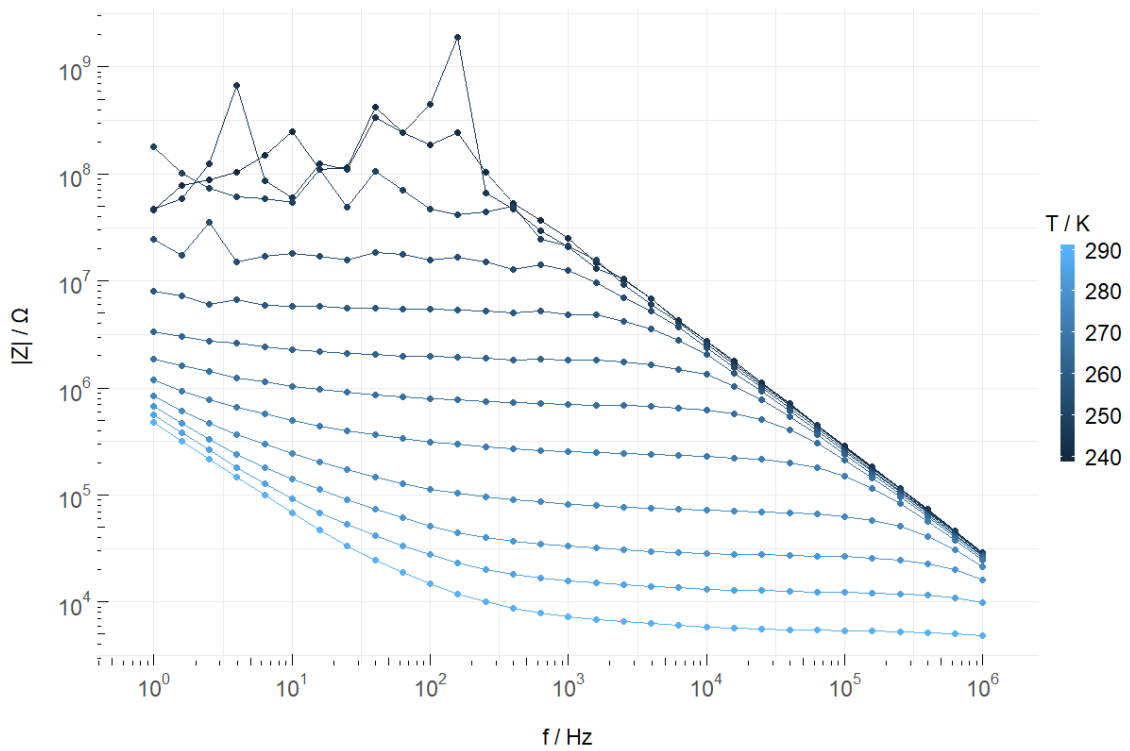


Figure 4.22: Bode plot of the impedance modulus as a function of frequency and temperature, of the DNA+AuNPs sensor (from 240 to 290 K, with a step of 4 K).

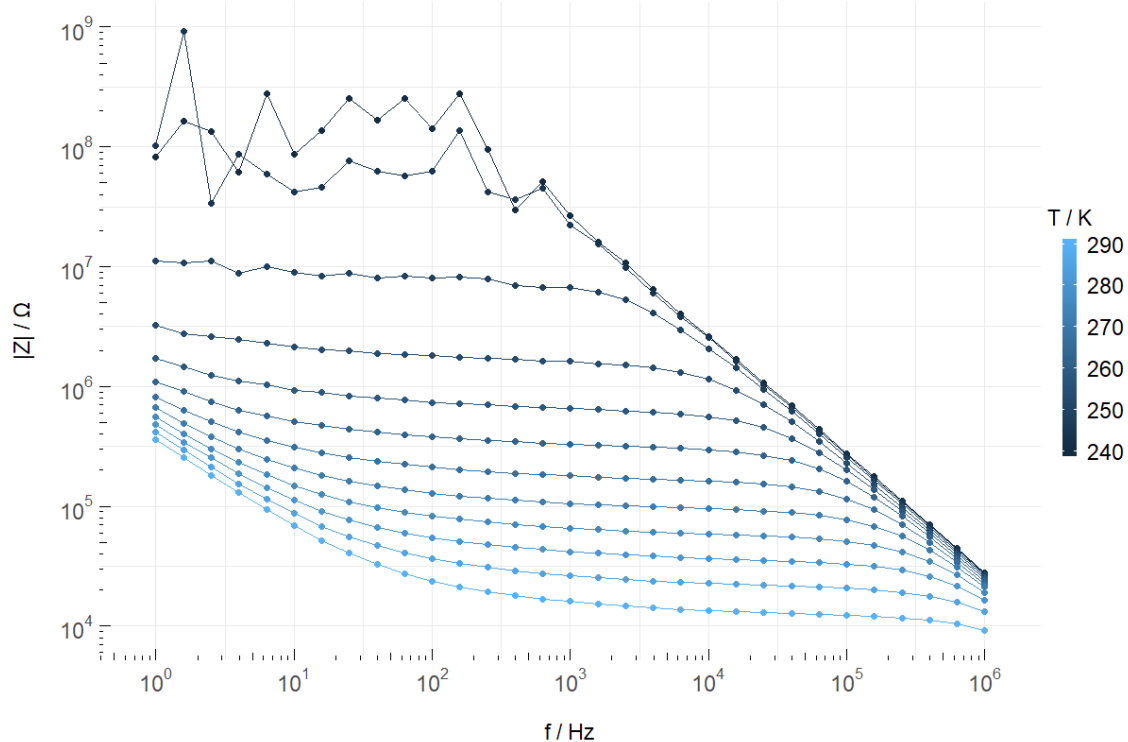


Figure 4.23: Bode plot of the impedance modulus as a function of frequency and temperature, of the UV irradiated DNA sensor (from 240 to 290 K, with a step of 4 K).

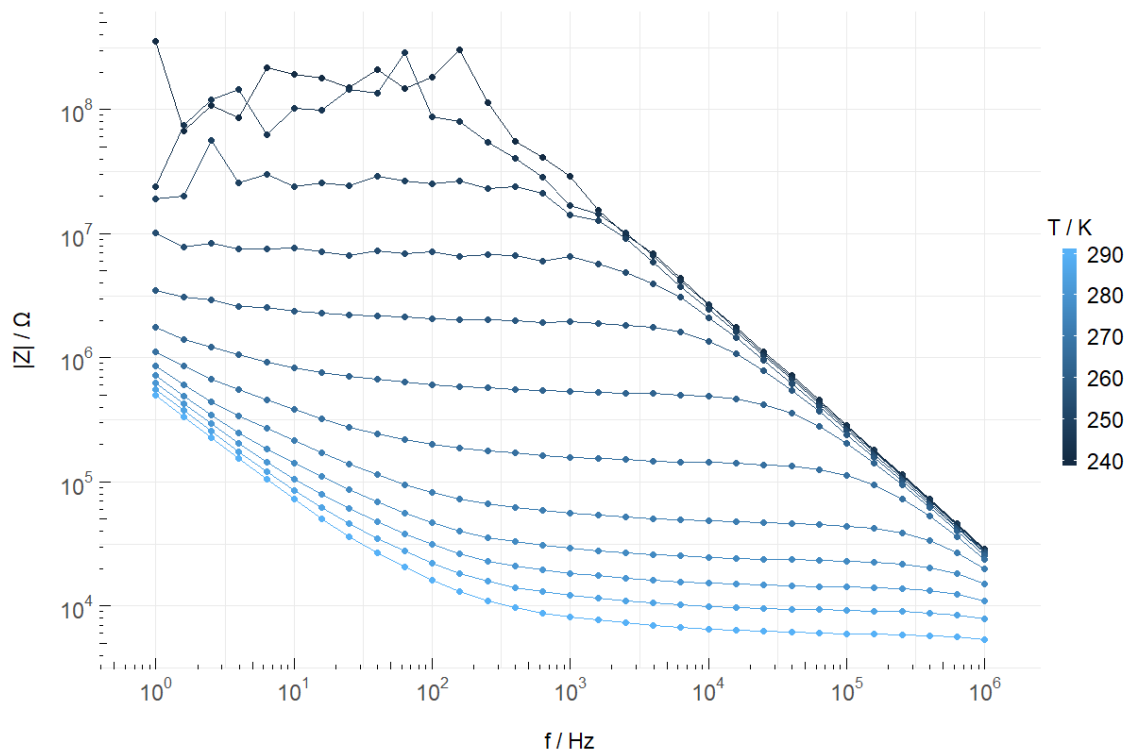


Figure 4.24: Bode plot of the impedance modulus as a function of frequency and temperature, of the UV irradiated DNA+AuNPs sensor (from 240 to 290 K, with a step of 4 K).

masking the DNA molecules' degraded state. If this is the case, then an IS is not the appropriate means of measuring damage done to the DNA molecule. In any case, more testing is required.

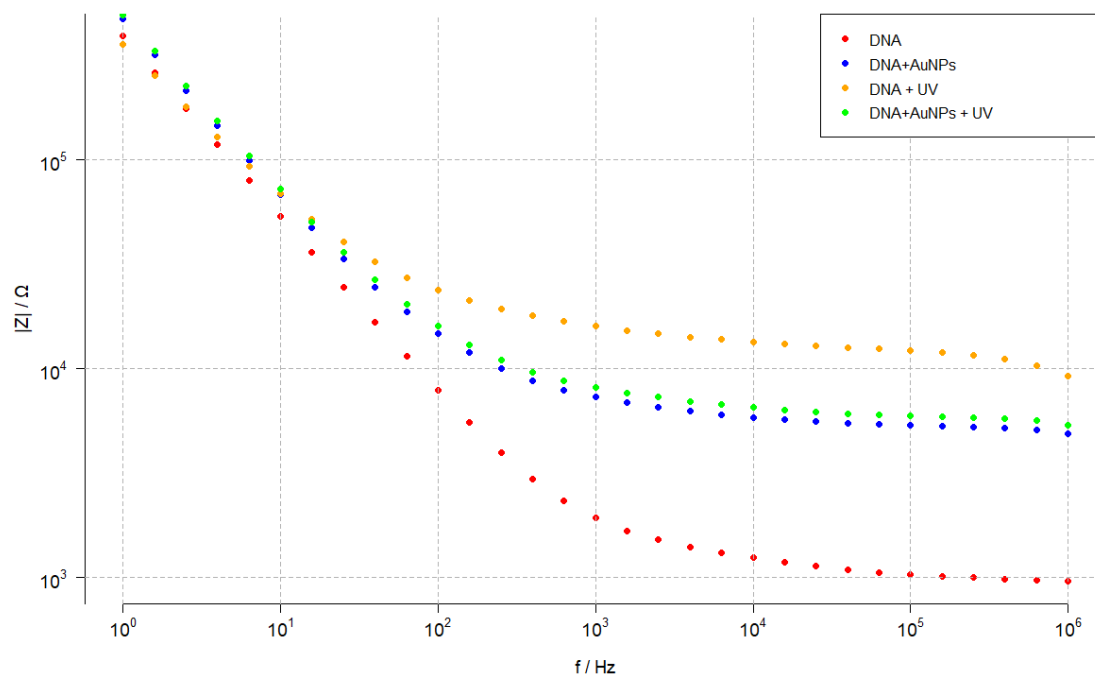


Figure 4.25: Bode plot of the impedance modulus as a function of frequency at 290 K, of the DNA (red), DNA+AuNPs (blue), UV irradiated DNA (yellow) and UV irradiated DNA+AuNPs sensor (purple).

CONCLUSION AND FUTURE PERSPECTIVES

This project's objective was to build a cryogenic system that would enable IS measurements of DNA and DNA+AuNPs samples on an interdigitated sensor. These measurements would automatically take place at temperatures defined by the user, within the range of 77 to 300 K. This objective was accomplished through the development of a user software and by the design and construction of two assemblies, with different designs. These two assemblies were then tested.

The first test intended to determine if the assemblies could replace the original connector (the blue connector) used to connect the sample to the impedance spectrometer. To this end a homemade circuit was developed and the measurement results of were compared between them and those obtained from measuring a circuit provided by AMETEK SI[®]. From this experiment it was found that the blue connector previously used has a parasitic capacitance, which causes the impedance values to be lower than they otherwise be for high frequencies. This led to the confirmation that the assemblies could replace the blue connector as an interface of measurement and to the validation of the homemade circuit, allowing it to be used as a reference circuit.

After testing the developed user interface with measurements of the homemade circuit, from low to around room temperature, the electrical impedance of the bare interdigitated sensors was measured. This test was conducted in order to know the response of the sensors in the 77 to 290 K range. It was found that, within the chosen range, their response is independent of the temperature. It was also found that there was a slight difference between the two assemblies, with Assembly B having a small parasitic capacitance.

The following step was to record the differences between using the Impedance Analyzer 1260A alone or paired with 1296A, with the software used previously (SMaRT) and the developed user interface. It was found that 1296A was key for measurements

of samples with impedance values above the threshold of $10^7 \Omega$ and without it, values that would otherwise continue to follow a pattern above this limit, do not. However, due to how the 1260A and 1296A work when paired together, it is impossible to control them both with LabVIEWTM - as confirmed by AMETEK SI[®] - which led to the use of only 1260A with the developed software. Additionally, the obtained results did not show differences between SMaRT or the developed user software. This makes the developed software the better choice due to its ability to monitor the temperature and automatically start a measurement when a defined temperature has been reached.

The response of consecutive measurements with several voltage amplitudes, of DNA and DNA+AuNPs was studied. It was found that, up until the value of 25 mV, DNA samples are not affected by consecutive measurements, nor the increase in the voltage amplitude. However, the same response was not obtained regarding DNA+AuNPs samples, where the first measurements could have induced an irreversible change in their response to an IS. It is unclear if this effect is a response of the AuNPs to the first measurement, altering the whole sample, or if an error had occurred somewhere in the manufacturing of the sample or when the measurement was taking place. This experiment would need to be repeated, possibly from lower to higher voltage amplitude values and more measurements per voltage amplitude.

The final objective of this project was achieved when measurements of DNA and DNA+AuNPs samples, before and after UV irradiation, along the temperature range of 77 to 290 K were made. These preliminary results show that from 77 to around 250 K, the impedance values would be similar to that of an interdigitated sensor with no sample. Only after this range, would they show their presence in the data. Additionally, in the case of the DNA sample, irradiation resulted in an increase of one order of magnitude to the sample's impedance, while slightly increasing the impedance of the DNA+AuNPs sample. These results confirm that UV radiation irreversibly damages the DNA molecule, while the same cannot be stated about the DNA+AuNPs sample.

Due to time constraints, two experiments were not performed and should be done in the future. The first would be to have a control for the samples. Specifically, an interdigitated sensor with only ultra-pure water and another with only the solution that contained the AuNPs should be made, followed by their measurement before and after UV irradiation. This experiment would help understand their response and their role in the tested samples. The second would be to see if the process of cooling and heating damages the samples, causing them to have different responses to an IS before and after said process. These two experiments should be performed in the future where the behavior of DNA and DNA+AuNPs samples is studied, which could help to better understand some of the results obtained. Additionally, the conduction phenomena should be studied at different temperatures, as well as the effect of AuNPs concentration in the DNA+AuNPs sample.

Regarding the assemblies, despite being composed of different materials, their response to the variation of temperature are similar. Since the temperature is always increasing, the temperature at the beginning of the measurement is different than that of the end. The results obtained show that, due to its slower variation of temperature for temperatures above 250 K, Assembly B would be a better candidate for an experiment with monitored but uncontrolled temperature. However, there is an option to keep the temperature constant when a measurement takes place. In that case, proportional–integral–derivative (PID) should be implemented in the future. If this happens, Assembly A should be the chosen assembly because there is good thermal conduction between the two aluminium parts that compose it, allowing for a better temperature control.

Finally, in order to facilitate sensor swapping, an assembly support should be designed and built in the future. This support should be adequate to the chosen assembly, since one of their main differences is how the sensor is swapped, and it should have an automatic height controller, so that the distance to the bottom of the dewar is constant throughout the project.

Additionally, it should be added that 3D printing can be an alternative to the normal means of building small components with many details, due constraints associated with machining small materials. Also, the plastic is a surprisingly good option for a cryogenic material, due to the fact that it can withstand temperatures as low as 77 K while being a cheap material. However, there are two drawbacks. One is the fact that it has a low fusion point, which can be a problem if the situation requires soldering near it. The other is that generally, plastics contract more than metals with the decrease in temperature, which can be a problem in certain situations.

BIBLIOGRAPHY

- [1] *1260A Impedance Analyzer*. <https://www.ameteki.com/products/frequency-response-analyzers/1260a-impedance-analyzer>. Accessed: 2019-09-01.
- [2] *1296A Dielectric Interface System*. <https://www.ameteki.com/products/materials-testing-systems/1296a-dielectric-interface>. Accessed: 2019-09-01.
- [3] N. S. Abadeer and C. J. Murphy. “Recent Progress in Cancer Thermal Therapy Using Gold Nanoparticles.” In: *The Journal of Physical Chemistry C* 120.9 (2016), pp. 4691–4716. DOI: 10.1021/acs.jpcc.5b11232.
- [4] *Basics of Electrochemical Impedance Spectroscopy*. <https://www.bio-logic.net/wp-content/uploads/part-i-basics.pdf>. Accessed: 2019-09-01.
- [5] J. Berdys, I. Anusiewicz, P. Skurski, and J. Simons. “Damage to Model DNA Fragments from Very Low-Energy (<1 eV) Electrons.” In: *Journal of the American Chemical Society* 126.20 (2004). PMID: 15149241, pp. 6441–6447. DOI: 10.1021/ja049876m.
- [6] B. Boudaiffa, P. Cloutier, D. Hunting, M. A. Huels, and L. Sanche. “Resonant Formation of DNA Strand Breaks by Low-Energy (3 to 20 eV) Electrons.” In: 287.5458 (2000), pp. 1658–1660. DOI: 10.1126/science.287.5458.1658.
- [7] *Capacitor ESR, Dissipation Factor, Loss Tangent Q*. https://www.electronics-notes.com/articles/basic_concepts/capacitance/esr-dissipation-factor-loss-tangent-q.php. Accessed: 2019-09-01.
- [8] D. Chinaglia, G. Gozzi, R. Alfaro, and R. Hessel. “Espectroscopia de impedância no laboratório de ensino.” In: *Revista Brasileira de Ensino de Física* 30 (Dec. 2008), pp. 4504.1–4504.9. DOI: 10.1590/S1806-11172008000400013.
- [9] *Complex impedance method for AC circuits*. <http://www2.physics.umd.edu/~jacobson/273c/impedance.pdf>. Accessed: 2019-09-01.
- [10] *Dielectric Permittivity*. https://em.geosci.xyz/content/physical_properties/dielectric_permittivity/index.html. Accessed: 2019-09-01.
- [11] S. P. Egusquiaguirre, M. Igartua, R. M. Hernández, and J. L. Pedraz. “Nanoparticle delivery systems for cancer therapy: advances in clinical and preclinical research.” In: *Clinical and Translational Oncology* 14.2 (Feb. 2012), pp. 83–93.

BIBLIOGRAPHY

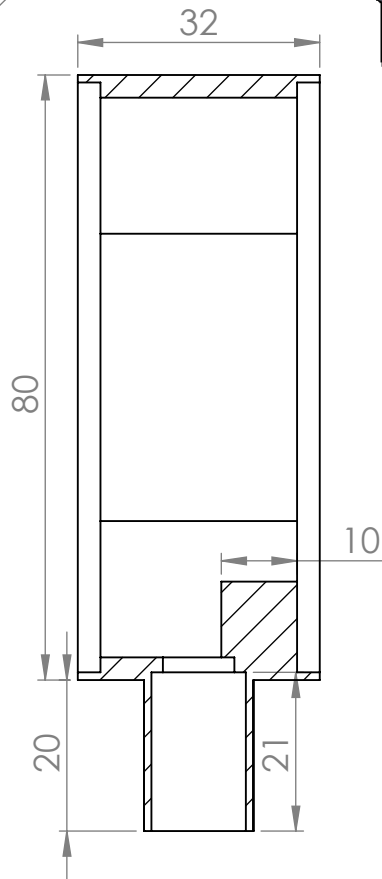
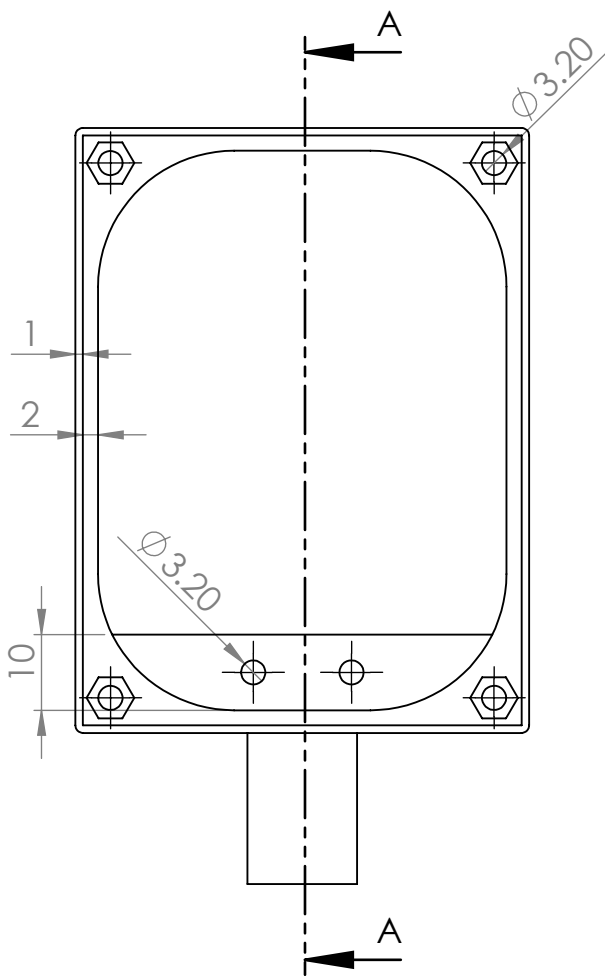
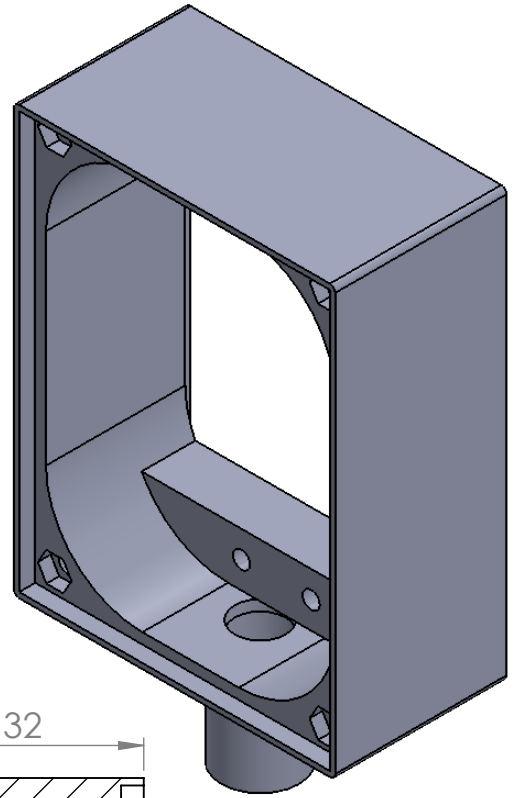
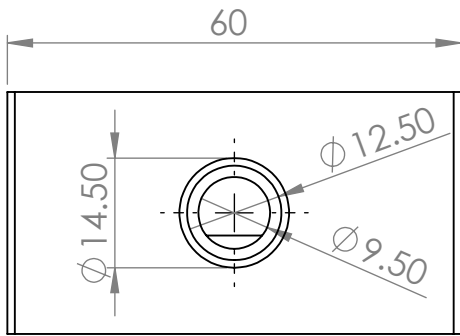
- [12] *Electromagnetic Dissipation*. http://web.mit.edu/6.013_book/www/chapter11/11.5.html. Accessed: 2019-09-01.
- [13] *File:DNA Structure+Key+Labelled.pn NoBB.png*. https://en.wikipedia.org/wiki/File:DNA_Structure%2BKey%2BLabelled.pn_NoBB.png. Accessed: 2019-09-01.
- [14] A. I. G. Francisco. “Montagem Didática para Medições de Resistividade de Metais na Gama 77 K a 300 K.” Master’s thesis. FCT/UNL, 2018, p. 78.
- [15] “Gold nanoparticles: Optical properties and implementations in cancer diagnosis and photothermal therapy.” In: *Journal of Advanced Research* 1.1 (2010), pp. 13–28.
- [16] P. J. Gomes, A. M. Ferraria, A. M. Botelho do Rego, S. V. Hoffmann, P. A. Ribeiro, and M. Raposo. “Energy Thresholds of DNA Damage Induced by UV Radiation: An XPS Study.” In: *The Journal of Physical Chemistry B* 119.17 (2015). PMID: 25844940, pp. 5404–5411. DOI: 10.1021/acs.jpcc.5b01439.
- [17] P. J. Gomes, M. Coelho, M. Dionísio, P. António Ribeiro, and M. Raposo. “Probing radiation damage by alternated current conductivity as a method to characterize electron hopping conduction in DNA molecules.” In: *Applied Physics Letters* 101.12 (2012), p. 123702. DOI: 10.1063/1.4754287.
- [18] *GPIO*. <https://www.raspberrypi.org/documentation/usage/gpio/>. Accessed: 2019-08-11.
- [19] *Introduction to EIS (Electrochemical Impedance Spectroscopy) with ECLab®/EC-Lab® Express*. <https://www.gamry.com/application-notes/EIS/basics-of-electrochemical-impedance-spectroscopy/>. Accessed: 2019-09-01.
- [20] *Introduction to Electrochemical Impedance Spectroscopy*. <https://www.gamry.com/assets/Uploads/Basics-of-Electrochemical-Impedance-Spectroscopy.pdf>. Accessed: 2019-09-01.
- [21] J. Laudát and F. Laudát. “Dielectric study of charge motion in DNA.” In: *European Biophysics Journal* 21.3 (July 1992), pp. 233–239. DOI: 10.1007/BF00196768.
- [22] J. R. Macdonald and W. B. Johnson. “Fundamentals of Impedance Spectroscopy.” In: *Impedance Spectroscopy Theory, Experiment, and Applications*. Ed. by E. Barsoukov and J. R. Macdonald. 2nd. Hoboken: John Wiley & Sons, Inc., 2010. Chap. 1, pp. 1–26. DOI: <https://doi.org/10.1002/0471716243.ch1>.
- [23] P. Martins, D. Rosa, A. Fernandes, and P. Baptista. “Nanoparticle Drug Delivery Systems: Recent Patents and Applications in Nanomedicine.” In: *Recent Patents on Nanomedicine* 3 (Jan. 2013), pp. 105–118. DOI: 10.2174/1877912304666140304000133.
- [24] “Metal nanoparticles: a theranostic nanotool against cancer.” In: *Drug Discovery Today* 20.9 (2015), pp. 1143–1151.

- [25] P. Ribeiro. “Caracterização Dielétrica e Eletroóptica do Copolímero Acrílico Funcionalizado com o Cromóforo 4-[N-etil-N-(2-hidroxietyl)]amino-2'-cloro-4'-nitroazobenzeno.” Doctoral dissertation. São Carlos: Universidade de São Paulo, July 1999.
- [26] *Tan Delta Test | Loss Angle Test | Dissipation Factor Test*. <https://www.electrical4u.com/tan-delta-test-loss-angle-test-dissipation-factor-test>. Accessed: 2019-09-01.
- [27] “UV degradation of deoxyribonucleic acid.” In: *Polymer Degradation and Stability* 94.12 (2009), pp. 2134–2141.
- [28] J. Walker, D. Halliday, and R. Resnick. “Electromagnetic Oscillations and Alternating Current.” In: *Fundamentals of Physics*. 9th. Hoboken: John Wiley & Sons, Inc. Chap. 31, pp. 826–860. ISBN: 978-0-471-75801-3. DOI: 10.1016/j.fsigen.2018.10.016.
- [29] J. Wang. “Electrical conductivity of double stranded DNA measured with ac impedance spectroscopy.” In: *Phys. Rev. B* 78 (24 Dec. 2008), p. 245304. DOI: 10.1103/PhysRevB.78.245304.
- [30] *What is electric permittivity?* <http://www.electrical4u.com/en/2018/11/02/what-is-electric-permittivity/>. Accessed: 2019-09-01.



APPENDIX 1: TECHNICAL DRAWINGS

A.1 General Components



SECTION A-A

UNLESS OTHERWISE SPECIFIED:
DIMENSIONS ARE IN MILLIMETERS
SURFACE FINISH:
TOLERANCES:
LINEAR: 0.2
ANGULAR: NA

FINISH:

DEBURR AND
BREAK SHARP
EDGES

DO NOT SCALE DRAWING

REVISION

	NAME	SIGNATURE	DATE
DRAWN	AM		
CHK'D	GB		
APP'VD	GB		

TITLE:

Frame

MATERIAL:	PLA
WEIGHT:	

DWG NO.

A4

SCALE:1:1

SHEET 1 OF 1

4 3 2 1

F

F

E

E

D

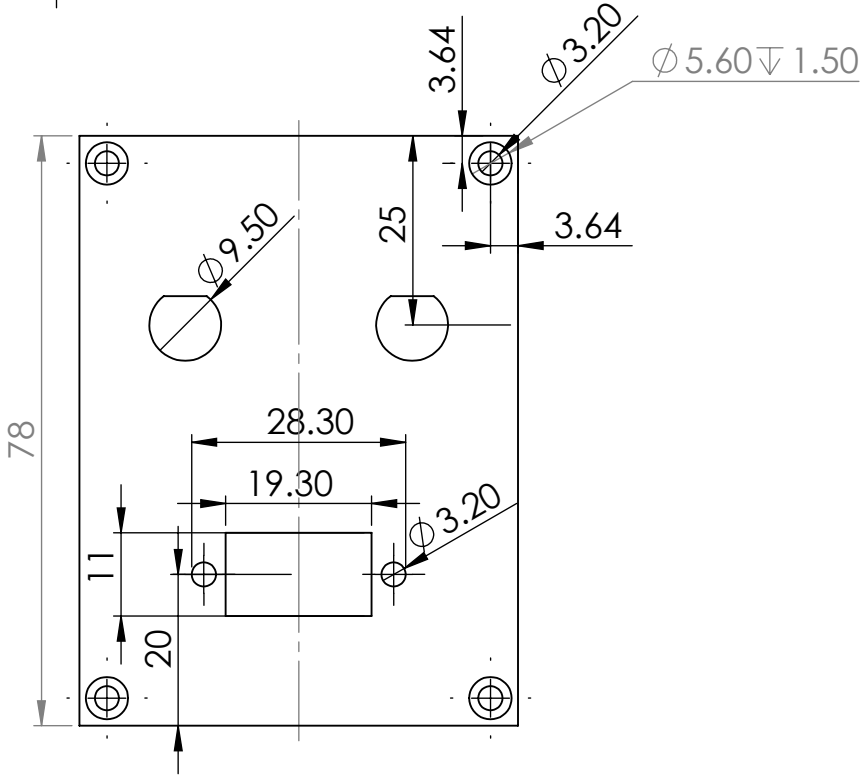
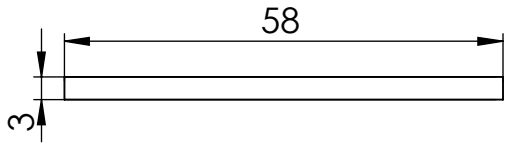
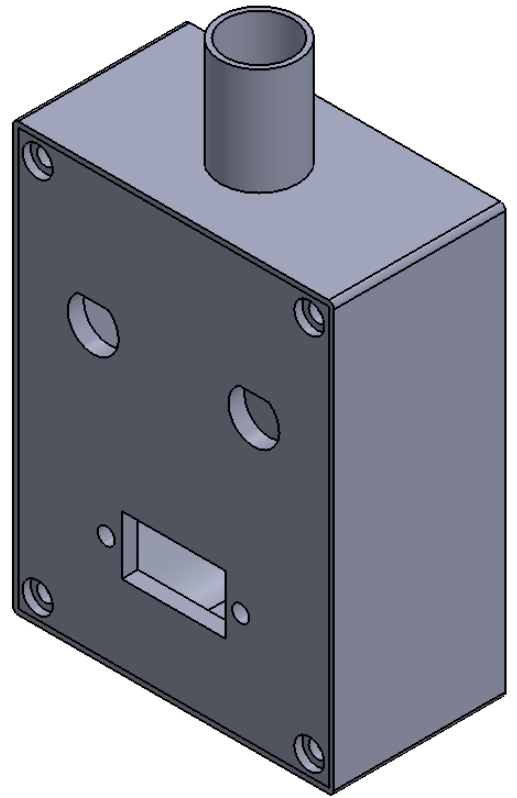
D

C

C

B

B



UNLESS OTHERWISE SPECIFIED:
DIMENSIONS ARE IN MILLIMETERS
SURFACE FINISH:
TOLERANCES:
LINEAR: 0.2
ANGULAR: NA

FINISH:

DEBURR AND
BREAK SHARP
EDGES

DO NOT SCALE DRAWING

REVISION

	NAME	SIGNATURE	DATE
DRAWN	AM		
CHK'D	GB		
APPV'D	GB		

TITLE: **Front Lid**

MATERIAL: PLA

DWG NO. _____

SCALE: 1:1

SHEET 1 OF 1

A4

4 3 2 1

A

A

4 3 2 1

F

F

E

E

D

D

C

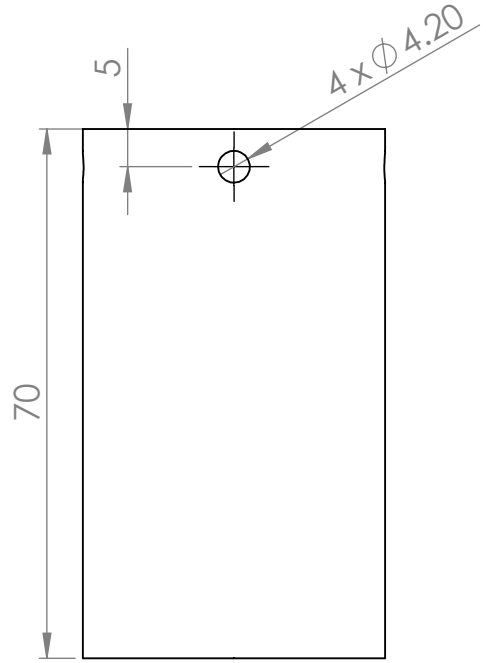
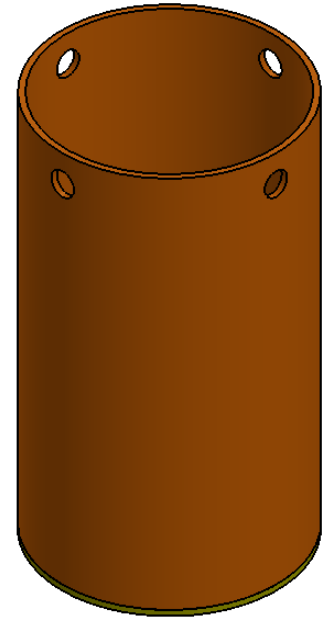
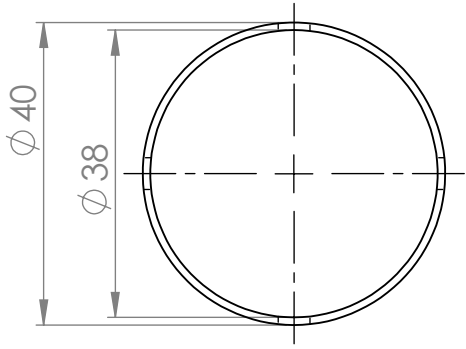
C

B

B

A

A



UNLESS OTHERWISE SPECIFIED:
 DIMENSIONS ARE IN MILLIMETERS
 SURFACE FINISH:
 TOLERANCES:
 LINEAR:
 ANGULAR:

FINISH:

DEBURR AND
 BREAK SHARP
 EDGES

DO NOT SCALE DRAWING

REVISION

	NAME	SIGNATURE	DATE
DRAWN	AM		
CHK'D	GB		
APP'VD	GB		

TITLE:

Screen

MATERIAL:
 Copper

DWG NO. A4

WEIGHT:

SCALE:1:1

SHEET 1 OF 1

4 3 2 1

4

3

2

1

F

F

E

E

D

D

C

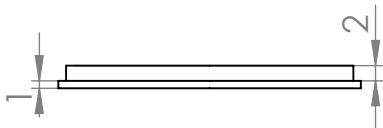
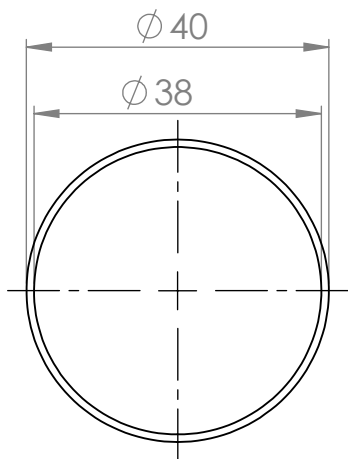
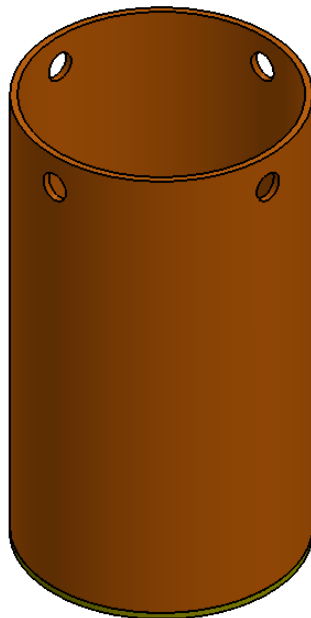
C

B

B

A

A



UNLESS OTHERWISE SPECIFIED:
 DIMENSIONS ARE IN MILLIMETERS
 SURFACE FINISH:
 TOLERANCES:
 LINEAR: 0.2
 ANGULAR: NA

FINISH:

DEBURR AND
 BREAK SHARP
 EDGES

DO NOT SCALE DRAWING

REVISION

	NAME	SIGNATURE	DATE
DRAWN	AM		
CHK'D	GB		
APP'VD	GB		

TITLE:
Bottom

MATERIAL:
Brass

DWG NO. _____

A4

WEIGHT: _____

SCALE: 1:1

SHEET 1 OF 1

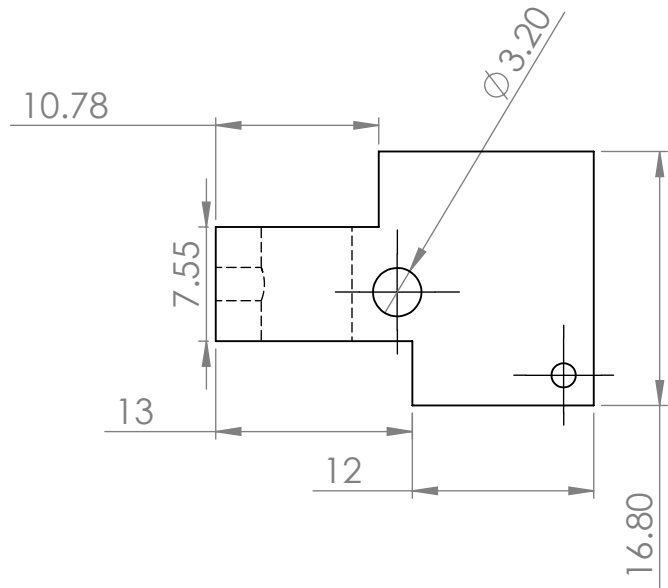
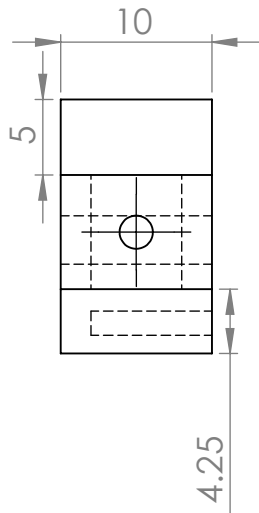
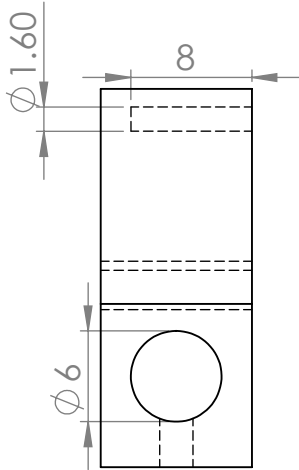
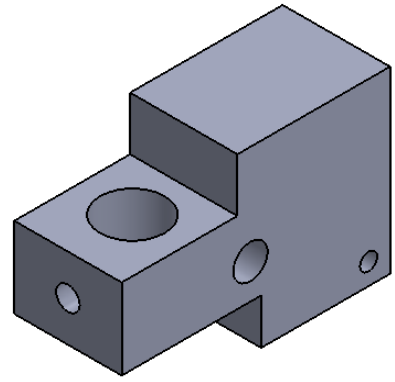
4

3

2

1

A.2 Assembly A



UNLESS OTHERWISE SPECIFIED:
DIMENSIONS ARE IN MILLIMETERS
SURFACE FINISH:
TOLERANCES:
LINEAR: 0.2
ANGULAR: NA

FINISH:

DEBURR AND
BREAK SHARP
EDGES

DO NOT SCALE DRAWING

REVISION

	NAME	SIGNATURE	DATE
DRAWN	AM		
CHK'D	GB		
APP'VD	GB		

TITLE:
**Electrode Support
A**

MATERIAL:

Aluminum

DWG NO.

A4

WEIGHT:

SCALE:2:1

SHEET 1 OF 1

4

3

2

1

F

F

E

E

D

D

C

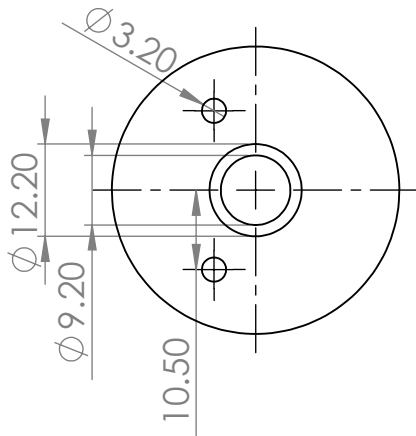
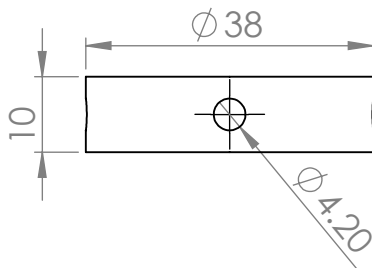
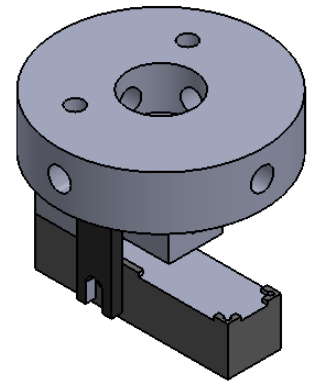
C

B

B

A

A



UNLESS OTHERWISE SPECIFIED:
 DIMENSIONS ARE IN MILLIMETERS
 SURFACE FINISH:
 TOLERANCES:
 LINEAR: 0.2
 ANGULAR: NA

FINISH:

DEBURR AND
BREAK SHARP
EDGES

DO NOT SCALE DRAWING

REVISION

	NAME	SIGNATURE	DATE
DRAWN	AM		
CHK'D	GB		
APP'VD	GB		

TITLE:

Flange A

MATERIAL: <h2 style="text-align: center;">Aluminum</h2>		
WEIGHT:		

DWG NO.	A4
SCALE: 1:1	SHEET 1 OF 1

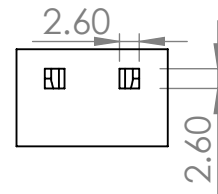
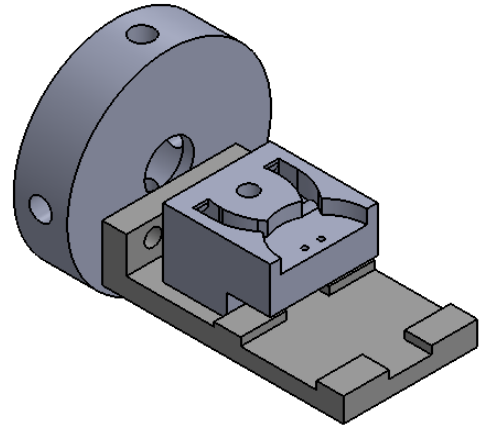
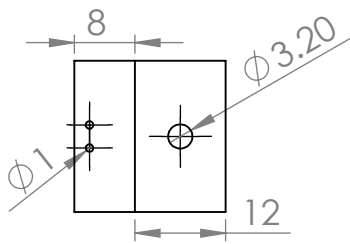
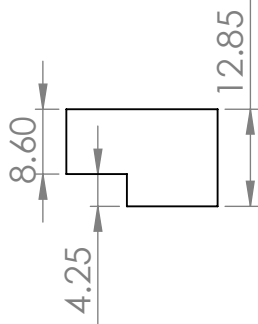
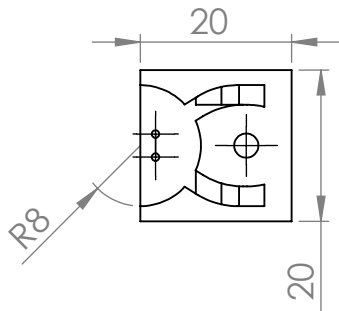
4

3

2

1

A.3 Assembly B



UNLESS OTHERWISE SPECIFIED:
DIMENSIONS ARE IN MILLIMETERS
SURFACE FINISH:
TOLERANCES:
LINEAR: 0.2
ANGULAR: NA

FINISH:

DEBURR AND
BREAK SHARP
EDGES

DO NOT SCALE DRAWING

REVISION

	NAME	SIGNATURE	DATE
DRAWN	AM		
CHK'D	GB		
APPV'D	GB		

TITLE:
**Electrode Support
B**

MATERIAL:
PLA

DWG NO.

A4

WEIGHT:

SCALE:1:1

SHEET 1 OF 1

APPENDIX 2: PYTHON CODE

Listing B.1: A listing of Python code used to establish communication between the Raspberry Pi and the computer.

```
1
2 import time
3 import board
4 import busio
5 import digitalio
6 import adafruit_max31865
7
8 # imports communication
9 import time
10 import serial
11
12 import threading
13 import os
14 from time import sleep
15
16 ser = serial.Serial("/dev/ttyUSB0", baudrate = 9600,
17                   parity=serial.PARITY_NONE,
18                   stopbits=serial.STOPBITS_ONE,
19                   bytesize=serial.EIGHTBITS)
20
21 spi = busio.SPI(board.SCK, MOSI=board.MOSI, MISO=board.MISO)
22
23 cs1 = digitalio.DigitalInOut(board.D5)
24 cs2 = digitalio.DigitalInOut(board.D6)
25
```

```
26 sensor1 = adafruit_max31865.MAX31865(spi, cs1, rtd_nominal=100, ref_resistor
    ↪ =431.0, wires=4)
27 sensor2 = adafruit_max31865.MAX31865(spi, cs2, rtd_nominal=100, ref_resistor
    ↪ =431.0, wires=4)
28
29 os.system('clear')
30
31 while True:
32
33     data = ser.read()
34     data = str(data)
35
36     s1t = sensor1.temperature
37     s1r = sensor1.resistance
38     s2t = sensor2.temperature
39     s2r = sensor2.resistance
40
41     if data == "b't'":
42         string = str(s1t) + ";" + str(s2t) + ";" + "\n"
43         byteArray = bytearray(string, "utf-8") # Convert string into a b$
44         data = ''
45
46     elif data == "b'r'":
47         string = str(s1r) + ";" + str(s2r) + ";" + "\n"
48         byteArray = bytearray(string, "utf-8") # Convert string into a b$
49         data = ''
50
51     elif data == "b'a'":
52         string = str(s1t) + ";" + str(s1r) + ";" + str(s2t) + ";" + str(s2r) +
    ↪ "\n"
53         byteArray = bytearray(string, "utf-8") # Convert string into a b$
54         data = ''
55
56     elif data == "b'e'":
57         data = ''
58         break
59         sleep(2)
60         s.close()
61
62     elif (data != "b't'") & (data != "b'r'") & (data != "b'a'") & (data != "b'e
    ↪ '"):
63         print('5\n')
64         data = ''
65
66
67     try:
```

```
68     ser.write(byteArray)
69     time.sleep(1)
70     byteArray = bytearray('', "utf-8")
71
72     except:
73         #print("Envio Impossível\n")
74         break
75         sleep(2)
76         ser.close()
```


APPENDIX 3: BODE PLOTS OF DNA AND DNA+AuNPs, FROM 240 TO 290 K

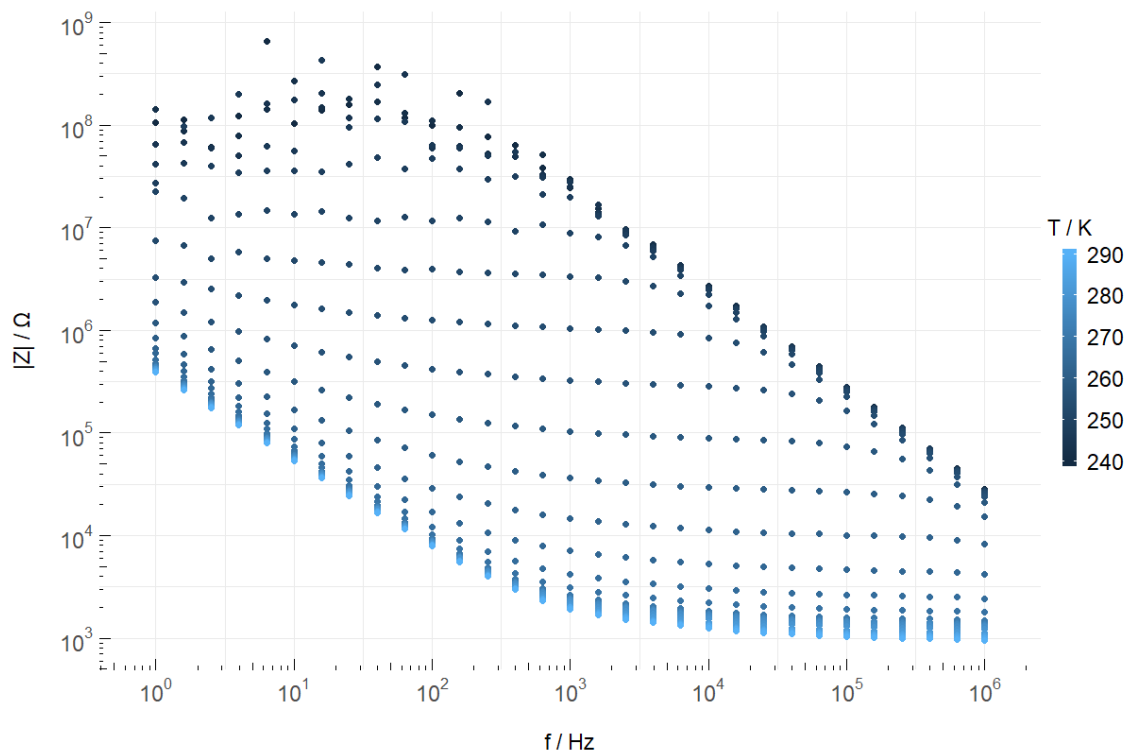


Figure C.1: Bode plot of the impedance modulus as a function of frequency and temperature, of the DNA sensor.

APPENDIX C. APPENDIX 3: BODE PLOTS OF DNA AND DNA+AuNPs, FROM 240 TO 290 K

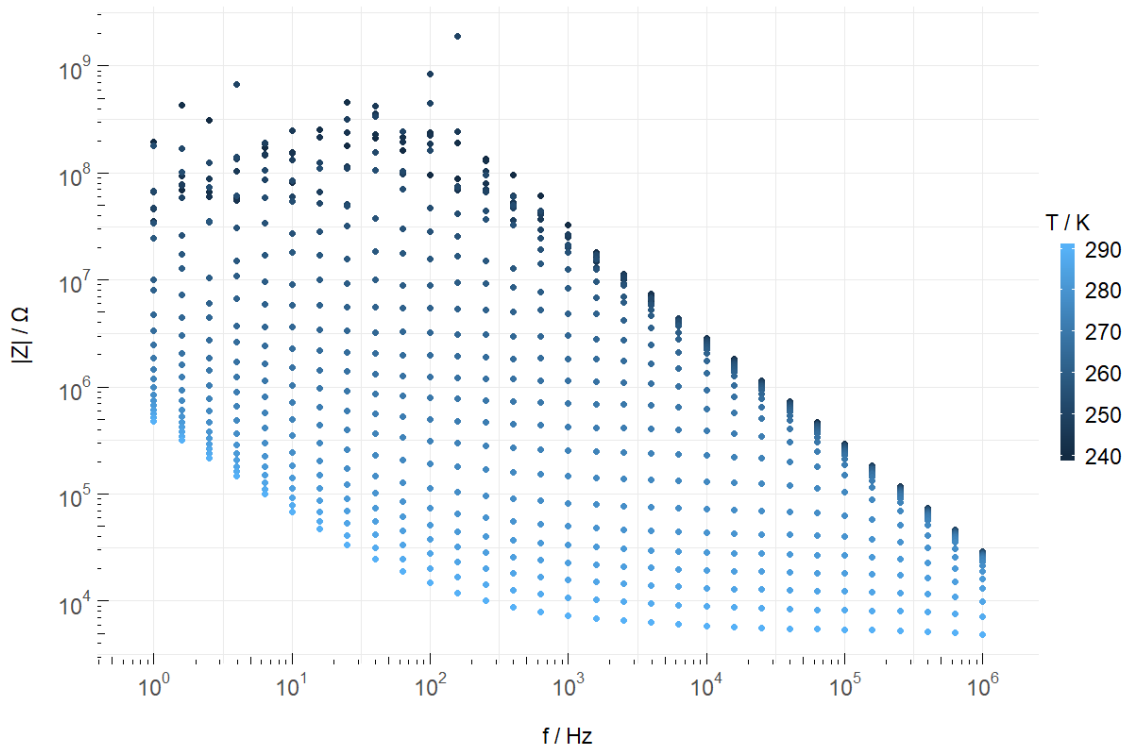


Figure C.2: Bode plot of the impedance modulus as a function of frequency and temperature, of the DNA+AuNPs sensor.

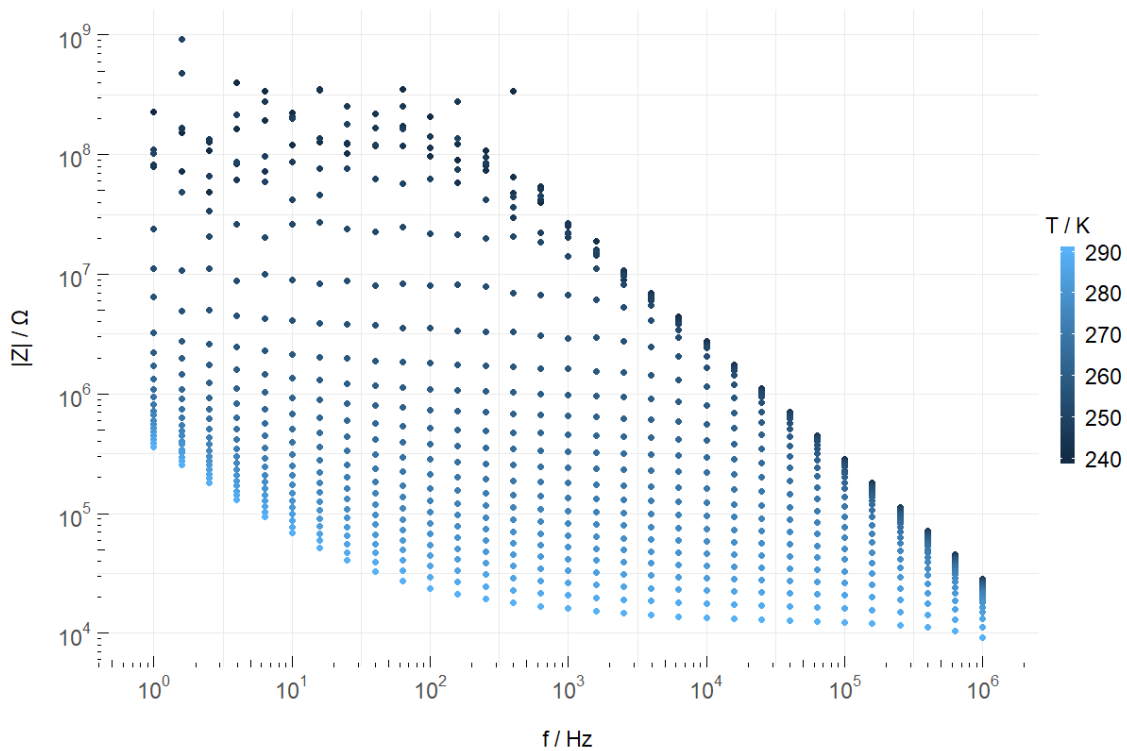


Figure C.3: Bode plot of the impedance modulus as a function of frequency and temperature, of the UV irradiated DNA sensor.

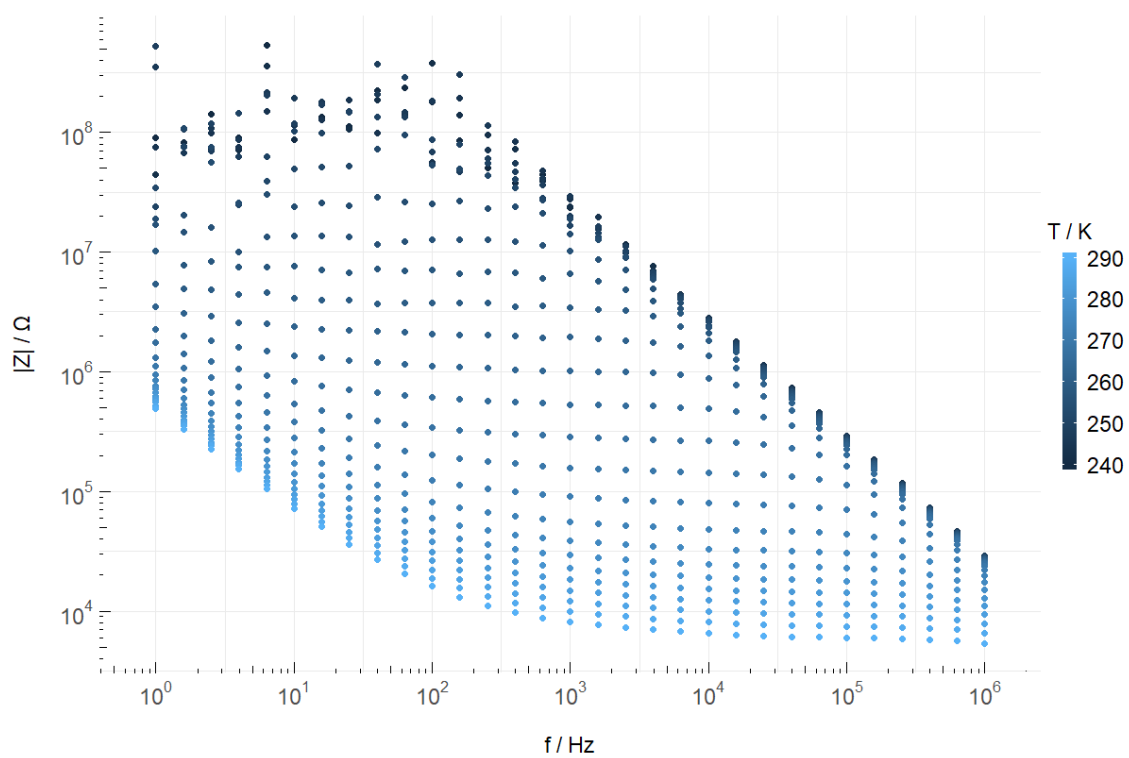


Figure C.4: Bode plot of the impedance modulus as a function of frequency and temperature, of the UV irradiated DNA+AuNPs sensor.

A N N E X



AUNPs DATASHEET

EM.GC40 - 40nm Gold Data Sheet

Information	
Product	Gold colloid – 40nm
Product Code	EM. GC40
Batch Number	#####
Storage Buffer	Suspended in H ₂ O, no preservative Residual chemical left from manufacture
Storage Instructions	Store at 2-8°C – DO NOT FREEZE
Expiry Date	##### #### (Use within one month of opening)

Technical Data	
Mean Diameter	37.0 nm – 43.0 nm
Coefficient of Variation	≤8%
Optical Density @ 520nm	1.00
Gold Chloride Concentration	0.01%
No. of Particles per ml (Estimated from theoretical calculation)	9.00 x 10 ¹⁰

USA: 1-800-423-8199 | International: +44 (0)2920 767 499 | info@bbisolutions.com | www.bbisolutions.com

Part of **BBI Group**

Registered office: c/o Berry Smith LLP, Haywood House, Dumfries Place, Cardiff, CF10 3GA.
BBI Solutions is the trading name of BBI Solutions OEM Limited. Registered in England and Wales Number 8368483

A N N E X

The image shows the word "ANNEX" written vertically in a bold, serif font. To its right is a square graphic containing the Roman numeral "II" in a white, serif font, set against a dark gray background.

MAX31865 DATASHEET

General Description

The MAX31865 is an easy-to-use resistance-to-digital converter optimized for platinum resistance temperature detectors (RTDs). An external resistor sets the sensitivity for the RTD being used and a precision delta-sigma ADC converts the ratio of the RTD resistance to the reference resistance into digital form. The MAX31865's inputs are protected against overvoltage faults as large as ±45V. Programmable detection of RTD and cable open and short conditions is included.

Applications

- Industrial Equipment
- Medical Equipment
- Instrumentation

Ordering Information appears at end of data sheet.

Benefits and Features

- Integration Lowers System Cost, Simplifies Design Efforts, and Reduces Design Cycle Time
 - Simple Conversion of Platinum RTD Resistance to Digital Value
 - Handles 100Ω to 1kΩ (at 0°C) Platinum RTDs (PT100 to PT1000)
 - Compatible with 2-, 3-, and 4-Wire Sensor Connections
 - SPI-Compatible Interface
 - 20-Pin TQFN and SSOP Packages
- High Accuracy Facilitates Meeting Error Budgets
 - 15-Bit ADC Resolution; Nominal Temperature Resolution 0.03125°C (Varies Due to RTD Nonlinearity)
 - Total Accuracy Over All Operating Conditions: 0.5°C (0.05% of Full Scale) max
 - Fully Differential VREF Inputs
 - 21ms (max) Conversion Time
- Integrated Fault Detection Increases System Reliability
 - ±45V Input Protection
 - Fault Detection (Open RTD Element, RTD Shorted to Out-of-Range Voltage, or Short Across RTD Element)

Typical Application Circuits

